



Développement par le procédé d'extrusion-gonflage de films polymères cellulaires à base de polyéthylène pour des applications piézoélectriques

Thèse

Ouassim Hamdi

Doctorat en génie chimique
Philosophiæ doctor (Ph. D.)

Québec, Canada

© Ouassim Hamdi, 2019

**Développement par le procédé d'extrusion-gonflage de films
polymères cellulaires à base de polyéthylène pour des
applications piézoélectriques**

Thèse

Ouassim Hamdi

Sous la direction de :

**Denis Rodrigue, directeur de recherche
Frej Mighri, codirecteur de recherche**

RÉSUMÉ

Cette thèse de doctorat présente une contribution à la fabrication de films polymères cellulaires. Ces matériaux ont récemment fait l'objet d'un vif intérêt aux niveaux académique et industriel grâce à leurs propriétés intéressantes combinant les avantages des polymères et des mousses, et en particulier leur potentiel pour des applications piézoélectriques. En fait, sous l'effet d'un chargement électrique approprié (décharge corona), les films polymères cellulaires peuvent fournir une conversion entre des énergies mécanique et électrique pour être utilisés comme capteurs ou actionneurs.

Tout d'abord, une méthode de production de films cellulaires en polyéthylène (PE) combinant le moussage chimique et l'extrusion-gonflage de film a été développée. Ce processus permet d'imposer un étirement biaxial aux échantillons lors de la formation de la structure cellulaire, ce qui favorise l'activité piézoélectrique de l'échantillon. Plusieurs compromis ont été faits pour améliorer la qualité du moussage. Cette optimisation était principalement basée sur une revue de la littérature et des observations directes lors des essais préliminaires. Les propriétés morphologiques ont été présentées et discutées en termes de paramètres de mise en œuvre, à savoir le profil de température, la vitesse de rotation des vis, le débit d'alimentation, le taux d'étirage (TUR), le taux de gonflage (BUR), ainsi que la composition de la matrice. Ces paramètres ont été optimisés pour produire une structure cellulaire homogène présentant des morphologies bien définies et une structure cellulaire bien développée avec des cellules de forme oculaire. Ceci a permis de diminuer le module élastique dans le sens de l'épaisseur et aussi de créer plus de surface spécifique pour la capture de charges conduisant ainsi à améliorer du coefficient piézoélectrique d_{33} .

Ensuite, des traitements de pression/température ont été appliqués pour mieux contrôler la morphologie cellulaire des films, afin d'optimiser les propriétés mécaniques et la surface spécifique interne de la structure cellulaire.

L'étape suivante était le chargement électrique par le procédé corona permettant aux films cellulaires d'acquérir la propriété piézoélectrique. Une amélioration supplémentaire a été

obtenue en optimisant le gaz utilisé lors du chargement (azote) et sa pression (15 psi) associés à des conditions de traitement telles que la tension de charge et la distance aiguille-échantillon.

Enfin, des traitements thermiques (recuit) et chimiques (acide phosphorique) ont été proposés pour mieux contrôler la microstructure des films et fournir une bonne stabilité temporelle et thermique. Dans l'ensemble, le traitement chimique s'est révélé le plus efficace. À la suite de ces étapes, un échantillon optimisé avec une densité de 450 kg/m^3 , une épaisseur de $162 \text{ }\mu\text{m}$, un facteur de forme longitudinale (AR-L) de 7.0 et un facteur de forme transversale (AR-T) de 4.1 a été fabriqué. Les propriétés piézoélectriques rapportées sont très élevées (même comparées au polypropylène (PP) qui est la polyoléfine la plus utilisée dans ce domaine) avec un coefficient d_{33} initial de 1315 pC/N se stabilisant après 50 jours à 792 pC/N et une bonne stabilité thermique, car les films restent chargés avec de bons coefficients piézoélectriques (280 pC/N) jusqu'à 80°C . Ces valeurs ont été améliorées par l'application d'un procédé combiné d'inversement de charge et d'empilement de trois couches donnant un d_{33} initial de 3270 pC/N , un d_{33} stabilisé de 1580 pC/N après 50 jours et une valeur de 641 pC/N à 80°C . Ces films de PE ferroélectrets aux propriétés piézoélectriques importantes peuvent être maintenant exploités pour la production à grande échelle de capteurs et de transducteurs à base d'électret.

ABSTRACT

This doctoral thesis presents a contribution on the fabrication of cellular polymer films. These materials have recently experienced a great interest at academic and industrial levels thanks to their interesting properties combining the advantages of both polymers and foams, in particular their potential for piezoelectric applications. In fact, after charging by an appropriate method (corona discharge), cellular polymers can provide high electrical/mechanical energy conversion to be used as sensors or actuators.

Firstly, a method to produce polyethylene (PE) cellular films using extrusion film-blowing was developed. This process allowed to impose biaxial stretching on the samples while foaming, which is believed to enhance the piezoelectric activity of the samples. Several compromises were made to improve the foaming quality. This optimization was mainly based on a literature review and direct observations during preliminary trials. Morphological properties were presented and discussed in terms of processing parameters, namely the temperature profile, screw rotational speed, feeding rate, take-up ratio (TUR), blow-up ratio (BUR), as well as the matrix composition. These parameters were optimized to produce a homogeneous cellular structure with defined morphologies and a well-developed eye-like cellular structure, which is important to decrease the elastic stiffness in the thickness direction and to provide more surface for charge capturing via cell deformation, thus improving the piezoelectric coefficient d_{33} .

Then, pressure/temperature treatments were applied to further control the cellular morphology of the films and optimize the mechanical properties and internal specific surface area of the cellular structure.

The next step was the electric charging by corona discharge producing cellular films with piezoelectric activity. Further improvement was obtained by optimizing the gas used (nitrogen) and its pressure (15 psi) combined with processing conditions such as the charging voltage and the needle-sample distance.

Finally, thermal (annealing) and chemical (phosphoric acid) treatments have been proposed to further control the microstructure of these films and to provide good time and thermal stability. Overall, the chemical treatment was found to be the most efficient. Following these steps, an optimized sample with a density of 450 kg/m^3 , a thickness of $162 \text{ }\mu\text{m}$, a longitudinal cell aspect ratio (AR-L) of 7.0 and a transversal cell aspect ratio (AR-T) of 4.1 was developed. The piezoelectric properties reported are very high (even compared to PP which is the most used polyolefin in this field) with an initial d_{33} of 1315 pC/N stabilizing after 50 days at 792 pC/N and a good thermal stability since the films remained charged with good piezoelectric coefficients (280 pC/N) up to 80°C . The values were further improved when a three-layered reverse charging method was applied giving an initial d_{33} of 3270 pC/N , a stabilized d_{33} of 1580 pC/N after 50 days and a value of 641 pC/N at 80°C . These ferroelectret PE films with important piezoelectric properties can now be exploited for the large-scale production of electret-based sensors and transducers.

TABLE DES MATIÈRES

RÉSUMÉ.....	III
ABSTRACT	V
TABLE DES MATIÈRES	VII
LISTE DES TABLEAUX	X
LISTE DES FIGURES	XI
Abréviations.....	XIII
Symboles	XV
QUOTE	XVII
REMERCIEMENT	XVIII
AVANT-PROPOS	XX
INTRODUCTION GÉNÉRALE	1
Introduction aux mousses thermoplastiques	1
Introduction au procédé d'extrusion-gonflage	3
Introduction à la piézoélectricité et aux ferroélectrets.....	5
Choix du polyéthylène: Avantages et défis	6
Intérêts, objectifs et originalités	8
CHAPITRE 1. PIEZOELECTRIC CELLULAR POLYMER FILMS: FABRICATION, PROPERTY AND APPLICATIONS	10
RÉSUMÉ.....	10
ABSTRACT	11
1.1. INTRODUCTION	12
1.2. PIEZOELECTRICITY	13
1.2.1. Fundamentals	13
1.2.2. Modeling	16
1.3. FABRICATION OF FERROELECTRET FILMS	17
1.3.1. Development of the cellular structure.....	17
1.3.2. Foaming steps.....	18
1.3.3. Polymer ferroelectret films processing	22
1.3.4. Electrical charging.....	24
1.3.5. Paschen's law	28
1.4. OPTIMIZATION OF THE PIEZOELECTRIC PROPERTIES OF CHARGED CELLULAR POLYMERS	29
1.4.1. Morphological and mechanical effects	29
1.4.2. Different methods used to enhance piezoelectricity of ferroelectrets	31
1.4.3. Enhanced thermal and temporal stability of the piezoelectric coefficient	32
1.5. POLYMERS USED AS FERROELECTRETS AND THEIR PROPERTIES	32
1.6. APPLICATIONS	34
1.6.1. Impact sensors	34
1.6.2. Human body	35
1.6.3. Transport applications.....	36
1.6.4. Acoustic applications	36
1.6.5. Tactile sensing applications	37
1.6.6. Other applications.....	37
1.7. CONCLUSIONS AND FUTURE DIRECTIONS IN THE FIELD	38

ACKNOWLEDGMENTS	39
CHAPITRE 2. OPTIMIZATION OF THE CELLULAR MORPHOLOGY OF BIAXIALLY STRETCHED THIN POLYETHYLENE FOAMS PRODUCED BY EXTRUSION FILM BLOWING.....	40
RÉSUMÉ.....	40
ABSTRACT	41
2.1. INTRODUCTION	42
2.2. EXPERIMENTAL	44
2.2.1. Materials	44
2.2.2. Film blowing	44
2.2.3. Characterization.....	45
2.3. RESULTS AND DISCUSSION	46
2.3.1. Challenges in producing thin foamed PE films of good quality.....	46
2.3.2. Optimization of the processing conditions to obtain high quality cellular films	48
2.3.3. Morphological results	54
2.4. CONCLUSION	59
ACKNOWLEDGEMENTS	60
CHAPITRE 3. PIEZOELECTRIC PROPERTY IMPROVEMENT OF POLYETHYLENE FERROELECTRETS USING POSTPROCESSING THERMAL-PRESSURE TREATMENT	61
RÉSUMÉ.....	61
ABSTRACT	62
3.1. INTRODUCTION	63
3.2. EXPERIMENTAL.....	66
3.2.1. Material preparation.....	66
3.2.2. Corona charging	67
3.2.3. Piezoelectric coefficient measurement.....	67
3.2.4 Temperature-pressure treatment.....	68
3.2.5. Morphological and density characterizations	70
3.2.6. Mechanical characterization.....	71
3.3. RESULTS AND DISCUSSION	72
3.3.1 Optimization of corona charging: needle-sample distance and charging time.....	72
3.3.2. Morphology effect on the piezoelectric coefficient and elastic stiffness	74
3.3.3 Elastic stiffness and piezoelectric coefficient correlations	77
3.3.4. Improving the d_{33} piezoelectric coefficient by using reverse charging.....	81
3.4. CONCLUSION	83
ACKNOWLEDGEMENTS	84
CHAPITRE 4. TIME AND THERMAL STABILITY IMPROVEMENT OF POLYETHYLENE FERROELECTRETS	85
RÉSUMÉ.....	85
ABSTRACT	86
4.1. INTRODUCTION	87
4.2. EXPERIMENTAL.....	89
4.2.1. Materials used and film preparation procedure	89
4.2.2. Differential Scanning Calorimetry (DSC) characterization	90

4.2.3. Piezoelectric coefficient measurement.....	91
4.2.4. Fourier-transform infrared (FTIR) spectroscopy characterization	91
4.2.5. Morphological and density characterizations	91
4.3. RESULTS AND DISCUSSION	92
4.3.1. Effect of the annealing temperature and time on crystallinity.....	92
4.3.2. Effect of polymer crystallinity on the piezoelectric stability of the cellular film	93
4.3.3. Effect of the chemical treatment on piezoelectric stability of the cellular films	95
4.3.4. Improvement of d_{33} piezoelectric coefficient using reverse charging and multi-layered films.....	100
4.4. CONCLUSIONS	104
ACKNOWLEDGEMENTS	105
CONCLUSION ET RECOMMANDATIONS.....	106
CONCLUSIONS GÉNÉRALES	106
RECOMMANDATIONS	108
Références	110

LISTE DES TABLEAUX

Table 1.1 List of different methods to improve the piezoelectric properties of ferroelectrets.	13
Table 1.2 Comparison of the piezoelectric properties of typical ferroelectrets.	34
Table 2.1 Optimized processing conditions for cellular PE blown films.	55
Table 2.2 Properties of the best polyethylene cellular films morphology (optimized conditions).	56
Table 3.1 Morphological parameters, elastic stiffness, and piezoelectric coefficient and their corresponding standard deviations (values in parentheses).	66
Table 3.2 Properties of the cellular polyethylene films.	79
Table 3.3 Piezoelectric coefficient (d_{33}) of multicharged cellular polyethylene films.	82
Table 4.1 Fitting parameters for Equation 4-4 based on the data of Figure 4-2.	94
Table 4.2 Morphological parameters of untreated and treated samples S1. (Values in parentheses represent standard deviations).	96
Table 4.3 d_{33} (pC/N) of the untreated and treated samples as a function of temperature. (Values in parentheses represent standard deviations).	97
Table 4.4 Initial d_{33} values (pC/N), as well as their time and thermal stability for three-layered reversely charged cellular polyethylene films. (Values in parentheses represent standard deviations).	101

LISTE DES FIGURES

Figure 1.1 Schematic representation of the piezoelectric effect (direct and reverse) of ferroelectrets [Li et al. 2017].	14
Figure 1.2 (a) Representation of a cellular film and (b) the simplified structure of the voided film with multiple layers of solid and gas [Rychkov et al. 2016].	16
Figure 1.3 Most simplified model of a charged cellular polymers [Rychkov et al. 2016].	17
Figure 1.4 Production of a cellular structure by stretching a filler loaded polymer (process 1) or foaming by a physical blowing agent (supercritical carbon dioxide, CO ₂) [Wegener 2010].	18
Figure 1.5 Phase diagram of a pure component showing the supercritical fluid (SCF) region [Hossieny 2010].	19
Figure 1.6 Schematic representation of homogeneous and heterogeneous nucleation [Chen et al. (2013)].	20
Figure 1.7 (a) Extrusion-calendaring foaming process and (b) its corresponding uniaxial stretched foamed film in the longitudinal direction (circular cells in the transversal direction), (c) extrusion-blowing foaming process and its corresponding biaxial stretched foamed film in the (d) longitudinal and (e) transversal stretched directions (same scale) [Mohebbi et al. (2017a); Hamdi et al. (2018b)].	23
Figure 1.8 Corona discharge (left) and direct contact charging (right) set-ups to perform film charging [Ramadan et al. (2014)].	25
Figure 1.9 Model description of the charging process [Qiu et al. (2007a)].	27
Figure 1.10 Effective charge density as a function of the bias voltage (V_{bias}) for a commercial cellular PP films (tradename PQ50) with a charging voltage directly applied on both metallized sides by means of a high voltage amplifier [Qiu et al. (2007a)].	27
Figure 1.11 Relative density effect on the piezoelectric coefficient and elastic stiffness [Wegener (2006)].	30
Figure 2.1 Schematic representation of the blown-film extrusion set-up.	45
Figure 2.2 Typical states of the foam during the optimization step: a) unfoamed PE film, b) film with 0.8% CBA, c) film with 1% CBA, d) PE film having surface defects and bubble stability problems, e) film with stable bubbles and good cellular quality, f) typical structure of a film presenting a non-uniform cellular structure and g) typical structure of a film presenting a uniform and well-developed cellular structure.	47
Figure 2.3 Schematic representation of the different temperature zones in an extrusion-blowing machine.	49
Figure 2.4 Left: bubble cooled by the cooling ring. Right: bubble cooled by ambient air presenting the bottleneck phenomenon.	50
Figure 2.5 SEM pictures for the transversal section of two film samples: (a) S1.2-6.4-1.8 and (b) S1.2-6.4-1.	52

Figure 2.6 (a) SEM picture for the longitudinal section of S1.5n-12.8-1 and (b) presence of tear lines when TUR=12.8 and BUR=1.8.....	53
Figure 2.7 SEM images of cellular polyethylene films: Sample S1.2-6.4-1.8 in the (a) transversal and (b) longitudinal directions, and S1.2n-6.4-1.8 in the (c) transversal and (d) longitudinal directions.....	54
Figure 2.8 SEM images of cellular polyethylene films: S2n-6.4-1.8 in the (a) transversal and (b) longitudinal directions and S2n-3.2-1.8 in the (c) transversal and (d) longitudinal directions.....	57
Figure 2.9 Typical SEM pictures for the longitudinal section of S1.5n-TUR-1.8 with different take-up ratios: (a) TUR=3.2 and (b) TUR=6.4.....	57
Figure 2.10 Effect of take-up ratio (TUR) and blowing agent content on the morphological properties of the cellular films.....	58
Figure 3.1 Illustration of the corona charging setup.....	67
Figure 3.2 Schematic description of the two TPT studied: (A) TPT1: stepwise temperature increase and (B) TPT2: 1-step temperature increase (both under 5 MPa of N ₂ pressure).....	70
Figure 3.3 Piezoelectric coefficient (d_{33}) as a function of needle-sample distance under air and different N ₂ atmospheres.....	73
Figure 3.4 Typical structures of the original and TPT samples (S2n-6.4). (Red lines represent a 100- μ m scale).....	75
Figure 3.5 Relationships between the piezoelectric coefficient (d_{33}) and the aspect ratio in both longitudinal (AR-L) and transversal (AR-T) directions.....	77
Figure 3.6 Experimental dielectric spectrum of S2n-6.4-TPT1 ferroelectret sample.....	78
Figure 3.7 Schematic representation of the developed process from manufacturing to characterization: (A) materials used, (B) biaxially stretched cellular PE films manufactured via optimized extrusion-blown film process, (C) cellular PE films with optimized morphology following a postprocessing temperature-pressure treatment (TPT), and (D) charged PE cellular films (ferroelectrets).....	82
Figure 4.1 Effect of annealing temperature and time on PE cellular films crystallinity.....	93
Figure 4.2 Variation of the piezoelectric coefficient with respect to time.....	94
Figure 4.3 Typical cellular structures of the untreated sample (S1) and treated sample (S1/PA). <i>Red lines represent a 100 μm scale.</i>	96
Figure 4.4 Piezoelectric coefficient d_{33} and its corresponding decrease in (%) at different temperatures.....	97
Figure 4.5 Typical SEM pictures of sample S1/PA at different magnifications.....	99
Figure 4.6 FTIR spectra of samples S1 and S1/PA.....	99
Figure 4.7 Schematic view of a multi-layer ferroelectret PE system.....	101
Figure 4.8 Processing steps and parameters leading to the optimized sample S1/PA.....	103

NOMENCLATURE (ABRÉVIATIONS/ SYMBOLES)

Abréviations

Ar	Argon
CaCO ₃	Carbonate de calcium
CBA	Agent de moussage chimique
CFC	Chlorofluorocarbures
CO ₂	Dioxyde de carbone
COC	Copolymère
COV	Composés organiques volatils
DSC	Calorimétrie différentielle à balayage
FLH	Position de figeage
FTIR	Spectroscopie infrarouge à transformée de Fourier
HCFC	Hydrochlorofluorocarbures
HDPE	Polyéthylène de haute densité
He	Hélium
HFC	Hydrofluorocarbures
LDPE	Polyéthylène de basse densité
LLDPE	Polyéthylène linéaire de basse densité
N ₂	Azote
NA	Agent nucléant
PA/H ₃ PO ₄	Acide orthophosphorique
PBA	Agent de moussage physique

PCl_3	Trichlorure de phosphore
PE	Polyéthylène
PET	Polyéthylène téréphtalate
PP	Polypropylène
PVDF	Polyfluorure de vinylidène
PZT	Zirconate de plomb
SCF	Fluide supercritique
SEM	Microscopie électronique à balayage
SiO_2	Quartz
TPT	Traitement de pression et température

Symboles

AR	Ratio de forme (-)
AR-L	Ratio de forme longitudinal (-)
AR-T	Ratio de forme transversal (-)
BUR	Taux de gonflage (-)
c_{33}	Module élastique en compression (MPa)
CST	Température de service continu (°C)
d_{33}	Coefficient piézoélectrique (pC/N)
E	Module élastique en traction (MPa)
F	Force (N)
F_a	Fréquence anti-résonance (Hz)
L/D	Ratio longueur sur diamètre (-)
MFI	Indice de fluidité (g/min)
N	Densité de cellules (cells/cm ³)
Q	Quantité de charge (pC)
R_0	Rayon de la bulle à la sortie de la filière (cm)
R_f	Rayons de la bulle à la position de figeage (cm)
T_c	Température de Curie (°C)
T_f	Température de fusion (°C)
T_g	Température de transition vitreuse (°C)
TUR	Taux d'étirement (-)
V_0	Vitesse d'écoulement à la sortie de la filière (g/cm)

V_f	Vitesse d'écoulement de la matière à la position de figeage (g/cm)
V_{thr}	Minimum de Paschen (V)
X_c	Degré de cristallinité (%)
E	Permittivité (F/m)
P	Masse volumique (kg/m ³)
σ	Densité surfacique de charge (pC/cm ²)
ΔH	Enthalpie (J/g)

QUOTE

“A scientist must be absolutely like a child. If he sees a thing, he must say that he sees it, whether it was what he thought he was going to see or not. See first, think later, then test. But always see first. Otherwise you will only see what you were expecting.”

Douglas Adams

REMERCIEMENT

Cette thèse est le fruit de plusieurs années de travaux intenses effectués aux laboratoires du Département génie chimique de l'Université Laval. Toutes ces années n'auraient pas été les mêmes sans les personnes avec qui j'ai travaillé pendant cette période.

*Je tiens tout d'abord à remercier le **Professeur Denis Rodrigue**, mon directeur de recherche, pour son accueil au sein de son groupe, son encadrement de haute qualité, son inestimable soutien et sa confiance. À son contact, j'ai bien progressé au niveau de mes connaissances et j'ai surtout acquis une certaine maturité dans la recherche et dans la manière d'aborder les problèmes scientifiques. Cette thèse a aussi été effectuée sous la codirection du **Professeur Frej Mighri**, que je remercie profondément pour son soutien, sa confiance et son aide grandement apprécié tant du côté humain que du côté scientifique. Je remercie aussi **mes directeurs de recherche** pour le financement qu'ils m'ont accordé, ce qui m'a permis d'être dans des conditions adéquates pour mener à bien ce projet de thèse jusqu'à son terme.*

*Je voudrais aussi remercier notre cher technicien de recherche **Yann Giroux** pour son aide technique et sa formation sur les différents équipements, et aussi pour sa sympathie et son support moral inestimable tout au long de ma période de thèse.*

*Je salue aussi tous mes anciens professeurs spécialement le **Professeur Mohamed Jaziri (ENIS)** qui m'a initié au domaine des polymères, ainsi que le **Professeur Sayed Taghavi (ULaval)** pour m'avoir donné l'opportunité d'assistanat au cours transfert de chaleur durant mon doctorat.*

J'aimerais aussi remercier le Centre de Recherche sur les Matériaux Avancés (CERMA), le Centre de Recherche sur les Matériaux Renouvelables (CRMR), le Centre de recherche sur les systèmes polymères et composites à haute performance (CREPEC) ainsi que le Centre Québécois sur les matériaux fonctionnels (CQMF) qui ont mis à ma disposition les appareils et le personnel qui leur sont affiliés pour la bonne marche et la réalisation de ce projet de thèse.

*Enfin, je tiens à remercier tous mes chers amis, mes collègues et ma large famille, en particulier mes parents **Afif (Pa)** et **Naima (Ma)**, mes sœurs **Syrine** (Félicitations pharmacienne), **Sinda** (Sandouda) et **Yasmine** (Yasmouna), et ma chère fiancée (et collègue!) **Saoussen** (Saw) pour leur amour, leur soutien, leur patience, leur compréhension et leurs encouragements. Je remercie aussi toute la famille*

*de ma tante **Sonia** et son mari **Adel** et les cousins **Wajih**, **Baha** et **Dhia** pour leur accueil et leur inestimable support au début de mon arrivée au Canada ainsi que ma **grand-mère** (Mima) et toute ma grande familles (oncles, tantes, cousins et cousines). Je remercie aussi mes collègues spécialement **Hejer** (Hajour), **Mustapha**, **Valerian** (Vale) et **Shan** ainsi que mon cher ami **Hichem** (Hich). Je vous aime tous et je vous souhaite beaucoup de bonheur!*

AVANT-PROPOS

Le présent travail a été réalisé sous la direction de Denis Rodrigue et sous la codirection de Frej Mighri, tous deux professeurs titulaires au Département de génie chimique de l'Université Laval. Ce travail de recherche a été effectué dans plusieurs laboratoires au Québec. Il s'agit du Centre Québécois sur les matériaux fonctionnels (CQMF), le Centre de recherche sur les matériaux avancés (CERMA) et du Centre de recherche sur les matériaux renouvelables (CRMR), ainsi que le Centre de recherche sur les systèmes polymères et composites à haute performance (CREPEC). En outre, le financement du projet provient d'une part du Conseil de recherches en sciences naturelles et en génie du Canada (CRSNG) et d'autre part du Centre de recherche sur les systèmes polymères et composites à haute performance (CREPEC). Cette thèse comprend six chapitres dont quatre sous forme d'articles scientifiques qui ont été acceptés/soumis pour publication dans des revues spécialisées.

Le premier chapitre est une introduction générale. Il présente une description des procédés de moussage, d'extrusion-gonflage et des ferroélectrets, ainsi que les objectifs de la thèse.

Le deuxième chapitre présente une littérature pertinente sur les films cellulaires piézoélectriques (fabrication, propriétés et applications). Il a été présenté sous la forme d'un article de revue déjà publié sous la référence:

Ouassim Hamdi, Frej Mighri, Denis Rodrigue (2018a) Piezoelectric cellular polymer films: Fabrication, properties and applications. *AIMS Materials and Science* 5: 845-869.

Les trois chapitres suivants (III à V) forment l'essentiel de cette thèse et présentent les résultats expérimentaux sous la forme d'articles scientifiques.

Le chapitre III présente le développement d'une méthode de production de films cellulaires en polyéthylène (PE) combinant le moussage chimique et l'extrusion-gonflage des films. On a détaillé l'effet des différents paramètres de mise en œuvre sur la structure cellulaire des films fabriqués. On a aussi réussi à fabriquer des films moussés à base de polyéthylène ayant une structure cellulaire riche (des cellules fines et denses avec une distribution uniforme) et

à déterminer la combinaison optimale des paramètres de mise en œuvre permettant d'obtenir des films convenables aux applications piézoélectriques (après chargement). Ce chapitre, a été publié avec la référence:

Ouassim Hamdi, Frej Mighri, Denis Rodrigue (2018b) Optimization of the cellular morphology of biaxially stretched thin polyethylene foams produced by extrusion film blowing. *Cellular Polymers* 37:153-168.

Dans le chapitre IV, les paramètres de chargement électrique moyennant le procédé Corona ont d'abord été optimisés (tension de charge, distance entre l'aiguille et l'échantillon, ainsi que du type et la pression du gaz utilisé) et leur effet sur le coefficient piézoélectrique quasi-statique (d_{33}) a été étudié en détail. De plus, deux différents traitements de pression et température ont été imposés pour obtenir une structure cellulaire de forme ellipsoïdale avec différents ratios de forme (AR) pour chaque direction (longitudinale et transversale). Ce chapitre a été accepté avec la référence:

Ouassim Hamdi, Frej Mighri, Denis Rodrigue (2018c) Piezoelectric properties improvement of polyethylene ferroelectrets using post-processing treatments. *Polymers for Advanced Technologies* 1-9.

Dans le chapitre V, on a essayé d'améliorer la stabilité du coefficient piézoélectrique en fonction de la température et du temps. Pour ce faire, des traitements ont été appliqués sur les films afin d'améliorer leur microstructure. Principalement, les films ont été traités avec de l'acide orthophosphorique ce qui a entraîné des améliorations substantielles de la stabilité de la charge, en particulier à une température plus élevée. Globalement, il a été possible d'augmenter la température de service continu (CST) des ferroélectrets à base de PE de 40 à 80°C, ce qui est similaire au CST typique du PP. Quant aux valeurs du coefficient piézoélectriques, on est arrivé (suite aux différentes optimisations évoquées dans tout le travail) à des valeurs importantes de d_{33} atteignant 1315 pC/N et allant jusqu'au 3270 pC/N par l'application d'un procédé combiné d'inversement de charge et d'empilement de trois couches. Ces films peuvent être exploités pour la production à grande échelle de capteurs et de transducteurs à base d'électrets. Ce chapitre a été soumis avec la référence:

Ouassim Hamdi, Frej Mighri, Denis Rodrigue (2018d) Time and thermal stability improvement of polyethylene ferroelectrets. *Journal of Applied Polymer Science*. Submitted.

Mes contributions, en tant qu'auteur principal de ces articles de recherche, incluent la planification et la réalisation des travaux expérimentaux, la collecte, l'analyse et l'interprétation des données, ainsi que la rédaction entière des manuscrits (version initiale). Mes co-superviseurs, Denis Rodrigue et Frej Mighri, sont les coauteurs dans les différents articles. Leur rôle était de vérifier l'ensemble des résultats, de m'aider à interpréter certains résultats et apporter des corrections nécessaires aux manuscrits avant leur soumission aux revues scientifiques choisies.

Enfin, le chapitre VI présente une conclusion générale et des recommandations pour des travaux futurs.

De plus, les résultats issus de ce travail de recherche ont également fait l'objet de communications dont

- Des affiches techniques lors de colloques scientifiques de CREPEC à Montréal:

Ouassim Hamdi, Frej Mighri, Denis Rodrigue (10 juin 2016) Production and optimization of cellular polymer films for piezoelectric applications. *Colloque étudiant du CREPEC, Montréal (QC), Canada.*

Ouassim Hamdi, Frej Mighri, Denis Rodrigue (6 December 2017) Optimization of the morphological, mechanical and piezoelectric properties of biaxially stretched thin polyethylene foams. *Colloque étudiant du CREPEC, Montréal (QC), Canada.*

- Une présentation dans le cadre de Poly-Foam Conference en Allemagne:

Ouassim Hamdi, Frej Mighri, Denis Rodrigue (11-12 avril 2018) Biaxially stretched thin polyethylene foams produced by extrusion film blowing: Optimization of the processing conditions. *2018 Poly-Foam Conference, Mainz (DE), Germany.*

INTRODUCTION GÉNÉRALE

Introduction aux mousses thermoplastiques

Les mousses thermoplastiques sont des polymères expansés constitués de deux phases: une phase polymérique continue dans laquelle est dispersée une phase gazeuse sous forme de bulles. Généralement, une telle structure est produite par l'introduction d'un agent gonflant (ou agent moussant) dans une matrice polymérique. De plus, différents types de particules peuvent être ajoutées dans la matrice, à savoir les agents nucléants qui peuvent être organiques ou minéraux [Lee et al. (2000); Lee et al. (2010)].

Depuis leur apparition dans les années 1930, les polymères cellulaires ont obtenu un grand succès dans les applications industrielles grâce à leurs avantages à savoir leur faible coût, leur légèreté, leur excellent rapport propriétés mécaniques/masse volumique, etc. De plus, ces matériaux sont particulièrement attirants car ils peuvent être produits avec des tailles différentes de cellules allant de quelques nanomètres à plusieurs millimètres. Pour chaque polymère, l'utilisation de différents agents gonflants et de différentes conditions de mise en œuvre peut produire de nouveaux matériaux avec des densités, des structures et propriétés différentes [Coccorullo et al. (2008)].

Le moussage consiste à générer des bulles de gaz dans la phase de masse fondue de polymère afin de produire un matériau plus léger sans sacrifier les propriétés mécaniques et physiques du polymère. Grâce à la présence des bulles de gaz, les produits finaux (mousses) possèdent généralement de meilleures propriétés isolantes ainsi que des degrés plus élevés de résistance à l'impact [Lee et al. (2000)]. Pour obtenir une structure cellulaire, un agent de moussage est introduit dans une matrice polymérique. On introduit ici les différents agents qui peuvent intervenir dans le processus de moussage.

➤ **Les agents de moussage chimiques (CBA):** Ils se réfèrent aux matériaux qui se décomposent à la chaleur et génèrent de l'azote (N_2), du dioxyde de carbone (CO_2) ou les deux gaz en même temps. Il existe deux grands types d'agents de moussage chimique: exothermiques et endothermiques. La plupart sont exothermiques tel que l'azodicarbonamide

qui génère de l'azote lors de sa décomposition. En revanche, le gaz primaire généré à partir des agents endothermiques, tels que le bicarbonate de sodium et l'acide citrique, est le CO₂. Les agents chimiques exothermiques ont tendance à se décomposer plus facilement par rapport à leurs homologues endothermiques parce que la chaleur générée lors de leur décomposition peut déclencher la décomposition des particules voisines et ainsi de suite (réaction en chaîne et auto-catalytique). Les principaux avantages de l'utilisation des CBA est qu'ils ne nécessitent pas de modification de l'équipement existant pour les utiliser. Aussi, il est plus facile de réaliser une distribution uniforme du gaz dans la matrice de polymère. Toutefois, les CBA sont généralement plus coûteux que les agents physiques [Leung (2009)].

➤ **Les agents de moussage physique (PBA):** Les procédés de moussage physique utilisent la décompression de la matrice pour qu'un agent gonflant solubilisé, qui peut être un gaz comme N₂ ou CO₂ ou un liquide à savoir les fluorocarbures ou le pentane, puisse créer les bulles par simple changement de phase (instabilité thermodynamique) [Coccorullo et al. (2008)]. Les chlorofluorocarbures (CFC) et les hydrochlorofluorocarbures (HCFC) étaient les agents physiques les plus couramment utilisés pour les processus de formation de mousse plastique. Cependant, leur potentiel néfaste sur la couche d'ozone, le Protocole de Montréal [Rodrigue et al. (2002)] et les règlements connexes ont interdit leurs utilisations. Les composés organiques volatils (COV) peuvent également être utilisés comme agents gonflants, mais ils sont inflammables, préjudiciables à la santé et réagissent avec la lumière UV et les oxydes d'azote pour former de l'ozone troposphérique. Par conséquent, il existe une pression croissante pour réguler également leur utilisation. Afin d'éviter tous ces inconvénients, l'industrie des mousses plastiques a tourné son attention vers d'autres remplaçants potentiels. En particulier, des études sur les hydrofluorocarbures (HFC), réalisées pour étudier leur efficacité comme agents gonflants alternatifs, ont attiré beaucoup d'intérêts de l'industrie. Différents chercheurs ont également étudié les comportements du moussage de plastiques utilisant le CO₂ ainsi que des gaz inertes tels que le N₂, l'argon (Ar) et l'hélium (He). Cependant, les HFC, CO₂, N₂, Ar et He sont moins solubles et possèdent des diffusivités supérieures dans le polymère fondu que leurs homologues moins respectueux de l'environnement. L'obtention/contrôle des morphologies souhaitées devient donc technologiquement plus complexe [Lee (2010)].

➤ **Les agents nucléants (NA):** Pour enrichir la structure cellulaire, on peut ajouter des particules appelées agents nucléants (carbonate de calcium, talc, etc.) agissant comme des sites de germination et favorisant la création d'une structure plus riche en bulles de gaz. Cette nucléation est appelée hétérogène. Les agents de nucléation sont généralement ajoutés pour contrôler la qualité de la mousse et sa morphologie: des cellules de petites tailles avec des distributions de taille plus étroites. Les meilleurs agents de nucléation sont associés à leur capacité à augmenter le taux de nucléation en favorisant la nucléation hétérogène au détriment de la nucléation homogène. En effet, les agents de nucléation fournissent plusieurs sites de nucléation où la barrière d'énergie de surface est plus faible. C'est pourquoi, à l'échelle commerciale, la fabrication de mousse par la nucléation hétérogène a été plus efficace que la nucléation homogène pour faciliter la formation de bulles et produire une structure cellulaire uniforme [Rodrigue et al. (2002)]. Une description plus détaillée du phénomène physique se produisant lors de l'intervention de l'agent nucléant est rapportée dans le chapitre 1.

Introduction au procédé d'extrusion-gonflage

Le procédé d'extrusion gonflage constitue l'un des principaux procédés de fabrication des films plastiques. Il consiste à produire en continu des films thermoplastiques bi-orientés et minces [Kolarik (2012); Laffargue (2003); Gamache (2010)]. Les films gonflés sont utilisés dans plusieurs domaines à savoir l'emballage (sacs d'épicerie, sacs de transport, sacs à ordures, films d'emballage alimentaire), les films de barrière (viande ou conditionnement du fromage), les films agricoles (films de serre, films d'ensilage), les films médicaux et les séparateurs pour les batteries Li-ion. Tous ces produits bi-orientés sont principalement faits à partir de polyoléfines, de polystyrène, de chlorure de polyvinyle et de polyamide [Kolarik (2012)]. Au début, le polymère (sous forme de granulés ou de poudres) est introduit dans l'extrudeuse qui assure le transport, la plastification et l'homogénéisation de la matière et force le polymère fondu à passer à travers une filière annulaire. À la sortie de la filière, le film est étiré longitudinalement par des rouleaux pinceurs. Le taux d'étirement TUR (*Take Up Ratio*), nommé aussi le ratio d'étirage, définit l'étirement longitudinalement du film par les rouleaux pinceurs:

$$TUR = V_f/V_0 \quad (\text{I-1})$$

où V_f et V_0 sont respectivement les vitesses d'écoulement de la matière à la position de figeage et à la sortie de la filière.

Le soufflage de l'air par le centre de la filière crée une pression interne conduisant au gonflement du tube qui forme ainsi une bulle (ou gaine). Le volume d'air emprisonné dans la gaine est constant et mène au contrôle du taux de gonflement BUR (*Blow Up Ratio*) qui définit l'étirage transversal du film:

$$BUR = R_f/R_0 \quad (\text{I-2})$$

avec R_f et R_0 étant respectivement les rayons des bulles de la matière à la position de figeage et à la sortie de la filière. La gaine est refroidie par un jet d'air comprimé appliqué à la sortie de la filière par un anneau de refroidissement.

Un anneau de refroidissement projetant de l'air permet le figeage du polymère. La position à partir de laquelle le film est solidifiée est appelée la position de figeage FLH (*Frost Line Height*). Lorsque le polymère est entièrement solidifié, il n'est plus déformé. Un débit de refroidissement important implique un refroidissement rapide de la bulle et le diamètre final du film est atteint plus tôt. Inversement, plus le débit d'air de refroidissement est faible, plus le temps pour atteindre la solidification du polymère est important. Enfin, la bulle est rabattue sur elle-même sous l'effet de plaques et de rouleaux pinceurs, et le film est enroulé [Kolarik (2012); Laffargue (2003); Gamache (2010)]. Bien que la littérature libre ne présente pas suffisamment d'informations sur le procédé d'extrusion-gonflage des polymères cellulaires, ce procédé a été choisi puisqu'il assure un étirage biaxial permettant de bien contrôler les propriétés morphologiques et mécaniques du film cellulaire. Plus de détails sur ce procédé et ses différents paramètres sont détaillé dans le chapitre III.

Introduction à la piézoélectricité et aux ferroélectrets

Le mot piézoélectricité est une combinaison de deux mots: 'piezo' qui est un mot grec signifiant pression et 'électricité' faisant référence évidemment aux charges électriques. En effet, les matériaux piézoélectriques ont la capacité de générer des charges électriques en réponse aux contraintes mécaniques appliquées [*Padasalkar et al. (2015)*]. Ce phénomène de piézoélectricité peut se produire dans les deux sens: l'effet piézoélectrique direct qui correspond à la polarisation sous contrainte et l'effet piézoélectrique inverse qui correspond à la déformation du matériau sous l'action d'un champ électrique.

Les films polymères cellulaires piézoélectriques, appelés aussi 'ferroélectrets', ont attiré récemment une grande attention grâce à leurs propriétés diélectriques et piézoélectriques intéressantes. La structure interne de ces films est un composite de polymère et de cellules gazeuses dispersées dans ce dernier. Le mot ferroélectrets vient de la combinaison de deux termes:

- 1- Les électrets qui sont des matériaux ayant une polarisation électrique quasi-permanente (équivalent électrique d'un aimant). Les électrets polymères sont des diélectriques ayant subis un champ électrique externe permettant d'emprisonner des charges électriques aux surfaces du polymère [*Ende Dav et al. (2012)*].
- 2- Les ferroélectriques sont des matériaux ayant une polarisation électrique spontanée pouvant être réorientée à la suite d'une polarisation externe.

Les ferroélectrets sont donc des matériaux qui se chargent sous l'action d'un champ électrique externe (similaire aux électrets) et qui restent polarisés lorsque ce champ est retiré (tout comme la polarisation rémanente des ferroélectriques). Ces mousses doivent être électriquement chargées afin de générer une rupture de symétrie de la polarisation interne. Par conséquent, des champs électriques généralement élevés sont appliqués sur l'épaisseur de l'échantillon par un chargement corona ou en contact direct. Le champ électrique appliqué sur l'épaisseur de l'échantillon conduit à des décharges de barrière diélectrique à l'intérieur des vides accompagnées d'un piégeage de charges avec des polarités différentes sur des

surfaces de vides opposées. Les charges séparées représentent un grand dipôle électrique macroscopique dont la direction peut être commutée en effectuant à nouveau le processus de charge avec une tension de polarité opposée. Les ferroélectrets présentent un comportement d'hystérésis de la polarisation interne en fonction du champ électrique appliqué [Wegener (2010)].

Les ferroélectrets sont aujourd'hui à l'étude pour plusieurs applications à savoir les actionneurs, les contrôleurs de vibration, les transducteurs à ultrasons, les capteurs tactiles, les dispositifs ferroélectriques, les dispositifs de conversion d'énergie, les haut-parleurs, les microphones, les claviers, les capteurs de choc, etc. En effet, les capteurs traditionnels sont coûteux, nécessitent une alimentation constante et manquent de durabilité et de flexibilité pour répondre aux besoins des clients. Au contraire, les polymères cellulaires piézoélectriques peuvent être manipulés pour être compatibles avec n'importe quel produit. Généralement, ces polymères cellulaires piézoélectriques peuvent être exploités comme des capteurs dits « intelligents ». Ces capteurs ajoutent de la valeur puisqu'ils sont flexibles, légers et moins coûteux. La tension créée par la mousse lors de l'impact dépend de la force (ou l'énergie) appliquée. Ces informations peuvent être utiles dans plusieurs applications et plus de détails sont disponibles dans la section 1-6.

Choix du polyéthylène: Avantages et défis

Le polyéthylène (PE) est un polymère thermoplastique appartenant à la famille des polyoléfines. Son nom vient du fait qu'il est obtenu par polymérisation des monomères d'éthylène ($\text{CH}_2=\text{CH}_2$) en une structure de formule générique $-(\text{CH}_2-\text{CH}_2)_n-$ [Liu (1998)]. Le polyéthylène linéaire de basse densité (LLDPE) a été choisi comme résine principale pour la fabrication des films cellulaires dans ce projet. Plusieurs raisons nous ont poussé à faire ce choix:

- 1- Le polyéthylène est le polymère le plus disponible, il est peu coûteux et très utilisé dans les industries. Ceci convient parfaitement à notre objectif de fabriquer des films piézoélectriques bon marché.

- 2- Le polyéthylène possède un module élastique relativement faible en compression avec d'autres polymères. Ceci est important puisque le coefficient piézoélectrique (d_{33}) est inversement proportionnel au module d'élasticité [Wegener et al. (2005)], comme démontré dans l'équation 1-1 [Rychkov et al. (2016); Sessler et al. (1999); Zhang (2010)].

Cependant, le choix du LLDPE pose plusieurs défis qu'on doit surmonter pour arriver à obtenir des films compétitifs. Les deux défis principaux sont:

- 1- La résistance à l'état fondu (*melt strength*) du LLDPE : la plupart des PE linéaires ne possèdent pas une résistance à l'état fondu suffisante pour assurer une déformation importante pendant la formation de la mousse (expansion cellulaire) et le gonflage de film (étirement) [Zakaria et al. (2009)]. En effet, la faible résistance élongationnelle à l'état fondu limite la croissance des cellules avant l'effondrement et la coalescence, ce qui conduit à des structures cellulaires non homogènes. En outre, une résistance élongationnelle élevée est importante pour maintenir la stabilité des bulles et éviter les défauts de surface lors de la mise en œuvre des films. Donc, l'amélioration de la qualité du film doit passer par ce paramètre clé. Quelques méthodes comme l'addition d'un polymère branché ou d'un agent nucléant peuvent être utiles. Il est très important de bien contrôler les différents paramètres technologiques intervenant dans la mise en œuvre de ces films cellulaires afin d'assurer une qualité optimale des films produits.
- 2- Faible stabilité piézoélectrique: La faible stabilité thermique et temporelle des charges emprisonnées dans ce polymère. En fait, la littérature indique que le coefficient piézoélectrique des films de PE cellulaire commence à diminuer rapidement aux environs de 40°C (contre 60°C pour le polypropylène, PP), alors qu'à 90°C, ces ferroélectrets perdent presque complètement leur charge électrique (tombant à zéro à 100°C) [Rychkova et al. (2012); Paajanen et al. (2000); Neuschwandtner et al. (2001)]. Ici, l'application de traitements thermiques et

chimiques afin de modifier les propriétés surfaciques des films cellulaires doit être réalisée.

Intérêts, objectifs et originalités

L'objectif général de la présente thèse est d'utiliser les matériaux polymères les plus abondants et les procédés les plus standards de mise en œuvre des films polymères dans les applications piézoélectriques. Ceci permet de rendre leur utilisation plus accessible en termes de disponibilité et de coût tout en essayant d'obtenir les meilleures propriétés piézoélectriques possibles en termes du coefficient piézoélectrique quasi-statique (d_{33}) et des stabilités thermique et temporelle.

À cet effet, on présente ici les objectifs spécifiques de cette thèse avec les concepts et les étapes nécessaires pour y arriver:

- 1- Fabriquer des films cellulaires à base de polyéthylène ayant une structure cellulaire riche; c.à.d. des cellules fines et denses avec une distribution uniforme.
 - Une bonne compréhension des principes de mousage et d'extrusion-gonflage.
 - Une optimisation des différents paramètres (géométriques, technologiques, matériel) influant sur la qualité du film moussé par extrusion-gonflage.
 - Une investigation de l'effet des matières utilisées lors du processus (type et concentration) sur la stabilité du coefficient piézoélectrique.

- 2- Contrôler la morphologie et les propriétés mécaniques pour optimiser les propriétés piézoélectriques des ferroélectrets.
 - Avoir un bon contrôle de la morphologie cellulaire sur une large plage de ratios de forme (AR), de densités et de tailles de cellules.
 - Pouvoir lier les paramètres de mise en œuvre et la morphologie (plus précisément le ratio de forme AR).

- 3- Améliorer les conditions du chargement électrique via le procédé Corona.

- Une optimisation des différents paramètres de chargement électrique (tension de chargement électrique, distance entre l'aiguille et l'échantillon, type et pression du gaz utilisé, etc.) pour étudier leur effet sur le coefficient piézoélectrique (d_{33}).
- 4- Évaluer l'effet des traitements thermiques et chimiques sur les propriétés piézoélectriques.
- Comprendre la relation entre la microstructure du film polymérique et la stabilité piézoélectrique.
 - Analyser l'effet des traitements thermiques (comme le recuit) et des traitements chimiques (comme l'acide phosphorique) sur la stabilité de la charge, en particulier à une température plus élevée.

Ainsi ce travail traite toutes les étapes (fabrication, traitements post-fabrication, chargement électrique) conduisant à l'optimisation des ferroélectrets. L'utilisation de polyéthylène et du procédé d'extrusion-gonflage pour des applications piézoélectriques est innovante. Ceci constitue un avancement important au niveau du développement des matériaux piézoélectriques à faible coût pouvant être utilisés dans différents domaines tels que la médecine, la sécurité, l'environnement, le sport et les transports.

CHAPITRE 1. PIEZOELECTRIC CELLULAR POLYMER FILMS: FABRICATION, PROPERTIES AND APPLICATIONS

RÉSUMÉ

La piézoélectricité peut être définie comme la capacité de certains matériaux à fournir une conversion d'énergie mécanique-électrique. En plus des polymères ferroélectriques traditionnels (polyfluorure de vinylidène, PVDF) et les céramiques (titanate de zirconate de plomb, PZT), les films polymères moussés chargés électriquement ont également montré une activité piézoélectrique importante. En fait, lorsque ces films sont exposés à des champs électriques élevés, des charges positives et négatives sont créées sur les faces opposées de la surface de chaque cellule. En conséquence, les polymères cellulaires chargés peuvent présenter un comportement similaire aux matériaux ferroélectriques et peuvent donc être appelés ferroélectrets. On sait que l'effet piézoélectrique de ces matériaux dépend de plusieurs paramètres tels que la structure cellulaire (densité cellulaire, forme et taille des cellules), la densité relative et la rigidité élastique. Cependant, un contrôle minutieux de la morphologie est nécessaire pour optimiser la réponse piézoélectrique. Les ferroélectrets ont récemment suscité un vif intérêt, tant du point de vue académique qu'industriel, en raison de leur vaste éventail d'applications technologiques associées à leur coefficient piézoélectrique élevé, leur faible coût ainsi que leur flexibilité et légèreté. Dans cet article, un aperçu des différents polymères cellulaires piézoélectriques est présenté avec les progrès récents dans le développement de ces structures et leurs applications.

Mots-clés: piézoélectricité; ferroélectrets; polymères cellulaires; propriétés morphologiques et mécaniques; coefficient piézoélectrique; applications.

ABSTRACT

Piezoelectricity can be defined as the ability of certain materials to provide mechanical-electrical energy conversion. In addition to traditional ferroelectric polymers (such as polyvinylidene fluoride, PVDF) and ceramics (such as lead zirconate titanate, PZT), charged polymer film foams have also shown important piezoelectric activity. In fact, when cellular polymers are exposed to high electrical fields, positive and negative charges are created on the opposite faces of each cell surface. As a result, charged cellular polymers can exhibit ferroelectric-like behavior and may therefore be called ferroelectrets. The piezoelectric effect of these materials is known to be affected by several parameters such as the cellular structure (cell density, shape and size), relative density and elastic stiffness. However, a careful morphology control is mandatory to optimize the piezoelectric response. Ferroelectrets have recently received a great deal of academic and industrial interest due to their wide range of technological applications associated with high piezoelectric constants, low cost, flexibility and low weight. In this paper, an overview of different piezoelectric cellular polymers is presented with recent developments and applications.

Keywords: piezoelectricity; ferroelectrets; cellular polymers; morphological and mechanical properties; piezoelectric coefficient; applications.

Ouassim Hamdi, Frej Mighri, Denis Rodrigue (2018a) Piezoelectric cellular polymer films: Fabrication, properties and applications. *AIMS Materials and Science* 5: 845-869.

1.1. INTRODUCTION

Since the discovery of the piezoelectric effect in 1880, the demand for advanced functional materials in transducer technology has been increasing. Several applications have emerged because of the growing need for sensors and actuators (biomedical, transport, communication, robotic, electro-acoustic, etc.) [Dagdeviren (2016)].

Three main classes of piezoelectric materials are known: crystals, ceramics and polymers. Inorganic materials (crystals or ceramics) were the first to be discovered and are still commercialized due to their good piezoelectric coefficient. Compared to their inorganic counterparts, piezoelectric polymers have several advantages, namely being lightweight, low cost, highly flexible and thin, making them suitable for large-area applications [Mohebbi et al. (2018)]. However, most of the piezoelectric polymers, mainly poly(vinylidene fluoride) (PVDF) and its copolymers, have shown a relatively weak quasi-static piezoelectric coefficient (d_{33}) of around 20 to 28 pC/N [Harrison et al. (2002)]. Therefore, the need for polymer-based materials with good piezoelectric properties led to the development of piezoelectric cellular polymers, called ferroelectrets. These voided polymers, with artificial piezoelectric behavior, have shown interesting piezoelectric properties (see **Table 1.1**) with a wide range of possibilities for their optimization.

The paper is organized as follows. Firstly, definitions are given and the piezoelectric effect is discussed with a short historical perspective. Then, ferroelectrets and their differences with classical piezoelectric materials (ferroelectric materials) are presented. Finally, the preparation of these materials with their charging process, optimization, and recent applications is described.

Table 1.1 List of different methods to improve the piezoelectric properties of ferroelectrets.

STEP	METHOD/ TREATMENT	EFFECT	REFS.
DURING FILM PREPARATION	Blending with a high melt strength polymer (such as adding low density PE (LDPE) to linear low-density PE (LLDPE))	Morphological effect by stronger cell walls able to bear the extensional forces, thus preventing structure collapse.	[<i>Mohebbi et al. (2015)</i> ; <i>Hamdi et al. (2018b)</i> ; <i>Zhai et al. (2008)</i> ; <i>Rachtanapun et al. (2004a)</i> ; <i>Rachtanapun et al. (2004b)</i> ; <i>Huang (2005)</i> ; <i>Huang et al. (2005)</i>]
	Nucleating agents addition (such as talc, calcium carbonate, short carbon fibers, etc.)	Morphological effect by increasing cell nucleation density and producing more uniform and stable structure.	[<i>Huang et al. (2008)</i> ; <i>Ding et al. (2013)</i> ; <i>Wang et al. (2013)</i> ; <i>Zheng et al. (2010)</i> ; <i>Mohebbi et al. (2017a)</i> ; <i>Audet (2015)</i>]
	Biaxial stretching (such as film extrusion-blowing)	Morphological and mechanical effects by controlling cell shape and size in both longitudinal and transversal directions.	[<i>Hamdi et al. (2018b)</i>]
AFTER FILM PREPARATION (POST-PROCESSING)	Temperature and pressure treatment	Morphological and mechanical effects by controlling cell shape and size.	[<i>Wegener et al. (2004b)</i> ; <i>Sborikas et al. (2013)</i>]
	Multilayer films superposition (three or more layers)	Electrical effect: increased dipoles number leading to higher voltage under stress.	[<i>Qiu et al. (2007b)</i>]
	Charge storage stability (such as treatment with hydrofluoric acid or orthophosphoric acid)	Electrets properties improvement (thermal and time stability) by applying chemical treatments.	[<i>Rychkova et al. (2012)</i> ; <i>AN et al. (2009)</i>]

1.2. PIEZOELECTRICITY

1.2.1. Fundamentals

The term piezoelectricity is a combination of two words: “piezo” which is a Greek word meaning pressure, and “electricity”, obviously referring to electrical charges. In fact,

piezoelectric materials can convert mechanical energy into electrical energy. As shown in **Figure 1-1**, the piezoelectric effect can occur in all directions and can be divided in two main effects: the direct piezoelectric effect, corresponding to the production of electrical charges under mechanical stress, and the inverse piezoelectric effect associated to the deformation of a material when subjected to an electric field.

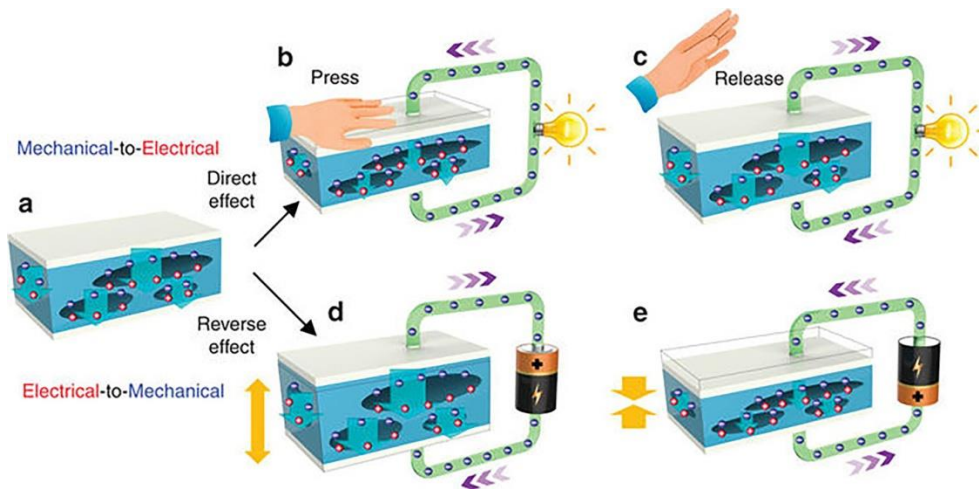


Figure 1.1 Schematic representation of the piezoelectric effect (direct and reverse) of ferroelectrets [Li et al. 2017].

Crystals, such as quartz (SiO_2), were the first piezoelectric materials discovered around 1880 [Curie et al. (1880)]. Their piezoelectricity comes from the displacement of atoms in their unit cells. When no stress is applied on the material, the positive and negative charges are equally distributed so that there is no potential difference. However, when a deformation is applied, the barycenters of the positive and negative charges are separated, hence, a change in the electric dipole moments occurs. The charges no longer cancel each other out and a potential difference exists.

Ferroelectrics constitute another piezoelectric family and represent the largest number of piezoelectric materials [Defay (2013)]. Their piezoelectric activity manifests itself as a result of external polarization [Defay (2013); Setter et al. (2006); Abraham (2011)]. In fact, ferroelectrics are materials having a spontaneous electric polarization below their ferroelectric Curie temperature (T_C). At temperatures above T_C , the crystals are nonpolar and no longer ferroelectric, thus behaving like normal dielectrics. On the other hand, the

polarization of ferroelectrics can be reoriented by the application of an external electrical field. Ferroelectrics are made of several very small randomly oriented ferroelectric domains (formed by self-assembly) so that the electric fields created cancel each other and there is no net polarization on the material. Each domain contains some polarized crystals in the same direction and every domain is separated from others by domain walls. The internal dipoles are reoriented by the application of an external electric field, leaving a remnant polarization after field removal [Defay (2013); Setter et al. (2006); Abraham (2011)]. This remnant polarization (electric dipoles) also changes when a stress is applied, leading to piezoelectricity. The most well-known ferroelectric materials are ceramics, such as PZT. Some polymers have also shown ferroelectric properties due to their polar structure containing molecular dipoles. Similar to ceramic materials, these dipoles can be reoriented and kept in a preferred orientation state by an external electric field. PVDF is one of the most commonly used piezoelectric polymers exhibiting considerable flexibility in comparison with PZT, but has a poor d_{33} coefficient [Defay (2013); Setter et al. (2006); Abraham (2011)].

To improve the polymer piezoelectric sensitivity, cellular structures were explored. Their development in the late 1980 was a response to the growing need to have piezoelectric materials combining the interesting properties of polymers and high piezoelectric coefficients [Graz et al. (2016); Kirjavainen (1987)]. The internal structure of polymer films is a two-phase morphology made from a solid polymer (continuous phase or matrix) and gaseous cells (dispersed phase or bubbles). When the polymer surfaces surrounding the voids are charged with an external electric field, the charged polymer foam behaves like a ferroelectric material. In fact, applying a large electric field across the film ionizes the gas molecules in the voids, thus opposite charges are accelerated and accumulated on each side of these voids. Such “artificially” embedded dipoles respond to mechanical stress (direct piezoelectric effect) or an externally applied electrical field (inverse piezoelectric effect) similar to piezoelectric materials [Savolainen et al. (1989)]. More details of the poling procedure will be discussed in **Section 1.3.3**.

1.2.2. Modeling

As discussed above, ferroelectrets are cellular charged polymer films with closed cavities exhibiting strong d_{33} coefficients. As a first approximation, the foam can be represented by a stack of alternating solid and gas layers characterized by the same macroscopic piezoelectric coefficient as the initial material (**Figure 1.2**).

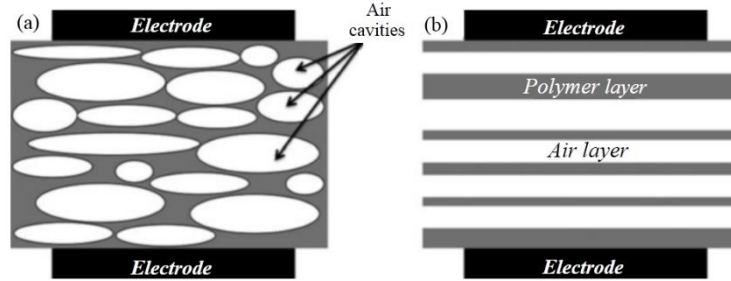


Figure 1.2 (a) Representation of a cellular film and (b) the simplified structure of the voided film with multiple layers of solid and gas [Rychkov *et al.* 2016].

The system is then simplified to a three-layer structure: an air layer enclosed by two polymer layers (**Figure 1.3**). The piezoelectric coefficient (d_{33}) can be defined as the ratio of the induced charge (Q) to the applied force (F) perpendicular to the film surface [Mohebbi *et al.* (2018)]. The main parameters controlling the piezoelectric behavior of a specific structure are the charge density on the cavities inner surface (σ), the polymer and the air permittivity (ϵ), the elastic stiffness c_{33} (elastic modulus), as well as the polymer (d_1) and gas (d_2) thickness layer leading to [Rychkov *et al.* (2016); Sessler *et al.* (1999); Zhang (2010)]:

$$d_{33} = \frac{Q}{F} = \frac{\epsilon\sigma}{c_{33}} * \frac{1+d_2/d_1}{1+\epsilon*d_2/d_1} \quad (1.1)$$

This simple model highlights the influence of the ferroelectrets mechanical and electrical properties on the macroscopic response of the cellular films.

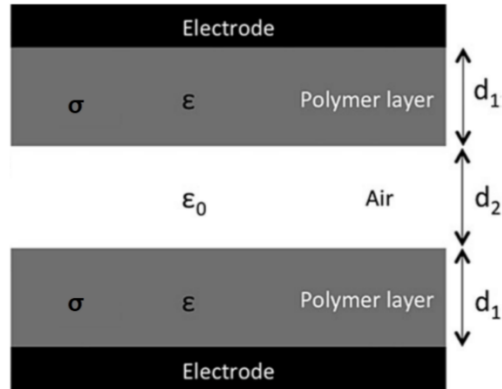


Figure 1.3 Most simplified model of a charged cellular polymers [Rychkov et al. 2016].

1.3. FABRICATION OF FERROELECTRET FILMS

The processing of piezoelectric cellular polymer films involves several stages, each one requiring the control and optimization of the different parameters involved, as well as the use of specific equipment. In this section, the conditions and techniques used for each step are presented and discussed based on existing work taken from the literature.

1.3.1. Development of the cellular structure

1. The first step is obtaining the cellular structure. In the literature, a wide variety of techniques for making cellular films has been proposed. These techniques can be classified in two categories: stretching and foaming methods (**Figure 1.4**). The stretching method consists of producing a polymer composite film filled with small solid particles and then stretching it to create voids around the solid particles by delamination at the particle-matrix interface [Mohebbi et al. (2015); Wegener (2010)]. In fact, the objective is to create micro-cracks generating a high level of interfacial stresses on the particles. Under mechanical loading (stretching), these particles are zones of crack initiation and propagation leading to the production of a cellular structure. On the other hand, foaming consists in generating a cellular structure via a blowing agent. Several blowing agents have been developed, depending on the desired foam morphologies.

They can be divided in two classes: physical blowing agents (PBA) where a gas (or a volatile liquid) is directly injected into the polymer, and chemical blowing agents (CBA), which are molecules generating the blowing gas after some heat-induced chemical decomposition [Mohebbi *et al.* (2015); Wegener (2010)]. The obtained gas is dissolved in a polymer, and then nuclei are created by imposing a thermodynamic instability (pressure drop or temperature jump).

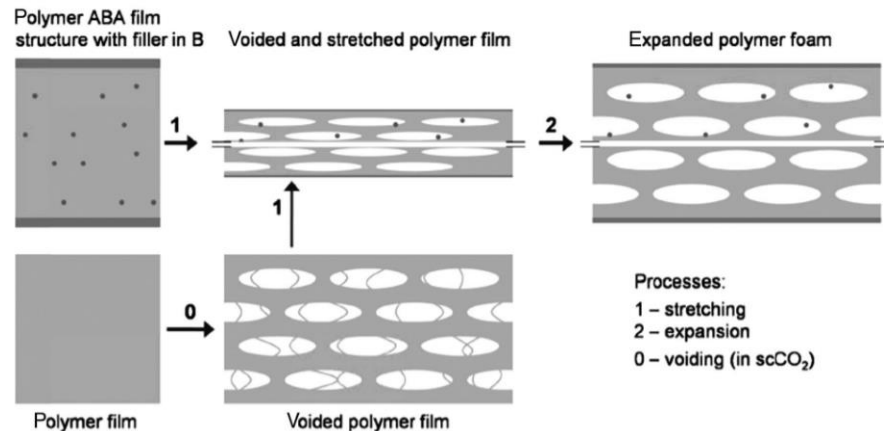


Figure 1.4 Production of a cellular structure by stretching a filler loaded polymer (process 1) or foaming by a physical blowing agent (supercritical carbon dioxide, CO₂) [Wegener 2010].

1.3.2. Foaming steps

The foaming process consists mainly of four main stages: saturation (blowing agent addition), nucleation (bubble formation), expansion (bubble growth) and stabilization (final morphology). The principles of each step are detailed next.

1.3.2.1. Saturation

This step involves the dissolution of a fluid (often supercritical) at high pressure. Again, the gas could be directly injected or generated via a chemical agent, and then dissolved in the polymer matrix. The objective is to obtain a homogeneous and uniform polymer–gas mixture, which is critical for high quality (homogeneous) foam production. For instance, the system pressure during extrusion or molding must be higher than the solubility pressure (also known as the saturation pressure) corresponding to the amount of injected blowing agent. Otherwise,

undissolved gas pockets (large voids) can form and this is detrimental to the foaming process and the cellular structure homogeneity. Therefore, it is important to determine the solubility data for various blowing agents in different polymers to determine the amount of gas to inject (PBA) or powder to add (CBA) depending on the targeted density reduction (amount of void to generate). This information is important for the production of homogeneous and stable cellular structures [Wegener (2010)].

It should be noted that the use of supercritical fluids as PBA is known to result in the creation of a large number of small cells which can grow to produce microcellular foams due to high mass transfer rates into polymers [Mohebbi et al. (2018)]. This state is reached when the fluid pressure and temperature are above the critical point (see **Figure 1.5**). Under these conditions, the fluid can behave simultaneously like a gas (easier diffusion) and a liquid (easier dissolution). The most commonly used supercritical fluids are nitrogen (N_2) and carbon dioxide (CO_2). In comparison with CO_2 , N_2 has the advantage of being above its supercritical temperature at room temperature. Thus, increasing the pressure above its supercritical pressure (3.4 MPa) is the only condition needed to create N_2 supercritical conditions [Mohebbi et al. (2015)].

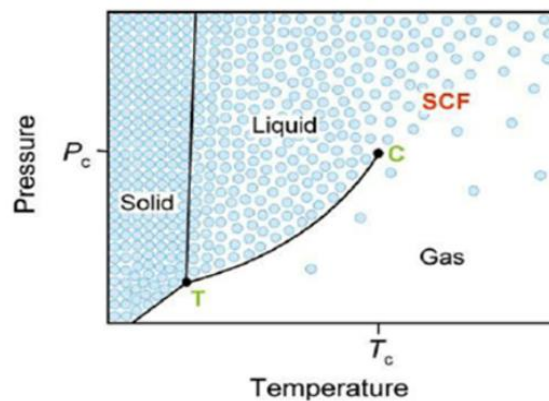


Figure 1.5 Phase diagram of a pure component showing the supercritical fluid (SCF) region [Hossieny 2010].

CBA can be classified in two categories: exothermic and endothermic. The majority of exothermic CBA generates N_2 upon decomposition (such as azodicarbonamide), while the

primary gas generated from endothermic CBA (such as sodium bicarbonate and citric acid) is CO₂ [Kumar et al. (1990)].

1.3.2.2. Nucleation

Nucleation is the transformation of a large number of gas molecules into small cells (micron-size). In fact, the already saturated system becomes supersaturated when the gas solubility is reduced through a thermodynamic instability. This instability can be achieved by either a temperature increase [Kumar et al. (1992); Schirmer et al. (2003); Park et al. (1997); Schirmer et al. (2003)] or a pressure drop [Park et al. (1997); Park et al. (1996)]. Consequently, the polymer-gas solution tends to form small bubbles (nuclei) so that a low-energy stable state can be restored. There are two nucleation types according to the classical theory, which is widely accepted to explain the nucleation process: homogeneous and heterogeneous nucleation (see **Figure 1.6**) [Chen et al. (2013); Colton et al. (1986); Colton et al. (1987a); Colton et al. (1987b)].

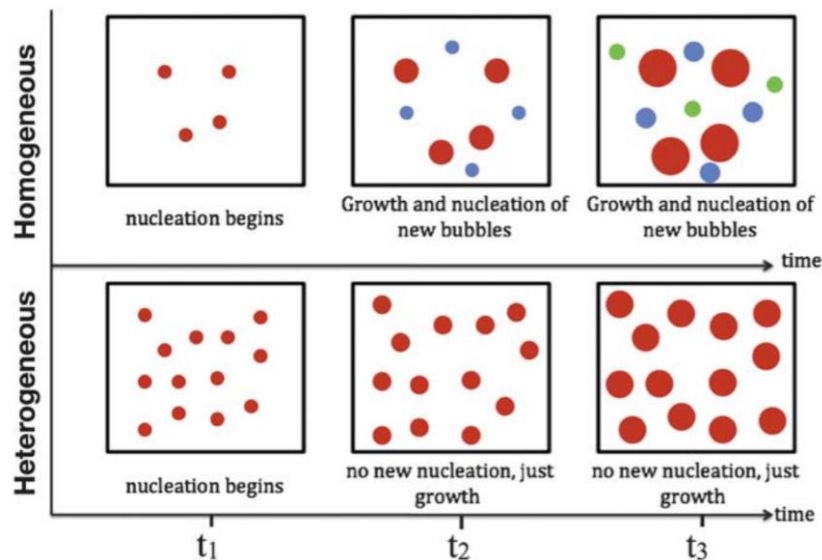


Figure 1.6 Schematic representation of homogeneous and heterogeneous nucleation [Chen et al. (2013)].

Homogenous nucleation is a phase separation process in which bubble nucleation randomly occurs throughout the neat polymer-gas solution. In fact, the dissolved gas (blowing agent)

forms a second phase (bubbles) in the primary phase (polymer matrix). On the other hand, heterogeneous nucleation requires preferred bubble nucleation sites such as impurities in the polymer matrix or sites provided by additives like nucleating agents (see **Table 1.1** for typical nucleating agents). Generally, heterogeneous nucleation requires less energy (activation energy barrier) than homogeneous nucleation.

1.3.2.3. Expansion (cell growth) and stabilization

Resulting from gas diffusion (from the matrix to the cells), the bubbles continue to grow after nucleation. This is due to the decreased gas solubility in the polymer associated to decreasing pressure, as well as the cells tendency to grow to minimize the pressure difference, as the pressure inside the cells is higher than the surrounding matrix due to surface tension effects [*Zhang (2010); Bae (2005); Liu (1998)*]. Several system parameters affect the cell growth mechanism such as gas concentration, viscosity, diffusion coefficient, and the number of nucleated bubbles. Cell expansion is mainly limited by the amount of gas available or the cooling level as the matrix becomes too stiff to allow further cell growth. To prevent cellular structure degradation during cell growth, three critical issues should be taken into consideration: cell coarsening, cell coalescence, and cell collapse. Proper strategies should be implemented to prevent these phenomena, which are detrimental to the cell-population density (number of cell per unit volume) and may degrade foam mechanical properties [*Zhang (2010); Bae (2005); Liu (1998)*].

1.3.2.4. Optimizing the temperature profile

To optimize the quality (homogeneity) of cellular films, the processing conditions must be carefully controlled. The temperature profile is one of the most important parameters influencing the foaming step. Generally, the temperature should be kept relatively low in the feeding zone to avoid premature decomposition of the blowing agent, which would cause gas losses. Then, the temperature must be increased in the melting zone to ensure complete CBA decomposition and achieve homogeneous dissolution/dispersion of the generated gases before the pumping zone. The most sensitive temperature is at the die: a temperature too high

leads to low melt strength of the matrix producing excessive foaming as well as bubble wall rupture, cell collapse, surface defects and bubble instability; but if the temperature is too low, limited bubble nucleation and growth occurs. So the temperature profile should be high enough in the intermediate section of the extruder (melting zone) to fully melt the polymer and fairly low near the die to increase the melt strength and avoid processing instability. More details about temperature profile and other parameters influencing foaming step can be found elsewhere [*Hamdi et al. (2018b)*].

1.3.3. Polymer ferroelectret films processing

Polymer ferroelectret cellular films are generally produced using standard polymer processes such as extrusion and injection. Since the cellular structure is very important for piezoelectric properties optimization, these methods must allow a good foam morphology control. Here, some of the recent foaming processes based on extrusion (which is the most used process in the plastic industries) are presented to obtain a suitable structure for electrical charging (**Figure 1.7**).

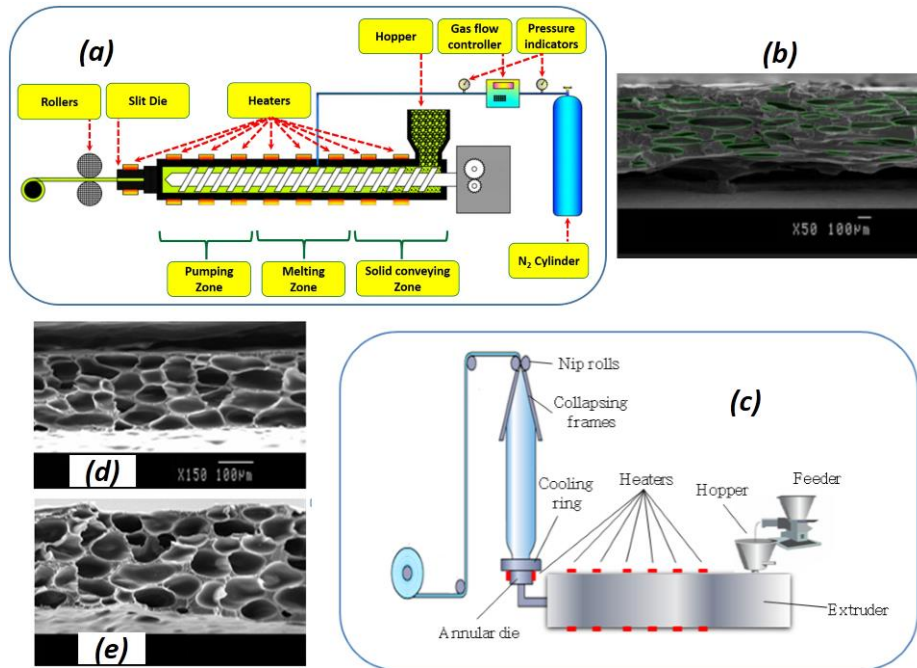


Figure 1.7 (a) Extrusion-calendaring foaming process and (b) its corresponding uniaxial stretched foamed film in the longitudinal direction (circular cells in the transversal direction), (c) extrusion-blowing foaming process and its corresponding biaxial stretched foamed film in the (d) longitudinal and (e) transversal stretched directions (same scale) [Mohebbi *et al.* (2017a); Hamdi *et al.* (2018b)].

1.3.3.1. Extrusion-calendaring foaming process (uniaxial stretching)

A continuous extrusion-calendaring foaming method was developed in 2017. Low cost thin cellular polypropylene (PP) foams were produced using nitrogen as a physical blowing agent and calcium carbonate (CaCO_3) as a nucleating agent [Mohebbi *et al.* (2017a)]. The developed films had a uniform eye-like structure with a cell aspect ratio of 5.4 in the longitudinal direction, which is needed for good cellular piezoelectric films (see **Figure 1.7a,b**) [Mohebbi *et al.* (2017a)]. This led to a good quasi-static piezoelectric coefficient (d_{33}) of around 800 pC/N.

1.3.3.2. Blown-film extrusion (biaxial stretching)

A method to produce polyethylene microcellular films using extrusion-blowing was developed in 2018 (**Figure 1.7c**). The 3D cellular structure was controlled for thin (less than 300 μm) polyethylene (PE) films using a chemical blowing agent (azodicarbonamide) and nucleating agent (talc) [*Hamdi et al. (2018b)*]. The main advantage of this process is that biaxial stretching is applied on the foaming samples providing a complete control of cell deformation in all directions. The different processing parameters, such as the take-up ratio (TUR), blown-up ratio (BUR), flow rate, screw speed, etc., were optimized resulting in a fine and uniform cell morphology (relative foam density of 0.62 and high cell density of 5.9×10^6 cells/ cm^3) of the foamed film with a well-developed ellipsoidal cellular structure (cell aspect ratio of around 4 in both longitudinal and transversal directions) which is required for high piezoelectric sensitivity (**Figure 1.7d,e**), since a high amount of surface area is generated per unit volume.

1.3.3.3. Other methods

Several other methods have also been proposed to produce ferroelectrets such as [*Liu (1998)*]:

- The template-based fabrication: This method consists of using a thermo-formed material to form a cellular structure in a sandwiched polymer films. Generally, the obtained cells are uniform and relatively large.
- Microfabrication: In this method, a structure with well-defined uniform micron-sized voids is formed by means of a microelectromechanical system (MEMS) fabrication process.
- Screen printing: It is a printing technique allowing to produce a uniform cell structure but with large cell sizes.

1.3.4. Electrical charging

Electrical charging is a crucial step in ferroelectrets manufacturing. It involves applying a

strong electric field leading to the accumulation of internal charges on the cell surfaces as shown in **Figure 1.8**. These charges of opposite polarity on opposite sides create the macroscopic dipoles. Mechanical stimulations causing a variation in the thickness direction of the electrically charged voids result in an electrical signal between the electrodes connected to the films' surface. Thus, ferroelectrets are obtained with ferroelectric properties [Gerhard-Multhaupt (2002); Bauer et al. (2004); Ramadan et al. (2014)].

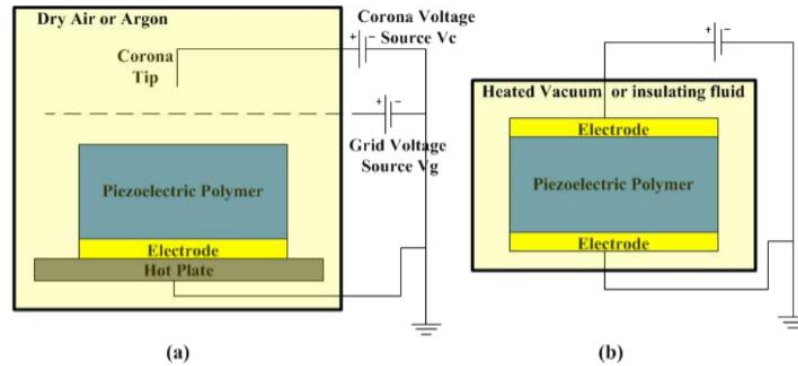


Figure 1.8 Corona discharge (left) and direct contact charging (right) set-ups to perform film charging [Ramadan et al. (2014)].

Several charging methods can be used to generate the dipoles in the polymer foam. The most common methods are direct contact charging and corona discharge. The direct contact charging method consists of directly applying a high electric voltage on the electrodes placed on either side of the film. The applied electric fields for different piezoelectric polymers are in the 5-100 MV/m range [Ramadan et al. (2014)]. The electrodes can be deposited under vacuum or glued by an adhesive tape. This method is simple but only allows charging the film section located between both electrodes and is relatively expensive compared to corona discharge. In fact, the latter is cheaper and more feasible on an industrial scale as the method consists in imposing a potential difference between a needle and a conductive plate, thus creating an electric field over the entire plate width. As shown in Figure 8, this assembly consists of three main parts: the tip of the positively charged electrode, the negatively charged metal plate, and the metal grid. The strong ionization resulting from the corona effect bombards with electrons the film surface, thus creating positive and negative charges on both sides of the film surface. A more intense field allows a better polarization of the ionizing gas

molecules, as described by Paschen's law (**Equation 1.2**). To get good contact with the ground, it is preferable that the sample bottom be coated with an electrode [*Schirmer et al. (2003)*; *Ramadan et al. (2014)*].

In general, the idea is to impose a potential difference on the cells allowing ionization of the gases they contain. The minimum voltage for a cell to be charged is related to the permittivity of the layers on the electric field created through the sample during electrical charging as [*Qiu et al. (2011)*]:

$$V_{\min} = E_{\min} \left(\frac{\epsilon_{\text{gaz}}}{\epsilon_p} d_1 + d_2 \right) \quad (1.2)$$

where V_{\min} and E_{\min} are respectively the minimum voltage to activate the micro-discharges and the electrical field obtained from the Paschen's law.

It is important to mention that there is no charge created below the minimum voltage (V_{\min}), also called the threshold voltage (V_{thr}) or simply the Paschen minimum, which is associated with the Paschen micro-discharges (dielectric barrier discharges or DBD). In addition, increasing the charging voltage beyond V_{\min} provides a field greater than the fields of the dipoles created, generating new micro-discharges and thus maximizing ion production. This directly results in d_{33} improvement [*Qiu et al. (2007a)*]. **Figure 1.9** is a model describing the charging process. The point A indicates the start of internal breakdown upon reaching the Paschen minimum. During DBD, charges are separated and trapped on the top and bottom cells surfaces. An electric field opposite to the externally imposed field is induced by the trapped charges. Point B is reached by further increasing the applied voltage. Thus, a second series of breakdown events may occur, increasing the charges density captured in the voids. The applied voltage is then reduced down to point C where a phenomenon of reverse discharge under the influence of trapped charges occurs tending to overcompensate the applied field [*Qiu et al. (2007a)*].

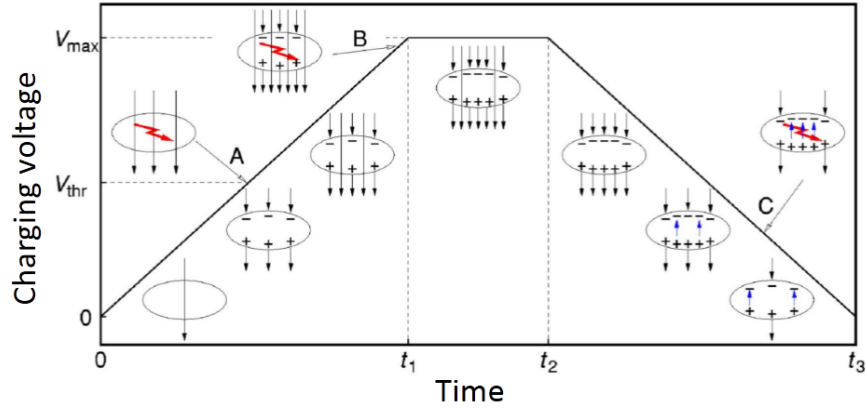


Figure 1.9 Model description of the charging process [Qiu et al. (2007a)].

The hysteresis curves of the surface charge density (ξ) allow the understanding of the discharge magnitude when the imposed voltage is removed ($V_c = 0$). **Figure 1.10** illustrates that the effective charge density after the electric field removal is about 0.5 mC/m^2 for a PQ50 film from Nan Ya Plastic Corporation [Qiu et al. (2008)].

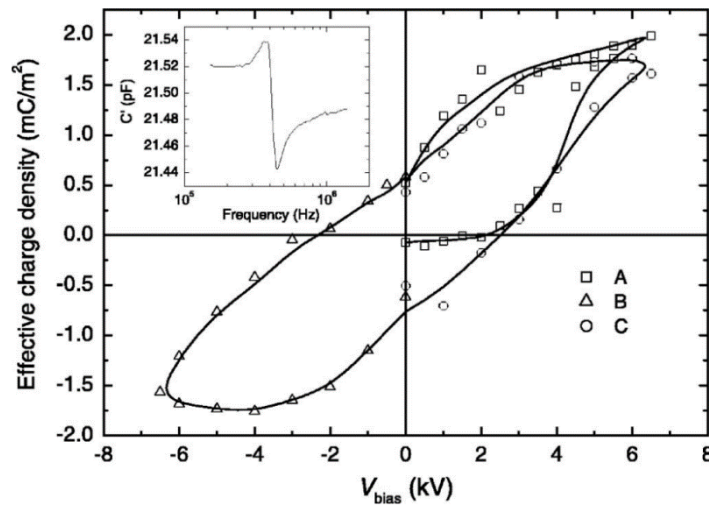


Figure 1.10 Effective charge density as a function of the bias voltage (V_{bias}) for a commercial cellular PP films (tradename PQ50) with a charging voltage directly applied on both metallized sides by means of a high voltage amplifier [Qiu et al. (2007a)].

The electrical field intensity inside the cells is of the order of 80-100 MV/m and the loading time of about 60 s for films between 37 and 100 μm placed 3-4 cm from the corona tip [Qiu

et al. (2008); Montanari et al. (2004); Zhang et al. (2005)]. The mechanism of charge separation is explained by Paschen’s law relating the arc formation to the product of gas pressure (p) and the distance (d) between the electrodes.

1.3.5. Paschen’s law

The electric charging is based on Paschen’s law, which represents the phenomenon of electrical discharges in an “initially” non-conductive gas between two electrodes. For cellular films, the internal cell walls play the role of the electrodes. Since gases are electrical insulators, electrical breakdowns can only occur under specific conditions for which local and temporary gas ionization takes place. At this point, the gas state is called a plasma and this state is electrically conductive. The charges then pass through the plasma under the influence of the electric field and each electron will collide with the gas atoms thus producing new electrons (avalanche phenomenon). When the field is removed, the positive and negative charges remain separated sticking to the internal cell walls. Paschen’s law (**Equation 1.3**) enables to calculate the minimum potential difference required (V_{min}) between the electrodes as a function of their distance to produce an electric discharge for a given gas:

$$V_{min} = \frac{B(pd)}{C + \ln(pd)} \quad (1.3)$$

$$C = \ln\left(\frac{A}{\ln(1+1/\gamma)}\right) \quad (1.4)$$

The term ($p d$) represents the pressure-distance product, while the parameters A and B are intrinsic to the gas used, and γ is the second ionization constant. So the product ($p d$) is proportional to the number of atoms or molecules located between the electrodes. This explains the existence of a minimum on the curves of **Figure 1.10**:

- When ($p d$) > ($p d$)_{opt}: The electrons undergo a large number of collisions passing from the anode to the cathode, slowing down their speed, hence a higher voltage is required.
- When ($p d$) < ($p d$)_{opt}: The avalanche phenomenon becomes less probable since the electrons are covering more space to meet atoms and ionize them, hence a lower voltage must be applied [*Koliatene (2009)*].

Therefore, the charging process is strongly influenced by the dimensions (height, b) of the cavities, the gas composition inside the cavities, and the pressure.

1.4. OPTIMIZATION OF THE PIEZOELECTRIC PROPERTIES OF CHARGED CELLULAR POLYMERS

1.4.1. Morphological and mechanical effects

The piezoelectric response of ferroelectrets originates from optimized cell morphology, elastic-foam properties and optimized charge trapping within the foam structure. The morphological properties (cells size, shape and density) of cellular polymers are related to the processing conditions and directly affect their mechanical and piezoelectric properties. On this basis, the optimization of ferroelectrets must pass through a careful morphological properties control and a good understanding of the relationship between the mechanical and piezoelectric properties.

To obtain a good piezoelectric activity, the cellular structure must be developed through the whole area of the samples. It is also advantageous to create a high cell density allowing to maximize the available charging area. However, the film mechanical integrity should not be lost by reducing too much the matrix density. So cell height (b) should be carefully considered. As detailed in Section 3.4, charging is not possible if b is too small, but the piezoelectric coefficient d_{33} is inversely proportional to the elastic modulus (**Equation 1.1**). So the elastic modulus control is of great importance. The literature reports that foam density is the main parameter affecting the elastic modulus. **Figure 1.11** experimentally confirmed the inverse relationship between the elastic stiffness c_{33} (elastic modulus) and the piezoelectric coefficient d_{33} , as well as the important effect of the relative density for anisotropic PP cellular films. For these samples, the lowest elastic stiffness is obtained for films having a relative density of about 0.45 [Wegener *et al.* (2006); Tuncer *et al.* (2006)]. In fact, a high relative density corresponds to a large elastic modulus (more material to resist the pressure) and less voids to charge, thus a smaller piezoelectric coefficient is consequently obtained. Similar observations about the effect of anisotropic foams density on the mechanical properties were reported via numerical simulations [Tuncer *et al.* (2006)].

However, the relative density is not the only parameter affecting the mechanical properties of a foam, which can also be represented by cell size, cell shape (or aspect ratio) and density. Several studies have investigated this effect [Tuncer et al. (2006)], while different models were developed to link the morphology to the mechanical properties. The most widespread model is the power-law model [Gibson et al. (1997)]:

$$\frac{E^*}{E_s} = C \left(\frac{\rho}{\rho_s} \right)^n \quad (1.5)$$

where E^* and E_s are respectively the Young's modulus of the foam and the solid (unfoamed matrix), while C and n are model parameters related to the micro-structure. Gibson and Ashby [Koliatene (2009)] presented experimental results on various cellular materials and their observations suggested that $n = 2$ is a good approximation. Since the dependence of effective properties on the micro-structure are not well understood in mixtures, the exact values for C and n are not known, which is a limitation to optimize and predict the composite/foam properties. However, several studies have reported that an eye-shaped cell structure with an aspect ratio $a/b > 4$ is optimum for good piezoelectric activity [Mohebbi et al. (2018); Qiu et al. (2011); Lindner et al. (2004); Xu et al. (2013)].

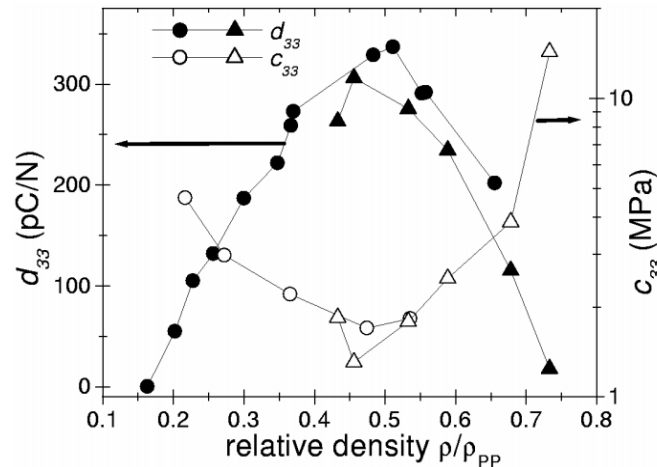


Figure 1.11 Relative density effect on the piezoelectric coefficient and elastic stiffness [Wegener (2006)].

Computer simulations have also been performed to predict the relations between the mechanical and morphological properties of cellular materials [Torquato (2001), Tuncer (2005)]. Tuncer simulated the elastic properties of ferroelectric cell structures using two different geometrical models: truss-like (straight boundary structure) and eye-shaped (curved boundary structure) [66]. The following quadratic power-law expression (modified **Equation 1.5**) was used:

$$\frac{E^*}{E_s} = C q^{aq^2+bq+c} \quad (1.6)$$

where q is the relative density and C is a model parameter. The results showed that the eye-shaped structure has lower Young's modulus than the truss-like at low solid concentrations ($q < 0.15$). However, negligible differences were obtained at intermediate ($0.15 < q < 0.85$) and high ($q > 0.85$) solid contents. Simulation results for three different unit-cell ratios ($a/b = 2, 4, \text{ and } 8$) were also presented for both structures. It was found that increasing the a/b ratio led to lower elastic moduli for the range of solid concentrations and type of structure studied [Tuncer (2005)].

Although numerical simulations are very interesting to allow a better trend understanding for the foam structural effects, they generally use perfect structures not achievable at laboratory and industrial scales. Experimental work is still needed for validation and more precise models must be further developed.

1.4.2. Different methods used to enhance piezoelectricity of ferroelectrets

Several methods and treatments are available to optimize the ferroelectrets' piezoelectric activity by controlling the mechanical and morphological properties, and also by improving the electrical charge conditions and electrets properties such as charge trapping capacity, charging time and thermal stability. These treatments can be performed before or after the cellular film preparation and **Table 1.1** reports on the most important works on ferroelectrets properties.

1.4.3. Enhanced thermal and temporal stability of the piezoelectric coefficient

In addition to its sensitivity, the stability of the piezoelectric coefficient of electromechanical transducer materials is a critical factor. Obviously, piezoelectric stability of ferroelectrets is highly dependent on the charge trapping properties of the polymer; i.e., on how effectively charges deposited on the inner surfaces of the voids can be retained over a wide range of times and temperatures [Qui (2016)]. The interfaces between amorphous and crystalline zones of the polymer are believed to limit electric charges drift [Qui (2016)]. Therefore, a film with more interface area should better retain its charges and piezoelectric effect. In the same context, it was shown that a higher degree of crystallinity gives a better charge stability towards temperature and time [Thyssen et al. (2015)].

Surface modification can also be a solution to improve the charge stability of ferroelectrets [Qui (2016); Thyssen et al. (2015); Fang (2010); Mellinger et al. (2006)]. Different treatments such as corona charging at elevated temperatures, quenching or pre-aging before charging, controlled aging or annealing after charging, have a significant effect. Some chemical treatments have also proved their efficiency. For example, the modifications of PE ferroelectrets with phosphorus trichloride (PCl_3) and titanium tetrachloride (TiCl_4) vapor, as well as orthophosphoric acid (H_3PO_4) all resulted in significantly enhanced charge stability. For PP ferroelectrets, treatment with fluorine gas was very efficient in terms of thermal stability. However, the effect of these different treatments on the degree of crystallinity and the piezoelectric stability is not yet well quantified and more efforts should be done to model the relation between these parameters [Qui (2016); Thyssen et al. (2015); Fang (2010); Mellinger et al. (2006)].

1.5. POLYMERS USED AS FERROELECTRETS AND THEIR PROPERTIES

The ferroelectret potential of different polymers was investigated using a variety of preparation methods. Cellular PP is the most investigated polymer in this context. It has become the workhorse of ferroelectret technology mainly due its high piezoelectric coefficient. Depending on the processing method and the characteristics of the applied electric field, a wide range of piezoelectric coefficient (130-2100 pC/N) has been reported [Mohebbi et al. (2018)]. Cellular PE has recently been investigated as a ferroelectret material

[Nakayama et al. (2009); Tajitsu (2011)]. Cellular PE films were fabricated with a thickness of 30 μm , a porosity ranging from 58 to 85% and pores diameter of about 0.3 μm distributed throughout the sample. The films were charged via corona poling with a distance (d) between the discharge tip and the cellular PE films of 8 mm and a needle voltage of 7 kV. A piezoelectric coefficient between 200 and 400 pC/N was recorded [Tajitsu (2011)]. Commercial closed cell PE foams of 480 μm were used in another study [Branaa et al. (2011)]. The films underwent “thermal stretching” consisting of simultaneous sample heating to 100 $^{\circ}\text{C}$ and mechanical stretching, thus decreasing film thickness and increasing cell deformation. Finally, a corona discharge voltage of 12 kV was applied for 5 min leading to a piezoelectric coefficient up to 170 pC/N [Branaa et al. (2011)].

Fluorocarbon polymers, such as several kinds of Teflon (polytetrafluoroethylene (PTFE), fluoroethylenepropylene (FEP), tetrafluoroethylene-per-fluoromethoxyethylene copolymer (PFA), and amorphous Teflon (AF)) have shown good electrets (charge storage) properties allowing them to be used as ferroelectrets [Qui 2016]. Porous AF films were prepared by casting a solution of Teflon (Dupont) resin in Fluorinert (FC-77). Cellular films were obtained, and 3 to 8 layers were cast on top of each other. The final thicknesses achieved were between 9 and 60 μm and typical densities were around 500 kg/m^3 [Branaa et al. (2011)]. The sandwich films were charged in a point-to-plane corona discharge at -15 kV for 15-30 s at room temperature. The surface potential applied were between 21.0 and 21.5 kV. As a result, a strong piezoelectric effect was generated with a coefficient up to 600 pC/N and a stable piezoelectric sensitivity up to 120 $^{\circ}\text{C}$ [Branaa et al. (2011)]. Tubular-channel FEP-film ferroelectret has also been produced by laminating two FEP films around a PTFE template at 300 $^{\circ}\text{C}$. Then, the PTFE template was removed from the laminated stacks. A piezoelectric coefficient up to 160 pC/N was recorded with a thermally stable charge up to 130 $^{\circ}\text{C}$ [Altafim et al. (2009)].

Polyester ferroelectrets have also been investigated such as polyethylene terephthalate (PET) foams [Wirges et al. (2007), Wegener et al. (2005)] and polyethylene naphthalate (PEN) [Fang et al. (2007); Fang et al. (2008); Fang et al. (2010)] produced through physical foaming with supercritical CO_2 . The optimized PET and PEN ferroelectrets exhibited high

piezoelectric coefficient of 500 and 140 pC/N respectively, with a stable sensitivity up to 80 °C, slightly higher than cellular polyolefin ferroelectrets. For example, PEN ferroelectrets are still piezoelectrically active even after storage at 100 °C for 5 days. Finally, cyclo-olefin polymer (COP) and copolymer (COC) ferroelectrets with a maximum d_{33} of about 1000 pC/N and a continuous service temperature (CST) of 100 °C were also developed [Li et al. (2013)].

The piezoelectric properties of typical ferroelectrets are summarized in **Table 1.2**.

Table 1.2 Comparison of the piezoelectric properties of typical ferroelectrets.

Ferroelectrets	d_{33} range (pC/N)	CST (°C)	References
Cellular PP	140–2100	50	[Mohebbi et al. (2018); Qui (2016)]
Cellular PE	200–400	-	[Qui (2016); Tajitsu (2011); Branaa et al. (2011)]
Cellular AF	600	120	[Mellinger et al. (2011)]
Cellular FEP	50–160	-	[Altafim et al. (2009)]
Cellular PET	23–500	-	[Wirges et al. (2007); Wegener et al. (2005)]
Cellular PEN	60–140	80	[Fang et al. (2007); Fang et al. (2008); Fang et al. (2010)]
COP and COP	15–1000	100	[Li et al. (2013)]

1.6. APPLICATIONS

Several ferroelectret applications have been proposed, demonstrated and commercially realized. An overview of the recent applications of cellular polymer films is presented to highlight their potential for innovative new products.

1.6.1. Impact sensors

Impact sensors are one of the main ferroelectrets common use. In fact, stresses created by the foam deformation during impact depend on speed and force of the striking object which are controlling impact energy. When the shock exceeds a predetermined threshold, an alert can be sent to a connected electronic device (computer, tablet or phone), thus leading to more

informed decisions. For example, head trauma is common in sport, such as American football. Unfortunately, the signs are not always visible and several players say they feel good, even if they are not. Produced by XOnano smart foam company [<http://xonano.com>] piezoelectric polymer foams inside the helmet emits an electric charge at the moment of impact. This charge is picked up by a microprocessor placed on the helmet top. The impact is evaluated and the results are transmitted to the trainer or team doctor. A coach will know in just a few seconds how hard his player has been hit and have a better idea if the player can continue playing or must leave immediately and be examined for concussion.

Also, with this technology, a car can give a virtual image of an accident, helping first responders to know the severity of a collision even before they arrive on the scene. Insurance companies can also use this technique to assess the details of a car accident. Due to the subjectivity of most evaluation methods, insurance companies pay billions of dollars every year on fake or inflated insurance claims. Once an automobile contains this piezoelectric cellular polymer film, claims evaluation can become very accurate [<http://xonano.com>].

1.6.2. Human body

Several ferroelectret sensors are developed to detect human body activities. For example, the registration of body motion is an interesting technique allowing the control of human–computer interfaces or real devices. Information related to muscle activity is important for the study of body motion (biomechanics). Such information must be registered for different purposes such as diagnostics, rehabilitation and entertainment [*Dobkin et al. (2011); Patel et al. (2012)*]. For example, muscle activities are recorded in rehabilitation training for patients with motor-function impairments to evaluate treatment performance [*Li et al. (2015)*]. Likewise, in biomedical devices such as prosthetic arms, the body-motion information is detected, then the motor commands are extracted and used for device control [*Jarrasse et al. (2017)*]. Force myography (FMG) is an important approach to detect body motion. In this case, the mechanical force signal associated with muscle activity is exploited. In fact, muscle contractions are accompanied by a change of muscle volume generating pressure in radial directions. The purpose of FMG is to record a force-distribution map [*Fang et al. (2018)*]. Ferroelectrets have recently been developed for FMG due to their large piezoelectric

coefficients, small elastic moduli, high flexibility, good stretchability and adaptability to various shapes. In fact, porous PP films (50 μm in thickness) with gas-filled cavities of the central section of around 100 μm in the lateral directions and 5 μm in thickness have been used as sensors recording the radially directed force-distribution signals generated by muscle contractions. By extracting the signal characteristics, the FMG models could be recognized with algorithms. Upper-limb motions of hand closing/opening and wrist pronation/supination/flexion/extension were registered with good accuracies [<https://emfit.com/>].

The respiration of humans can also be recorded with cellular polymers due to their good sensitivity, even if the transducers are not directly fixed to the skin [*Li et al. (2015)*]. Developed by Emfit (Finland), cellular PP films have been placed directly on beds for long-term respiration monitoring. The sensor signals measured during human motion are proportional to the respiration signal. The recorded information can give information on sleep quality [<https://emfit.com/>].

1.6.3. Transport applications

Ferroelectret sensors have also been developed to optimize the comfort of different transport means. For example, the noise in the cabins of cars, trains and aircrafts is a great source of nuisance for travelers, and a significant amount of research and development is devoted to active noise control. The noise-generating vibration may be detected by means of ferroelectret polymer layers to determine the vibration frequency and amplitude. After recording, a sound wave with optimum frequency and amplitude (anti-sound) is generated and focused to locally (at the human ears) cancel the noise [*Wegener et al. (2004)*].

Orthopedic diagnostics is also an interesting issue in automotive applications. Ferroelectrets were developed to monitor seats and backrests pressure distribution to optimize/design office chairs or seats in cars/trains/aircrafts for improved back comfort [*Wegener et al. (2004)*].

1.6.4. Acoustic applications

Including audio, ultrasonic and infrasonic frequency ranges, acoustic transducers are

vibration-based electromechanical transducers operating in the acoustic spectrum range (20-20,000 Hz). These transducers include microphones, loudspeakers, and hydrophones [<https://emfit.com/>; Kim (2013); Saarimaki et al. (2006)]. Microphone ferroelectret sensors are already on the market and produced by Emfit and B-Band (Finland) [Li et al. (2015); Wegener et al. (2004)].

Another type of electromechanical sensors is acoustic emission sensors (AES). These sensors passively detect the acoustic signals due to a system mechanical or shape change. Their main difference with ultrasonic transducers is that they detect the acoustic signal passively, while an ultrasonic transducer transmits a signal and receives the reflected signal to detect any change. AES are generally exploited where continuous monitoring is needed, such as material fracture or device failure, while ultrasonic transducers are used in automated machinery and medical imaging [Shi (2017)]. More examples of recent ferroelectric acoustic applications can be found in the literature [Doring et al. (2010); Lei (2017)].

1.6.5. Tactile sensing applications

A tactile sensor is a device measuring a physical phenomenon such as shape, force, temperature or softness. This type of sensor has potential uses in medicine as well as in robotics [<http://b-band.com/>]. Ferroelectrets are starting to be suitable for such applications, mainly in measuring force or pressure. For example, PP ferroelectret has been used in a large area touchpad sensor. To identify the touch location, this sensor analyzes four different voltage signals at the corners of a cellular PP. A flexible and self-powered keyboard converts the mechanical stimuli applied on the keyboard to an electrical signal used to show the pressed letter on a computer monitor also made from ferroelectret transducers [Kogler et al. (2011)].

1.6.6. Other applications

Several other ferroelectret applications have been studied and developed for different general applications. The most important ones are *accelerometers* [Hillenbrand et al. (2010); Hillenbrand et al. (2011)], *games* [<https://2020armor.com/>] and *robotics* [Zhuo et al.

(2015)]. Moreover, several applications are expected in the near future depending on the sensitivity level and the general performance/cost ratio of the materials developed.

More information on the subject can be obtained in reviews about electroactive polymers [Ning et al. (2018)], as well as about predicting the properties of ferroelectrets by numerical simulations [Zhang et al. (2005); Wan et al. (2012)].

1.7. CONCLUSIONS AND FUTURE DIRECTIONS IN THE FIELD

Despite their non-polar nature, internally charged cellular polymers provide a novel class of materials called ferroelectrets with close analogies to ferroelectrics. This allows the development of a wide range of applications, but also induces several challenges for materials and processing optimization, such as increasing the piezoelectric coefficient (d_{33}) as well as improving the long term and thermal stability of the piezoelectric activity.

Ferroelectrets are clearly distinguished from traditional piezoelectric materials, such as PZT, due to their softness, great ability to be developed and optimized, and their outstanding properties such as low cost, light weight, and good piezoelectric properties. Development of these materials needs a particular attention on polymer chemistry (materials synthesis), physics (materials characterization), mechanics (elastic properties), polymer processing and chemical engineering (development of industrial foaming processes), materials science (ferroelectric and ferroelectret materials), as well as the ability to develop engineering applications such as sensors, transducers, acoustics, and others. So, a great potential is expected for future applications. In fact, this paper may only be “surface” evaluation of their enormous potential. There is no doubt that other attractive topics or interesting applications are waiting to be discovered. It is expected that these materials will be integral components of numerous devices improving the quality of life by delivering high-quality audio and practically noise-free environments, vital medical information, enhanced security, etc.

It is also expected that improvement in material preparation techniques will allow obtaining more homogenous cellular structure and also the development of models quantifying the relationships between the mechanical, morphological and piezoelectric properties will be a key to optimize ferroelectrets capacities.

ACKNOWLEDGMENTS

Financial support from the Natural Sciences and Engineering Research Council of Canada (NSERC) and Fonds Québécois de la Recherche sur la Nature et les Technologies (FRQNT) was received for this work.

CHAPITRE 2. OPTIMIZATION OF THE CELLULAR MORPHOLOGY OF BIAXIALLY STRETCHED THIN POLYETHYLENE FOAMS PRODUCED BY EXTRUSION FILM BLOWING

RÉSUMÉ

Ce travail constitue une contribution pour la mise en œuvre de films polymères cellulaires utilisant le procédé d'extrusion-gonflage afin d'imposer un étirement biaxial à la structure cellulaire. Les matériaux choisis sont le polyéthylène linéaire de basse densité (LLDPE) et le polyéthylène de basse densité (LDPE) comme matrice, l'azodicarbonamide comme agent gonflant chimique et le talc comme agent de nucléation. Les paramètres de mise en œuvre, à savoir le profil de température, la vitesse de rotation des vis, le débit d'alimentation, le taux d'étirement (TUR), le taux de gonflement (BUR), ainsi que la composition de la matrice ont tous été optimisés pour produire une structure cellulaire homogène ayant des morphologies bien définies. Les films optimisés ont une épaisseur inférieure à 300 μm , une densité relative d'environ 0,6, une densité cellulaire supérieure à 2×10^6 cellules/ cm^3 et des cellules étirées de manière biaxiale avec des ratios de forme (AR) supérieurs à 4,0 longitudinalement et à 3,8 transversalement.

Mots clés: polyéthylène, mousse, étirement biaxial, forme cellulaire.

ABSTRACT

This work presents the production of cellular polymer films using extrusion blowing to impose biaxial stretching on the cellular structure while processing. The materials selected are linear low density polyethylene (LLDPE) and low density polyethylene (LDPE) as the matrix, azodicarbonamide as the chemical blowing agent, and talc as the nucleating agent. The processing parameters, namely the temperature profile, screw speed, feed rate, take-up ratio (TUR), blow-up ratio (BUR), as well as the matrix composition were all optimized to produce a homogeneous cellular structure with defined morphologies. The optimized films had a thickness below 300 μm , a relative density around 0.6, a cell density above 2×10^6 cells/ cm^3 and biaxially stretched cells with aspect ratios (AR) above 4.0 longitudinally and 3.8 transversally.

Keywords: Polyethylene, foam, biaxial stretching, cell deformation.

Ouassim Hamdi, Frej Mighri, Denis Rodrigue (2018b) Optimization of the cellular morphology of biaxially stretched thin polyethylene foams produced by extrusion film blowing. *Cellular Polymers* 37:153-168.

2.1. INTRODUCTION

Since their appearance in the 1930s, cellular polymers have received high interest thanks to their special structure containing two phases: a continuous polymer phase and a gaseous phase in the form of bubbles dispersed in a matrix [*Coccorullo et al. (2008)*; *Mohebbi et al. (2015)*]. This structure enables to combine the advantages of polymers and gases leading to interesting properties such as low material consumption, low weight, excellent specific mechanical properties, high fatigue life, and low thermal/electrical/acoustic conductivities [*Klempner et al. (1991)*; *Colton et al. (1987a)*; *Okolieocha et al. (2015)*; *Collais et al. (1995)*]. These properties lead to several industrial applications in the automotive, sporting equipment, packaging, and insulation sectors [*Kumar (1993)*; *Nofar et al. (2012)*; *Lambert (1991)*; *Suh et al. (2000)*].

Recently, cellular polymers have attracted new industrial and academic interest due to their potential for piezoelectric applications. In fact, after charging by an appropriate method (corona discharge), cellular polymers can provide high electrical/mechanical energy conversion and can be used as sensors or actuators [*Bauer (2006)*]. The concept of charged polymers, currently named ferroelectrets, was developed by studying cellular polypropylene (PP) films [*Mohebbi et al. (2015)*; *Mohebbi et al. (2017a)*; *Mohebbi et al. (2018)*]. The cellular structure of these films (cell density, cell size, cell shape, and cell orientation) is important to optimize the piezoelectric properties. Studies have confirmed that an eye-shaped (ellipsoidal) cellular structure provides better piezoelectric coefficients [*Lindner et al. (2004)*, *Tuncer (2005)*]. Thus, it is mandatory to develop a processing method allowing precise and biaxial control of the cell morphology. Different methods are already used to produce ferroelectrets such as extrusion, compression molding, injection molding, and micro-foaming [*Kumar et al. (1990)*; *Baldwin et al. (1994)*]. However, these methods are either discontinuous, and therefore not efficient due to their low production rate, or only apply uniaxial deformation, resulting in an incomplete control of the 3D cellular morphology. It has also been reported that increasing the cells aspect ratio (AR), defined as the ratio between cell length and width in a specific direction, can improve the piezoelectric sensitivity. In general $AR > 4$ is a target value to optimize the piezoelectric coefficient (d_{33}) [*Lindner et al. (2004)*; *Tuncer (2005)*]. By applying biaxial stretching, it would be possible

to reach this AR value in both transversal and longitudinal directions resulting in a higher piezoelectric response. Combining two processes (extrusion film blowing and foaming) to produce thin films having a controlled 3D cellular structure is therefore of interest.

Blown film extrusion is one of the main manufacturing methods for plastic films. It is a continuous production of bi-oriented and thin thermoplastic films. Polyethylene, as well as polypropylene, polystyrene and polyamide are typical materials prepared in this way [*Cantor (2006); Butler (2005); Kolarik et al. (2011)*]. On the other hand, foaming usually consists in a gaseous phase (blowing agent) dissolved in a polymer melt to generate a cellular structure following a thermodynamic instability. Depending on the desired foam morphologies or the final part applications, several blowing agents were developed and classified into physical (PBA) and chemical (CBA) blowing agents. The former is generally a gas (or volatile liquid) directly injected into the polymer melt, while the latter represents the transformation of a solid into gas after some heat-induced chemical decomposition. In general, a CBA is either dry-blended with the polymer (powder or pellets) or pre-mixed/compounded at a temperature below the CBA decomposition temperature (*masterbatch*) [*Mohebbi et al. (2015); Lee et al. (2000); Nawaby et al. (2004)*].

As reported several time in the literature, most linear PE do not have sufficient melt strength and elasticity above their melting point to ensure large deformation during foaming (cell expansion) and film blowing (stretching) [*Zakaria et al. (2009); Mohebbi et al. (2015)*]. Therefore, it is of high importance to control several parameters, not only related to processing conditions, but also with respect to the materials' properties.

The main objective of this work is therefore to produce, in a single continuous step, good quality thin cellular polymer films with stable and well-controlled morphology via biaxial stretching. To achieve this goal, an extrusion film blowing set-up is used to produce the samples. Polyethylene (PE) was chosen as the matrix due to its relatively low modulus and high crystallinity level since both parameters are known to improve the piezoelectric properties [*Kumar et al. (1990); Baldwin et al. (1994)*].

2.2. EXPERIMENTAL

2.2.1. Materials

In this work, a blend of linear low density polyethylene (LLDPE 8555 from Exxon Mobil Chemical, Irving, TX, USA) and low density polyethylene (LDPE LF-0219-A from NOVA Chemicals, Calgary, AB, Canada) was used as the matrix. LLDPE was chosen due to its significant commercial importance related to its good balance between mechanical properties and processability [Kim 2011], while LDPE was selected because of its high melt strength. After some preliminary trials, a ratio of 80/20 LLDPE/LDPE was selected. The LLDPE received has a density of 0.936 g/cm³ and a melt flow index (MFI) of 6.8 g/10 min (2.16 kg and 190°C), while the LDPE have a density of 0.919 g/cm³ and an MFI of 2.3 g/10 min (2.16 kg and 190°C). Celogen 754-A (Lion Copolymer Company, USA) was selected as the chemical blowing agent. This CBA has a decomposition temperature range of 165-180°C and produces 200 cm³/g of gas. Talc (Jetfine 3CC) was supplied by Imerys Talc (Houston, TX, USA) with an average particle size of 1.0 µm and used as a nucleating agent (foaming and crystallinity).

2.2.2. Film blowing

The set-up is composed of a co-rotating twin-screw extruder (Thermo Haake OS PTW16, Germany) with a 16 mm screw diameter (L/D = 40 mm). The extruder is coupled to a Haake PolyLab Blown Film Die and Blown Film Take-Off system as presented in **Figure 2.1**. The blown film die is designed as a vertical annular die (ring diameter of 24 mm and a gap of 0.8 mm) forming a thin-walled polymer tube. Air is introduced via a hole in the center of the die to blow the film up. The cooling ring (width of 48 mm) is designed to cool down the film, while the take-off rollers stretch the extruded film upward. The collapsing frame puts the film bubble onto a flat double-layered film. Finally, the film is drawn by a roller block with an adjustable take-off speed. The different processing parameters are presented in **section 2.3**.

For foaming, a simple dry-blending procedure (physical mixing) was carried out between the LLDPE/Celogen powders and LDPE pellets. The blend was then fed to the extruder at a flow rate of 22 g/min.

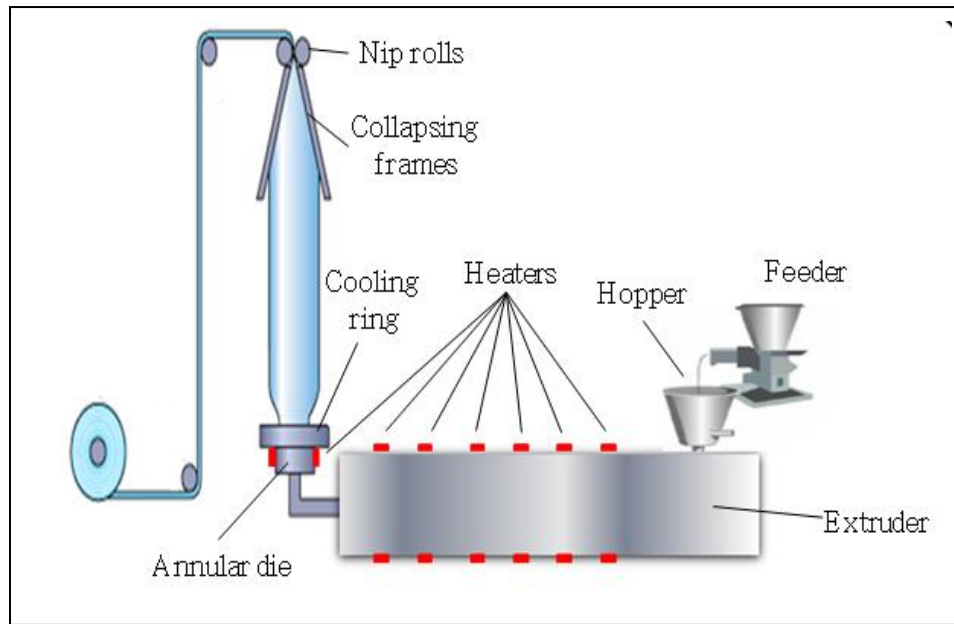


Figure 2.1 Schematic representation of the blown-film extrusion set-up.

2.2.3. Characterization

Scanning electron microscope (SEM) was used for morphological characterization in both longitudinal (L) and transversal (T) directions. The structure was exposed through a cryogenic fracture in liquid nitrogen. Then, the surface was coated with a thin layer of Au/Pd and characterized at different magnifications on a JEOL JSM-840A scanning electron microscope. The morphological characterization was analyzed using the Image Pro Plus software (Version 4.5). In both directions, the cells were approximated as ellipsoids and the major/minor axes were extracted. For cell density (N), due to cell deformation, the value was approximated by [Gosselin *et al.* (2005)]:

$$N = (N_1) (N_2)^{1/2} \quad (2.1)$$

where N_1 and N_2 are the surface cell densities in the longitudinal and transversal directions, respectively.

To perform tensile mechanical testing, an Instron model 5565 universal machine coupled with the Blue Hill software (Version 2) was used. The tests were carried out at room temperature with a drawing speed of 50 mm/min according to ASTM D882. Rectangular

samples (length = 5 cm and width = 1 cm) were cut in the films produced and the values reported are based on averaging at least five samples.

Finally, foam density was measured by a Quantachrome Ultrapyc 1200e gas (nitrogen) pycnometer. The reported values correspond to the average of a minimum of five measurements.

2.3. RESULTS AND DISCUSSION

2.3.1. Challenges in producing thin foamed PE films of good quality

The production of biaxially stretched foamed PE films by extrusion-blowing with a suitable 3D morphology for piezoelectric films presents different challenges as presented in **Figure 2.2**.

➤ A uniform unfoamed PE film was first produced as shown in **Figures 2.2a-c**. The film was initially transparent. Then, different CBA concentrations were used. At 0.8%, the films have a poor cellular structure (low cell density and non-homogeneous cell distribution). However, from 1% and above, the films are well foamed (the cells are evenly distributed with a homogeneous structure having higher cell density).

➤ **Figures 2.2d and 2.2f** illustrate the case of a cellular PE film having surface defects and bubble stability problems. Several parameters have to be controlled to optimize the foaming and blowing processes occurring simultaneously. The production of foamed polymer films requires a good understanding of the melt rheology, which plays an important role in both phenomena. In this context, melt strength is introduced as the main parameter. Melt strength is an engineering measure related to extensional viscosity and defined as the minimum tensile force required to break a molten polymer under well-defined conditions (extensional speed and temperature). Here, the shear rheology of the biphasic system (polymer with gas bubbles) is of limited importance, because during foaming the polymer is already out of the die and is mainly subjected to elongational stresses.

Bubble growth is also a phenomenon essentially involving an elongation flow. Cell growth is associated to a biaxial stretching of the cell walls. Therefore, low melt strength limits possible cell growth before collapse and coalescence, leading to non-homogeneous foam structures. In addition, high melt strength is important to maintain bubble stability and to

prevent surface defects during film processing. Therefore, improving the film quality must go through this key parameter. But a linear polyolefin like LLDPE generally has low melt strength. Nevertheless, several methods can be used to improve melt strength: addition of branched polymers [Wagner *et al.* (2004); Wagner *et al.* (2006)], addition of nucleating agents, or mixing with high molecular weight polymers. Addition of a branched polyethylene (LDPE) and a nucleating agent (talc) were selected here.

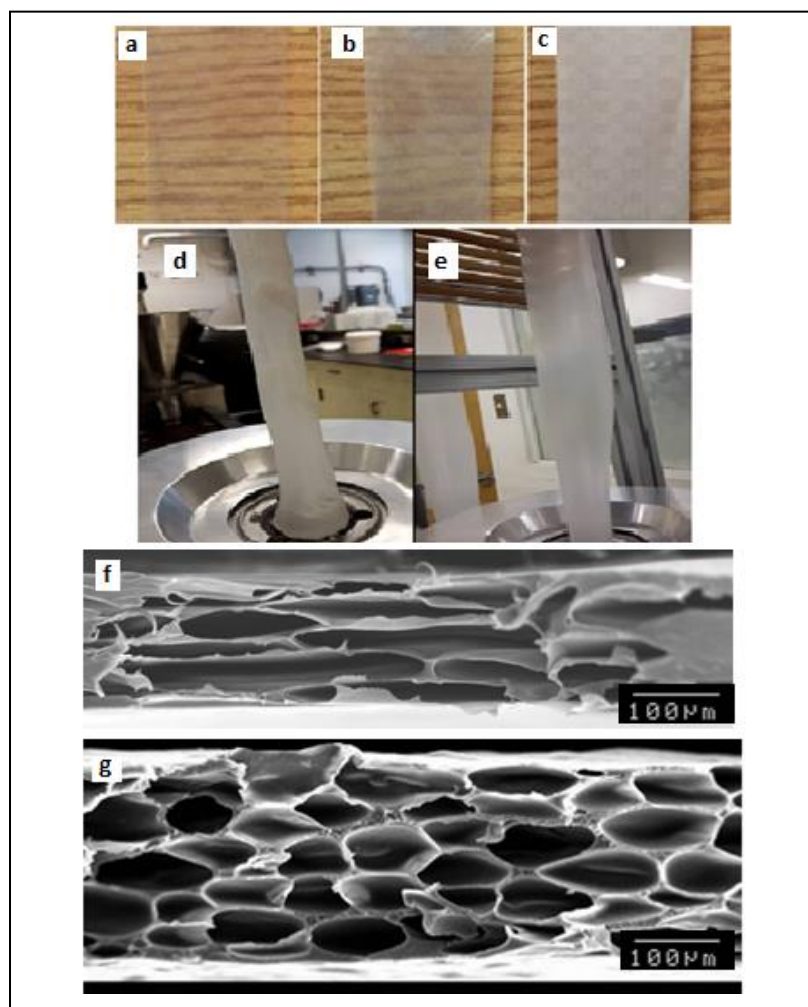


Figure 2.2 Typical states of the foam during the optimization step: a) unfoamed PE film, b) film with 0.8% CBA, c) film with 1% CBA, d) PE film having surface defects and bubble stability problems, e) film with stable bubbles and good cellular quality, f) typical structure of a film presenting a non-uniform cellular structure and g) typical structure of a film presenting a uniform and well-developed cellular structure.

2.3.2. Optimization of the processing conditions to obtain high quality cellular films

To optimize the quality of the cellular films, the processing must be carefully controlled. This optimization was mostly based on direct observation and information taken from the literature. During this step, an attempt was made to stretch the samples as much as possible without losing film integrity (rupture) while maintaining stable processing conditions. Several trials were carried out to produce high quality films. But to get a homogeneous and stable film, several compromises have to be made. A summary of the most important factors, as well as some remarks and recommendations, are presented next.

2.3.2.1. Addition of low density polyethylene

To improve the LLDPE melt strength, the addition of a branched polymer (LDPE) was very useful. These changes are easily visible by the naked eye (film quality). Several LDPE contents were tested (10, 20, 30 and 40% wt.), but 20% wt. was found to give an excellent foamed film quality.

2.3.2.2. Temperature profile

To achieve a homogeneous cellular structure, a suitable control of the temperature profile must be carried out (**Figure 2.3**). In the feeding zone, the temperature should be kept relatively low to avoid premature decomposition of the blowing agent, which would cause gas losses. In the melting zone, the temperature must be increased to ensure complete CBA decomposition and homogeneous dissolution/dispersion of the generated gases before the pumping zone. The die zone is the most sensitive, as it can lead to visible surface defects, non-homogeneous cells, and non-uniform cell structures. In fact, if the temperature is too high, the low melt strength of the matrix produces excessive foaming, leading to open cells which are detrimental for piezoelectric applications. In this case, bubble wall rupture, cell collapse, surface defects and bubble instability are obtained (**Figure 2.2d**). But if the temperature is too low, limited bubble nucleation and growth occurs. So the temperature profile should be high enough in the intermediate section of the extruder (melting zone) to fully melt the polymer and fairly low near the die to increase the melt strength and avoid processing instability.

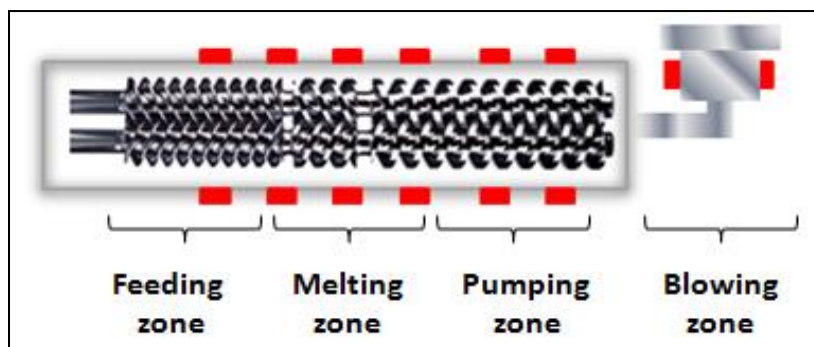


Figure 2.3 Schematic representation of the different temperature zones in an extrusion-blowing machine.

2.3.2.3. Cooling rate

The cooling rate provided by the cooling ring also makes a significant contribution to the foamed film quality. The higher the cooling rate, the faster the bubble temperature decreases and the earlier the final diameter is reached. Conversely, a low cooling rate leads to longer time to achieve polymer solidification (higher freeze-line height). The bubble remains thin for a longer time and widens to form a "bottleneck" shape at the die exit, as illustrated in **Figure 2.4**. Under optimum conditions, the bubble must not solidify too fast to prevent it from sticking to the die. On the other hand, it must solidify sufficiently rapidly to maintain its stability (not sticking to the collapsing frame/nip rolls). The speed of the extruder screws and the pulling rollers speed also play a role in bubble stability, as they determine the final film thickness.

In our case, cooling by free ambient air (cooling ring closed) gave better results. First, the cells tended to be more circular when the cooling ring was opened. When the cells were allowed to cool slowly, much higher aspect ratios were obtained, since the cells had more time to deform under the effect of stretching and gas inflation. In addition, higher elastic moduli in the machine direction were recorded when the films were cooled rapidly (see **section 2.3.3**). This is associated to the rapid freezing of the molecular chains resulting in more rigid films and also incomplete inflation of the cells in these films.



Figure 2.4 Left: bubble cooled by the cooling ring. Right: bubble cooled by ambient air presenting the bottleneck phenomenon.

2.3.2.4. Take-up ratio and blow-up ratio

The blow-up ratio (BUR) defines the transverse stretching of the film as:

$$\text{BUR} = R_f / R_0 \quad (2.2)$$

where R_f and R_0 are the radii of the bubble at the freeze-line position and at the die exit, respectively.

On the other hand, the take-up ratio (TUR) defines the longitudinal stretching of the film by the nip rolls as:

$$\text{TUR} = S_s / S_0 \quad (2.3)$$

where S_s and S_0 are the speeds of the material flow at the freeze-line (stretching speed) and at the die exit (extrusion speed), respectively.

S_0 was calculated from the mass flow rate of the molten polymer at the die exit taking into account the density change with temperature:

$$\alpha_v = -1/\rho * d\rho/dT \quad (2.4)$$

where α_v , ρ and T are the coefficient of volumetric thermal expansion, the density of the polymer and its corresponding temperature, respectively. For LLDPE, a value of $\alpha_v = 600 \times 10^{-6} \text{ K}^{-1}$ was used [Lechner (2005)].

The selection of a relatively high TUR was crucial to obtain a good cellular structure, since higher stretching speed allowed faster film cooling without opening the cooling ring, thus preventing late bubble solidification which would produce bubble instability.

Increasing the TUR and/or BUR both lead to a more elongated cell structure in the longitudinal and/or transverse directions respectively, thus producing higher deformation in both directions and increasing the cells aspect ratio (AR). However, in the case of excessive TUR or BUR, some defects and non-uniform cell structure are produced as presented next.

2.3.2.5. Feed rate and screw rotation speed

The feeding rate and screw rotation speed must also be selected based on a compromise because they have a direct effect on the flow rate (amount of material leaving the die) and the pressure inside the extruder (mostly at the die exit). Increasing the pressure inside the extruder favors nucleation rate through higher pressure drop rate [Park et al. (2004)]. However, if the pressure is too high, processing instability and material degradation can occur.

2.3.2.6. Blow-up ratio and take-up ratio effect

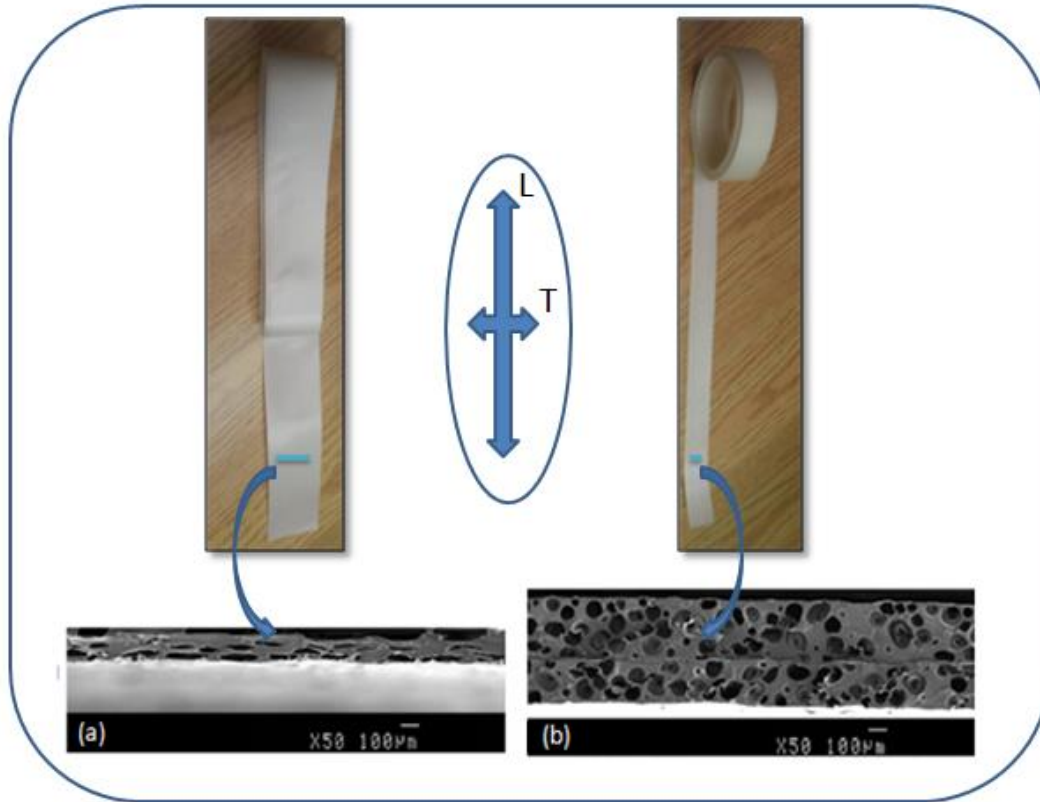


Figure 2.5 SEM pictures for the transversal section of two film samples:
(a) S1.2-6.4-1.8 and (b) S1.2-6.4-1.

Figure 2.5 presents the effect of BUR on the samples produced. Samples were coded as Sx-y-z where x represents the CBA content (wt.%), y represents the take-up ratio TUR (-) and z represents the blow-up ratio BUR (-). When a nucleating agent (talc) was added, 1 wt.% was found to be optimum and the sample code is changed to Sxn-y-z where n indicates the presence of talc.

The samples made at BUR=1.8 are approximately 80% wider than the films at BUR=1.0. It is clear that the cells in the transversal section of S1.2-6.4-1.8 are more elongated than for S1.2-6.4-1 (almost circular). As stated in the Introduction, an eye-shaped geometry is the most convenient for piezoelectric applications (electrical charging), so the BUR was fixed at 1.8 for the next samples as it was not possible to produce good quality (cell structure becomes

poor and non-homogeneous) and stable foams (break-up) at higher BUR (films become too thin).

For the TUR, three values were tested: 3.2, 6.4 and 12.8. The samples made with a TUR of 12.8 produced cells with high longitudinal aspect ratios. For example, S1.5n-12.8-1 (**Figure 2.6a**) shows cells with an average longitudinal aspect ratio of 20. However, with such a high TUR value, it was impossible to produce samples with BUR=1.8. In fact, the films become too thin and break easily (**Figure 2.6b**). Thus, only two TUR values were retained (3.2 and 6.4).

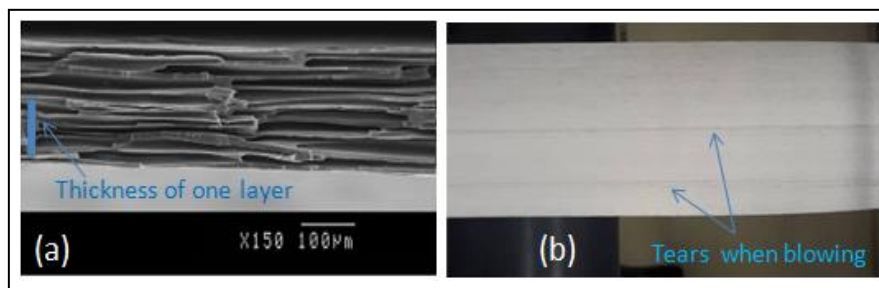


Figure 2.6 (a) SEM picture for the longitudinal section of S1.5n-12.8-1 and (b) presence of tear lines when TUR=12.8 and BUR=1.8.

2.3.2.7. Nucleating agents

Another way to control the cellular structure is by adding nucleating agents (heterogeneous nucleation) [Xu et al. (2003); Colton (1988); Han et al. (2003); Behravesht et al. (1996)]. As cell size and cell shape are very important to control the mechanical and piezoelectric properties of the films, an optimum was also searched for this effect as presented in **Figure 2.7**. It is clear that the average cell size is more uniform and finer when 1% talc is added. It is also clear that the addition of 1% talc favors nucleation (higher cell density). In this case, sample S1.2-6.4-1.8 has a major cell size of 671 μm in the longitudinal direction and 172 μm in the cross-section. These values decreased to 259 μm in the longitudinal and 123 μm in the transversal direction for S1.2n-6.4-1.8. Conversely, the cell density increased from 1.26×10^5 to 7.93×10^5 cells/cm³.

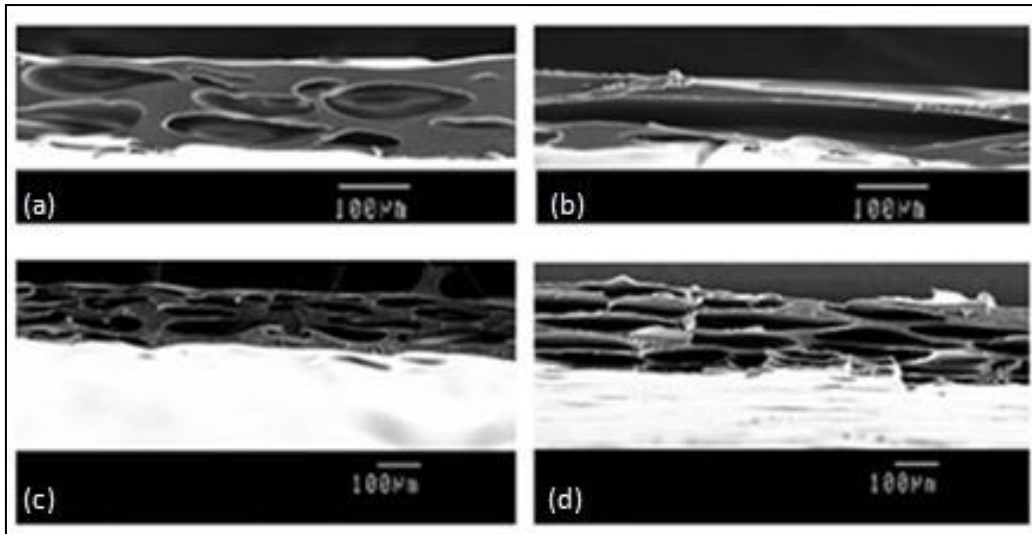


Figure 2.7 SEM images of cellular polyethylene films: Sample S1.2-6.4-1.8 in the (a) transversal and (b) longitudinal directions, and S1.2n-6.4-1.8 in the (c) transversal and (d) longitudinal directions.

This improvement in the cell structure (major cell size reduction of 61% in the L section and 28% in the T direction combined with a cell density increase of 529%) is explained by the lowering of the surface energy needed for cell nucleation as nucleation tends to occur at the interface between the matrix and the additive (heterogeneous nucleation) rather than within the polymer matrix (homogeneous nucleation) [Lee (2000)]. At the interface, the free energy barrier for nucleation is lower than for homogeneous nucleation (nucleation without nucleating agent). It should be noted that the addition of 2% talc was also tested, and the morphological results obtained were almost similar to the samples with 1% of talc.

2.3.3. Morphological results

The variation of several processing conditions allowed to control the cell morphology over a wide range. After processing and composition optimization as presented above, different foamed PE films were produced. **Table 2.1** presents the optimized conditions for the samples characterized.

Table 2.1 Optimized processing conditions for cellular PE blown films.

Parameters	Values
LLDPE/LDPE blend	80 / 20 wt.%
Blowing agent	1.5 - 2 wt.%
Nucleating agent (talc)	1 wt.%
Temperature profile in the extruder (feed to die)	162–165–172–172–170–166°C
Die temperature	147°C
Feed rate	22 g/min
Screw rotation speed	120 rpm
Cooling method	Free ambient air (cooling ring closed)
BUR	1.8
Stretching speed	125 - 250 cm/min
TUR	3.2 - 6.4

Table 2.2 presents the characterization of the best cellular films for piezoelectric applications. Firstly, the relative density (foam density divided by the matrix density) is quite low, indicating that good foaming occurred. In previous studies, optimum relative density for good piezoelectric coefficient is expected to be around 0.6 [Tuncer (2005); Wegener et al. (2004b)]. Again, this value represents a compromise between the total internal surface area to be charged (sensitivity) and the mechanical properties (modulus and strength), since the elastic modulus is inversely proportional to the piezoelectric coefficient (d_{33}) and foam density (ρ_F) [Wegener et al. (2005)]. The relative density and elastic modulus are also affected by cooling rate. In fact, rapid cooling rate inhibits cell expansion and thus relative density does not decrease much. In addition, the polymer chains are frozen more rapidly when cooling is applied, leading to lower crystallinity. For example, sample S1.5n-3.2-1.8 has an elastic modulus of 136 MPa (relative density of 0.53) in the longitudinal direction, while its counterpart cooled more rapidly (cooling ring opened) recorded an elastic modulus of 207 MPa (relative density of 0.69) which represents a 52% increase.

Secondly, the cell geometry and dimensions are also known to have a direct effect on the film's piezoelectric properties. In fact, it is believed that having an eye-shaped (ellipsoidal)

cellular structure positively affect the piezoelectric properties of the foamed films. Some studies reported that $AR > 4$ must be achieved [Lindner et al. (2004); Xu et al. (2013)]. Also, the cell height (b) should be higher than 5 μm for better charging ability [Qiu et al. (2008)].

Table 2.2 Properties of the best polyethylene cellular films morphology (optimized conditions).

Sample Code	Stretching speed	BUR	TUR	Relative density	Film thickness	Cell size-L		AR-L	Cell size-T		AR-T	Cell density
						major	minor		major	minor		
	(cm/min)	(-)	(-)	(-)	(μm)	(μm)		(-)	(μm)		(-)	(10^5 cells/ cm^3)
S1.5n-3.2-1.8	125	1.8 (0.2)	3.2 (0.5)	0.53 (0.02)	256 (12)	119 (41)	32.6 (9.9)	3.7 (0.8)	95 (34)	42 (16)	2.4 (0.6)	18.1 (2.2)
S1.5n-6.4-1.8	250	1.8 (0.2)	6.4 (1.0)	0.67 (0.03)	129 (11)	165 (62)	20.2 (4.9)	7.8 (2.8)	84 (35)	18.3 (6.6)	4.7 (1.4)	26.6 (3.1)
S2n-3.2-1.8	125	1.8 (0.2)	3.2 (0.5)	0.52 (0.01)	266 (12)	86 (33)	29.3 (7.6)	3.0 (1.0)	91 (30)	36 (12)	2.4 (0.5)	36.7 (4.5)
S2n-6.4-1.8	250	1.8 (0.2)	6.4 (1.0)	0.62 (0.02)	139 (10)	98 (32)	21.4 (7.2)	4.7 (1.6)	77 (24)	20.1 (5.5)	3.9 (1.0)	59.3 (4.9)

Values in parentheses correspond to standard deviation

As reported in **Table 2.2**, increasing the CBA content from 1.5 to 2% increased the cell density and decreased the relative density. For example, sample S1.5n-6.4-1.8 has a cell density of $26.6 \times 10^5 \text{ cells/cm}^3$ compared to $59.3 \times 10^5 \text{ cells/cm}^3$ for sample S2n-6.4-1.8 which represents a 122% increase combined with a 8% decrease in relative foam density (from 0.67 to 0.62). Typical SEM pictures for S2n-3.2-1.8 and S2n-6.4-1.8, which are the films having the highest cell densities, are presented in **Figure 2.8**.

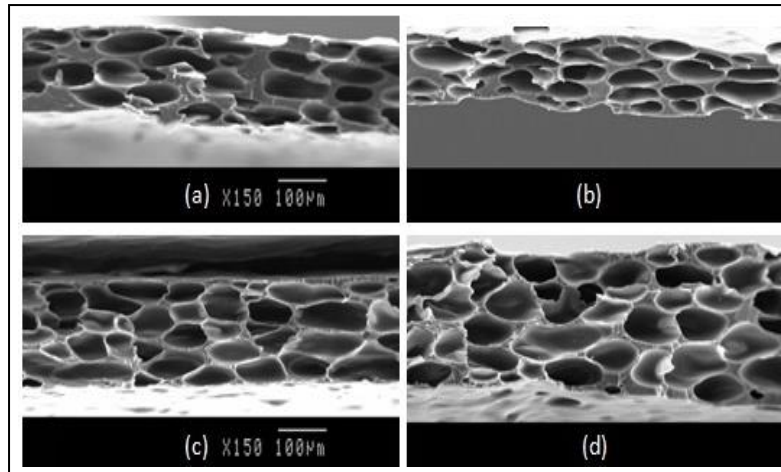


Figure 2.8 SEM images of cellular polyethylene films: S2n-6.4-1.8 in the (a) transversal and (b) longitudinal directions and S2n-3.2-1.8 in the (c) transversal and (d) longitudinal directions.

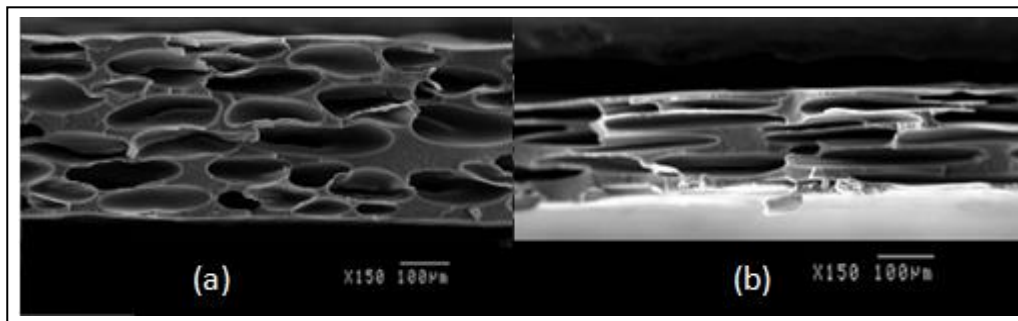


Figure 2.9 Typical SEM pictures for the longitudinal section of S1.5n-TUR-1.8 with different take-up ratios: (a) TUR=3.2 and (b) TUR=6.4.

Typical SEM images in the longitudinal (L) direction for the samples produced with 1.5% of CBA, 1% of talc, BUR=1.8, and different take-up ratios are presented in **Figure 2.9**. It can be seen that increasing the take-up ratio from 3.2 to 6.4 led to a more elongated cellular structure with higher AR values. The major cell sizes in the L direction for sample S1.5n-TUR-1.8 increased from 119 to 165 μm (**Figures 2.9 and 2.10**). Conversely, the minor cell sizes in the L direction of these films decrease from 32.6 to 20.2 μm . Therefore, the longitudinal aspect ratio (AR-L) shows a substantial increase from 3.7 to 7.8 under these conditions.

Despite having the same BUR, an important increase (83%) is also observed for the transversal aspect ratio (2.4 to 4.7) with increasing take-up ratio. This is explained by the significant decrease of the minor cell size (41.9 to 18.3 μm) combined with a negligible variation of the major cell size. Sample S1.5-6.4-1.8 has the highest transversal AR (4.7) making this film suitable for electrical charging in both (L) and (T) directions and should lead to good piezoelectric properties.

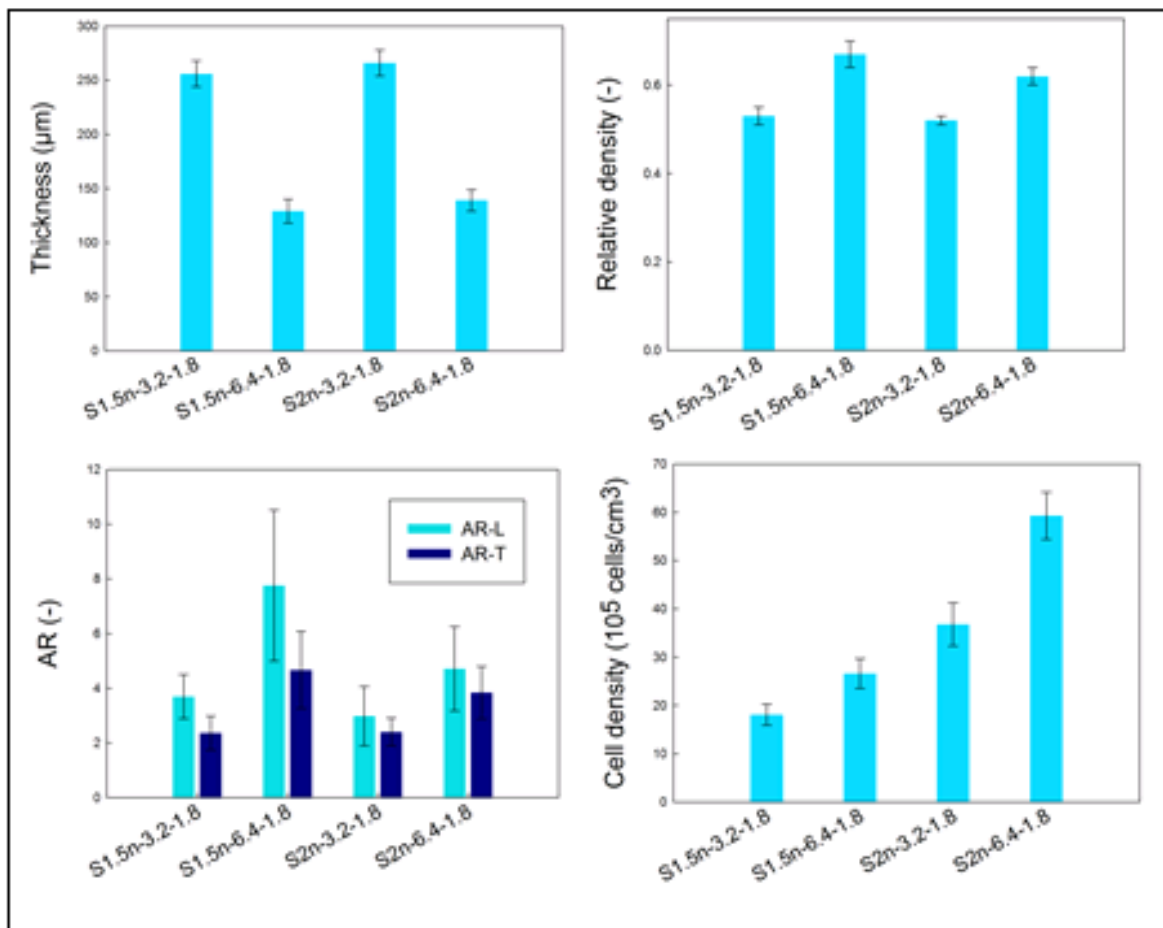


Figure 2.10 Effect of take-up ratio (TUR) and blowing agent content on the morphological properties of the cellular films.

As reported in **Figure 2.10**, the samples produced with 2% CBA have higher cell density than those produced with 1.5% CBA under the same processing conditions. Overall, sample S2n-6.4-1.8 has the highest cell density ($5.9 \times 10^6 \text{ cell/cm}^3$) with a well-defined eye-shaped cell morphology with good aspect ratios in both L (AR-L=4.7) and T (AR-T=3.9)

direction. These characteristics make this film a potential candidate for electrical charging and future piezoelectric applications.

2.4. CONCLUSION

In this work, the cellular structure in 3D was controlled for thin (less than 300 μm) polyethylene (PE) films produced by extrusion film blowing using a chemical blowing agent (CBA). This process allowed to impose biaxial stretching on the samples while foaming, which was shown to be continuous and stable.

The first challenge was to obtain a homogeneous and stable cellular structure. Several compromises were made to improve the foaming quality. This optimization was mainly based on literature review and direct observations during preliminary trials. The results showed that blending LLDPE with 20 wt.% of LDPE allowed to substantially improve the matrix melt strength leading to better film stability and homogeneity since polyethylene is known to have a very narrow foaming conditions window.

But process optimization here must include the extrusion and post-extrusion conditions. In our case, the optimum die temperature was 147°C and the formulation was optimized by using 1 wt.% of talc as a nucleating agent for a range between 1 and 2 wt.% of azodicarbonamide as a chemical blowing agent. All these conditions combined with careful selection of other processing parameters (flow rate=22 g/min, screw speed=120 rpm, BUR=1.8, TUR=6.4) resulted in a foamed film having a fine and uniform morphology (relative foam density=0.62 and high cell density=5.9x10⁶ cells/cm³) with a well-developed eye-like cellular structure (cell aspect ratio around 4 in both longitudinal and transversal directions) which are required for piezoelectric applications. Nevertheless, more work should be done to further improve on these values and determine their suitability for corona charging and different piezoelectric applications.

ACKNOWLEDGEMENTS

Financial support from the Natural Sciences and Engineering Research Council of Canada (NSERC) and Fonds Québécois de la Recherche sur la Nature et les Technologies (FRQNT) was received for this work. Materials samples were kindly supplied by Exxon Mobil (LLDPE), Nova Chemicals (LDPE) and Imerys (talc). The technical support from Mr. Yann Giroux is highly appreciated.

CHAPITRE 3. PIEZOELECTRIC PROPERTY IMPROVEMENT OF POLYETHYLENE FERROELECTRETS USING POSTPROCESSING THERMAL- PRESSURE TREATMENT

RÉSUMÉ

Dans ce travail, des films polymères moussés étirés bi-axialement avec des structures cellulaires bien définies ont été préparés à partir du polyéthylène par extrusion-gonflage et soumis à un chargement corona pour produire une réponse piézoélectrique. Les paramètres de chargement ont d'abord été optimisés en termes de tension de charge, de distance entre l'aiguille et l'échantillon, ainsi que le type et la pression du gaz utilisé, afin d'étudier leurs effets sur le coefficient piézoélectrique (d_{33}). Les résultats montrent que les échantillons chargés sous azote (N_2) à 100 kPa ont un meilleur coefficient d_{33} que ceux chargés sous air ambiant ou sous N_2 à 20 kPa. De plus, deux différents traitements de pression/température ont été imposés pour obtenir une structure cellulaire de forme ellipsoïdale allongée avec différents ratios de forme (AR). Les résultats ont montré que des cellules plus étirées dans les directions longitudinale et transversale (AR plus élevé) donnent des coefficients d_{33} plus élevés. Parmi les échantillons produits, les meilleurs résultats ont été obtenus pour l'échantillon ayant un ratio de forme longitudinal (AR-L) de 7,2, un ratio de forme transversal (AR-T) de 4,7 et une densité relative de 0,52 conduisant à un coefficient d_{33} de 935 pC/N. Ce coefficient a ensuite été augmenté à l'aide de films multicouches et avec un chargement électrique inverse, pour atteindre un maximum de 2550 pC/N. Cette valeur est beaucoup plus élevée que celle généralement rapportée jusqu'à présent pour tous les ferroélectrets de polyéthylène et de polypropylène. Ces résultats pourraient favoriser l'utilisation du polyéthylène dans les applications piézoélectriques, car ces matériaux sont très intéressants pour la production à grande échelle de capteurs et de transducteurs à base d'électrets en raison de leur faible coût et de leur fabrication plus facile.

Mots-clés: structure cellulaire, ferroélectrets, optimisation, polyéthylène, post-traitement.

ABSTRACT

In this work, biaxially stretched polymer foams with well-defined cellular structures were prepared from polyethylene via blown-film extrusion and subjected to corona charging to produce a piezoelectric response. The charging parameters were first optimized in terms of charging voltage and needle distance, as well as the gas type and pressure to investigate their effect on the piezoelectric coefficient (d_{33}). The results show that samples charged under nitrogen (N_2) at 100 kPa had better d_{33} coefficient than those charged under ambient air or N_2 at 20 kPa. Moreover, 2 different thermal pressure treatments were imposed to obtain an optimized eye-like cellular structure with different cell aspect ratios (AR). The results showed that when the cells were elongated in both the longitudinal and transverse directions (higher AR), higher d_{33} coefficients were achieved. From all the samples produced, the best results were obtained for a longitudinal aspect ratio (AR-L) of 7.2, a transversal aspect ratio (AR-T) of 4.7, and a relative foam density of 0.52 leading to a d_{33} coefficient of 935 pC/N. This coefficient was further increased using reverse charging and multilayered films, reaching a maximum of 2550 pC/N. This value is much higher than typical one reported so far for any polyethylene and polypropylene ferroelectrets. These results could increase the use of polyethylene in piezoelectric applications as these materials are very attractive for the large-scale production of electret-based sensors and transducers due to their low cost and easy processing.

Keywords: cellular structure, ferroelectrets, optimization, polyethylene, post-treatment.

Ouassim Hamdi, Frej Mighri, Denis Rodrigue (2018c) Piezoelectric properties improvement of polyethylene ferroelectrets using post-processing treatments. *Polymers for Advanced Technologies* 1-9.

3.1. INTRODUCTION

Interest in transducer technology based on advanced functional materials is witnessing a great evolution [*Qaiss et al. (2012)*; *Belhora et al. (2014)*; *Lang et al. (2006)*; *Ni et al. (2009)*]. In this context, new electromechanical (piezoelectric) materials based on electrets and thin cellular polymer films have recently been developed. These materials transform mechanical energy into electrical signals and vice versa [*Qiu et al. (2015)*]. They are suitable for a large range of uses in sensor technologies for different domains, such as impact signal measurement, detection of human body activities, tactile sensing, transportation, robotics, acoustics, etc. [*Patel et al. (2012)*; *Zhuo et al. (2015)*; *Li et al. (2015)*; *Saarimaki et al. (2006)*; *Fang et al. (2008)*; *Doring et al. (2010)*; *Kogler et al. (2011)*; *Hillenbrand et al. (2010)*; *Dobkin et al. (2011)*; *Wegener (2010)*].

The piezoelectric response of these materials (called ferroelectrets) originates from a combination of the foam cellular structure, their elastic properties, and their charge-trapping capacity [*Mohebbi et al. (2018)*]. The cellular structure of foamed films (cell density, size, shape, and orientation) has a direct effect on their piezoelectric activity, and previous studies confirmed that an eye-shaped (ellipsoidal) cellular structure provides better piezoelectric coefficients [*Lindner et al. (2004)*; *Tuncer (2005)*; *Mohebbi et al. (2017a)*; *Xu et al. (2013)*]. It is thus mandatory to develop a processing method allowing precise control of the cell morphology in two perpendicular directions; i.e. biaxial stretching.

In our previous work [*Hamdi et al. (2018b)*], different types of eye-like foamed polyethylene films with good cellular uniformity were successfully produced through blown-film extrusion using a chemical blowing agent (CBA). After a complete optimization of the process (temperature profile, screw speed, feed rate, take-up ratio, blow-up ratio (BUR), as well as matrix composition), an optimized cellular structure was obtained [*Hamdi et al. (2018b)*]. The next step, which is the main objective of this work, is to optimize the postprocessing conditions (electrical charging) which are crucial in ferroelectret manufacturing. In fact, by applying a high voltage to the structure, internal dielectric barrier micro-discharges are generated in the polymer voids, and charges of opposite signs are

created on the opposite sides of each cell creating macroscopic dipoles [Reimund (2002); Bauer et al. (2004); Ramadan et al. (2014)].

Mechanical stimulations, causing a variation in the thickness direction of the electrically charged voids, result in an electrical signal between the electrodes connected to the film surfaces. Thus, ferroelectrets are obtained with piezoelectric activity depending on the final material structure. The most common methods to generate dipoles in polymer foams are direct contact charging and corona discharge [Reimund (2002); Bauer et al. (2004); Ramadan et al. (2014)]. The latter is used in this work and is believed to be more suitable for an industrial scale. The method consists in imposing a potential difference between a needle and a conductive plate to create an electric field over the entire width. Parameters such as voltage, needle distance, and charging time are important to improve the charging effect [Mohebbi et al. (2017b)].

Another important parameter affecting the piezoelectric response is the elastic behavior of the film, mainly the elastic stiffness (c_{33}) in the surface-normal direction (thickness direction). The literature shows that the piezoelectric d_{33} coefficient has a maximum when the elastic modulus (c_{33}) exhibits a minimum. Generally, these two parameters present an inverse trend [Wegener et al. (2006)], which can be written as [Rychkov et al. (2016); Hillenbrand et al. (1999); Sessler et al. (1999)]:

$$d_{33} = \frac{\varepsilon \sigma}{c_{33}} \frac{1 + d_2/d_1}{(1 + \varepsilon d_2/d_1)^2} \quad (3.1)$$

where σ is the charge density on the inner surface of cavities, ε is the polymer permittivity, and c_{33} is the elastic stiffness (elastic modulus), while d_1 and d_2 are the polymer and gas phase layer thickness.

Although it has been shown that the relative film density has a great influence on c_{33} , the cell morphology was also shown to be important, making the prediction of d_{33} more complex. In fact, experimental [Wegener *et al.* (2006)] and numerical [Tuncer (2005)] studies have shown that the variation in Young modulus in the thickness direction (c_{33}) is inversely proportional to the cell aspect ratio (AR), meaning that flatter cells (more elongated) produce lower Young modulus and therefore higher piezoelectric coefficients.

Therefore, it can be deduced that the morphology of cellular films directly influences the piezoelectric activity in two ways: firstly by modifying the cellular-specific surface (total internal surface area to charge) via the charge density, and secondly by modifying the elastic modulus (c_{33}) controlling the resulting film deformation when a pressure is applied. In this work, the effect of cell morphology to improve the piezoelectric coefficient of polyethylene foam is investigated, as this information is highly important to produce materials, on larger scale, for piezoelectric sensors and transducers. Hence, a postprocessing treatment was also applied as the cavity sizes can be adjusted by a suitable pressure and/or temperature treatment (TPT), the gas diffusion expansion process [Wegener *et al.* (2006); Wegener *et al.* (2004b)]. In this process, the external gas pressure is usually increased and kept at a high value for a certain period of time at high temperature, so that the gases diffuse into the cavities and the cells are deformed/expanded.

The originality of this work lies in the fact that all the steps leading to optimize ferroelectret films are included, and also in the use of polyethylene, which is not a standard ferroelectret material. Therefore, this work is a contribution to the development of low-cost piezoelectric materials with potential applications in different fields such as medical, security, environment, sport, and transport.

3.2. EXPERIMENTAL

3.2.1. Material preparation

The material used in this study was a biaxially stretched foamed polyethylene (PE) film (80% LLDPE-20% LDPE) with an eye-like cellular morphology. The samples were produced through an optimized continuous chemical foaming process via blown-film extrusion using 2% of Celogen 754A (Lion Copolymer Company, USA) as a CBA and talc (Jetfine 3CC), supplied by Imerys Talc (USA), as a nucleating agent. The films had a relative density of around 0.60 and a thickness of around 300 μm . More details on film production and morphological analysis can be found in our previous work [Hamdi *et al.* (2018b)]. The main film properties are summarized in **Table 3.1**.

Table 3.1 Morphological parameters, elastic stiffness, and piezoelectric coefficient and their corresponding standard deviations (values in parentheses).

Sample code	Film density (kg/m ³)	Film thickness (μm)	Cell density (10 ⁶ cell/cm ³)	AR-L (-)	AR-T (-)	d_{33} (pC/N)
S2n-3.2	483 (10)	266 (12)	3.67 (0.45)	3.0 (1.0)	2.40 (0.51)	354 (33)
S2n-3.2-TPT1	561 (11)	174 (4)	5.63 (0.67)	6.6 (2.3)	4.05 (0.89)	783 (71)
S2n-3.2-TPT2	430 (15)	401 (4)	4.04 (0.51)	2.4 (0.7)	2.39 (0.87)	281 (35)
S2n-6.4	576 (20)	139 (10)	5.93 (0.49)	4.7 (1.6)	3.9 (1.0)	634 (43)
S2n-6.4-TPT1	490 (14)	151 (4)	4.83 (0.55)	7.2 (2.9)	4.7 (1.9)	935 (54)
S2n-6.4-TPT2	519 (8)	171 (5)	5.52 (0.50)	3.8 (1.2)	3.2 (1.0)	568 (57)

3.2.2. Corona charging

The foamed samples were charged by a corona process using a discharge generator with a needle voltage of -21 kV and a moveable needle to adjust the needle-sample distance between 2 and 6 cm (see **Figure 3.1**). The samples were then removed and metallized on both sides with conductive silver paint and connected with wires to a precise electrometer for d_{33} measurement.

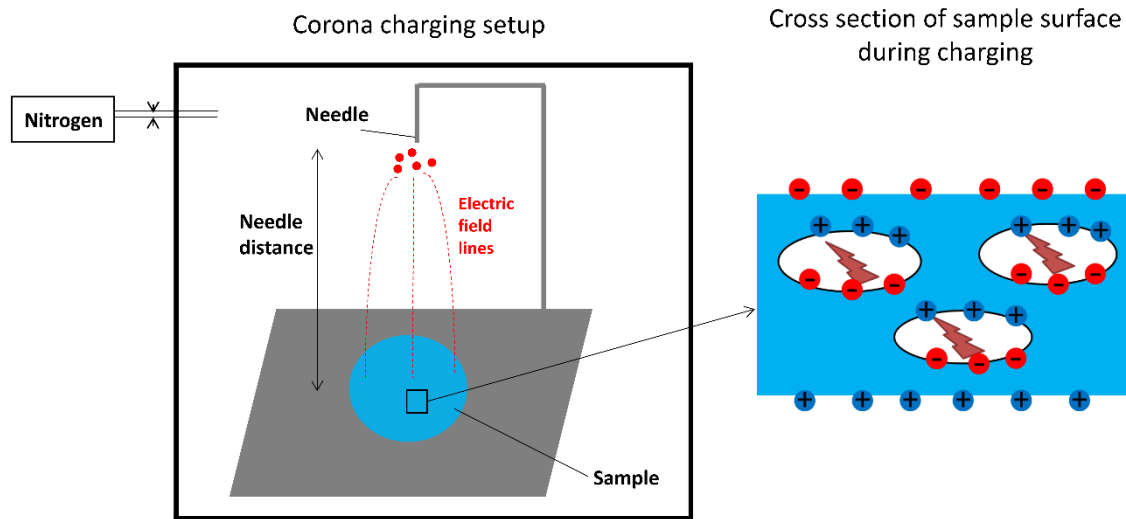


Figure 3.1 Illustration of the corona charging setup.

3.2.3. Piezoelectric coefficient measurement

Several procedures can be used to determine the d_{33} value of cellular electrets such as the quasi-static, dynamic, acoustic, and resonance methods [Mohebbi *et al.* (2017c)]. The quasi-static coefficient (determined by the quasi-static method) is the value commonly reported and compared with other piezoelectric materials [Mohebbi *et al.* (2017c)]. It is defined as the electric charge density generated per unit stress (or pressure) applied across the material at zero or very low frequency (few Hz) as:

$$d_{33} = Q/F = \sigma/p \quad (3.2)$$

where Q is the charge generated on the electrodes, F is the applied force, and σ is the charge density generated upon applying a mechanical pressure p .

A quasi-static setup was used to measure the piezoelectric d_{33} coefficient by applying a direct piezoelectric effect. A force of 0.5 N was applied on the sample, and the induced charge was detected by a programmable electrometer (Keithley 6514, USA) connected to a LabView software for data acquisition. The d_{33} coefficient was calculated using **Equation 3.2**. The procedure was repeated 3 times for each sample, and the average values with their standard deviations are reported in **Table 3.1**.

It is important to note that the test is very sensitive to the experimental conditions and requires some precautions to get precise and stable values: using very light wires, carefully adding the silver paint, and letting it dry sufficiently before taking measurements. Also, the metallization was not performed on the full film surface but limited to a small area in contact with the wires. The wires connected on the opposite surfaces must be separated (not superimposed across the film thickness) to avoid a short-circuit if metal penetration was to occur. The mass applied should not directly touch the paint or the wires because a static charge can be generated. It is also very important to eliminate vibration since these ferroelectrets are very sensitive to this type of low repeated mechanical motion. Finally, the use of a Faraday cage is necessary to shield out all possible electrical interference from other laboratory equipment (environment).

3.2.4 Temperature-pressure treatment

Two TPT, also known as gas diffusion expansion procedures, were applied to further optimize the eye-like cellular structure of the PE films; i.e. increase the cell AR. The samples were placed in a 1-L cylindrical high-pressure vessel (Autoclave Engineers, USA) connected to a N_2 (Praxair, Canada) cylinder. The vessel was first purged with N_2 to remove air. Then, the pressure was increased from atmospheric pressure up to 5 MPa to ensure a high N_2 diffusion into the samples. In both treatments, the temperature range was selected from room

temperature to 81°C (based on preliminary tests) to stay below the films melting point T_m , which is around 125°C for our samples, and prevent film deformation during the treatment, but well above the glass transition temperature T_g (about -78°C for polyethylene) to maintain the polymer chain mobility to accommodate N_2 diffusion.

As shown in **Figure 3.2**, the first treatment (TPT1) consisted in imposing a stepwise temperature increase at constant pressure (5 MPa) for the treatment duration. The temperature was increased from 25°C to 81°C, applying a 19°C increase every 10 minutes. When the temperature reached 81°C, temperature stabilization was imposed for around 14 minutes. The pressure was then kept constant during sample cooling to retain the final cell structure produced. This phase took about 2 hours. The second treatment (TPT2) consisted in imposing a rapid temperature increase from 25°C to 81°C at a heating rate of 28°C/10 minutes followed by 40-minute stabilization under a constant pressure of 5 MPa. Similar to TPT1, the pressure was then kept constant during sample cooling. The vessel was finally depressurized, and the samples were removed for analysis.

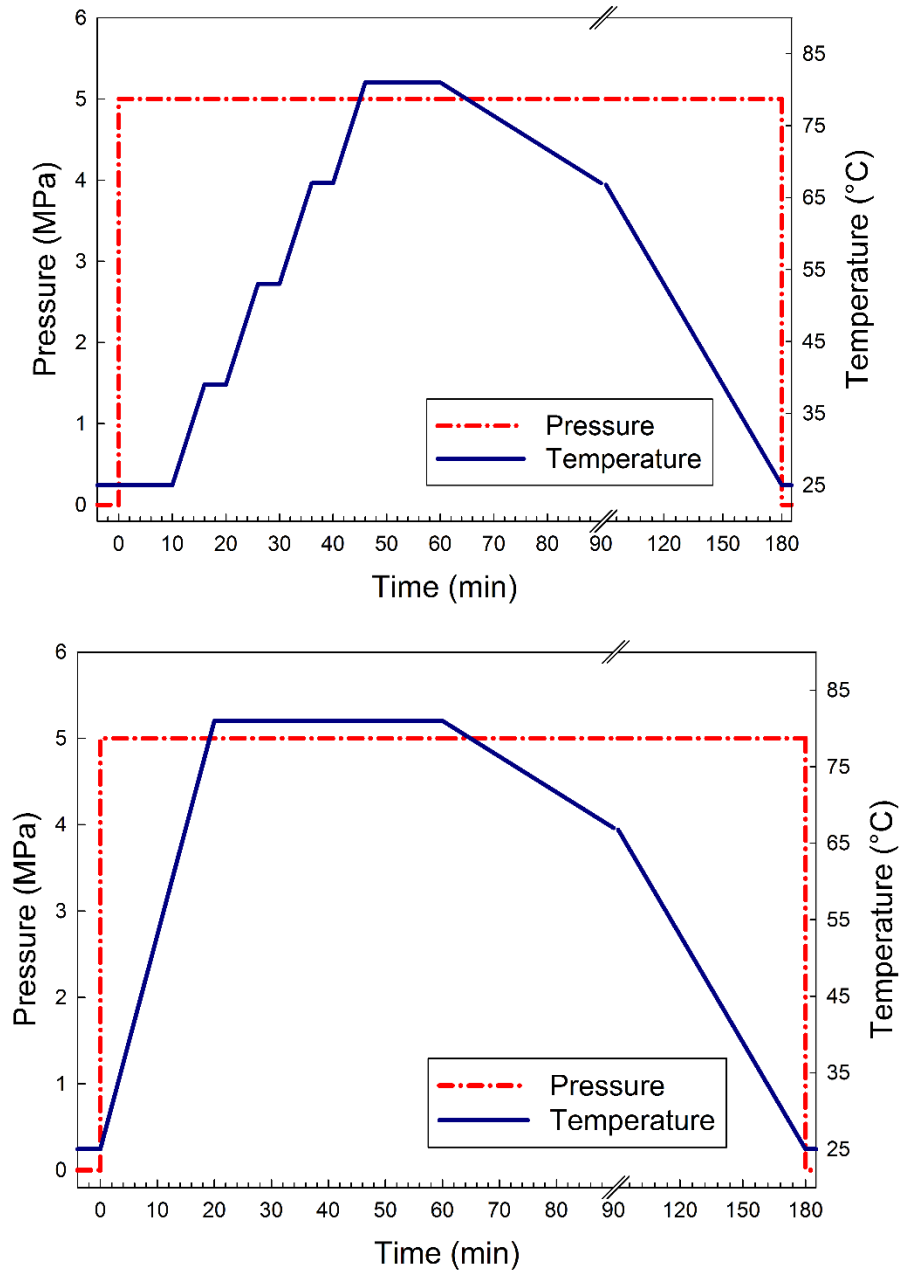


Figure 3.2 Schematic description of the two TPT studied: (A) TPT1: stepwise temperature increase and (B) TPT2: 1-step temperature increase (both under 5 MPa of N₂ pressure).

3.2.5. Morphological and density characterizations

A JEOL JSM-840A scanning electron microscope (SEM) was used for the morphological characterization in both longitudinal (L) and transversal (T) directions. The structure was

exposed through cryogenic fracture in liquid nitrogen. The surface was then coated with a thin layer of Au/Pd, and images were taken at different magnifications. The cells were approximated as ellipsoids, and the major/minor axes were extracted via the Image Pro Plus software. Due to cell deformation, the cell density (N) was approximated by [Gosselin et al. (2005)]:

$$N = (N_1) (N_2)^{1/2} \quad (3.3)$$

where N_1 and N_2 are the surface cell densities in the longitudinal and transversal directions, respectively.

A Quantachrome (USA) Ultrapyc 1200e gas (nitrogen) pycnometer was used to measure the foam density. The reported values correspond to the average of a minimum of 5 measurements.

3.2.6. Mechanical characterization

Ferroelectrets are electromechanical materials in which electrical and mechanical properties are equally relevant. Therefore, the compressive Young modulus in the thickness direction, also called the elastic stiffness (c_{33}), can be determined from their dielectric resonance spectrum [Gosselin et al. (2005)]. A high-precision impedance analyzer (Agilent 4294 A) was used to perform the measurements. The antiresonance frequency (f_a) is given at the dielectric (or mechanical) resonance of the free thickness-extension mode as [Zhang et al. (2012); Neugschwandtner et al. (2000)]:

$$f_a = \frac{1}{2s} \sqrt{\frac{c_{33}}{\rho}} \quad (3.4)$$

where ρ (unit) and s are the film density and thickness, respectively. Once the f_a value is determined from the dielectric resonance spectrum, the elastic stiffness can be calculated.

This resonance method can also be used to determine d_{33} via [Zhang *et al.* (2012); Neugschwandtner *et al.* (2000)]:

$$d_{33} = k_t \sqrt{\frac{\varepsilon_r(s) \varepsilon_0}{c_{33}}} \quad (3.5)$$

where $\varepsilon_r(s)$, ε_0 , and k_t are the relative permittivity of the sample, vacuum permittivity, and electromechanical coupling factor, respectively. The latter can be determined via [Neugschwandtner *et al.* (2000)]:

$$k_t^2 = \frac{\pi}{2} \frac{f_s}{f_p} \tan\left(\frac{\pi}{2} \frac{f_p - f_s}{f_p}\right) \quad (3.6)$$

The parallel (f_p) and series (f_s) resonance frequencies are defined as the frequencies at which the real part of the impedance and admittance have a maximum, respectively.

3.3. RESULTS AND DISCUSSION

3.3.1 Optimization of corona charging: needle-sample distance and charging time

In our previous work [Hamdi *et al.* (2018b)], the samples were coded as SXn-Y-Z where X represents the CBA content (wt.%), n indicates the presence of 1 wt.% of nucleating agent (talc), Y represents the take-up ratio (-), and Z represents the BUR (-). The latter is removed here since the optimized samples were all produced at BUR = 1.8. For example, sample S2n-6.4-1.8 in our previous work corresponds to S2n-6.4 here. The piezoelectric d_{33} coefficient was optimized as a function of needle-sample distance and charging time using the sample S2n-6.4. The charging field was fixed at -21 kV. It is important to mention that before carrying out charging, the samples were left for 15 minutes in the corona charging chamber under the gas and pressure under which they will be electrically charged.

As shown in **Figure 3.3**, films charged under air at atmospheric pressure had the lowest piezoelectric coefficients compared to those obtained by N₂ charging. Other papers reported similar results for polypropylene (PP) ferroelectrets [Mellinger (2003)]. This is explained by the higher breakdown strength of N₂ compared to air, resulting in more effective corona charging. For example, the relative breakdown strength of N₂ and air is 0.36 and 0.30, respectively.

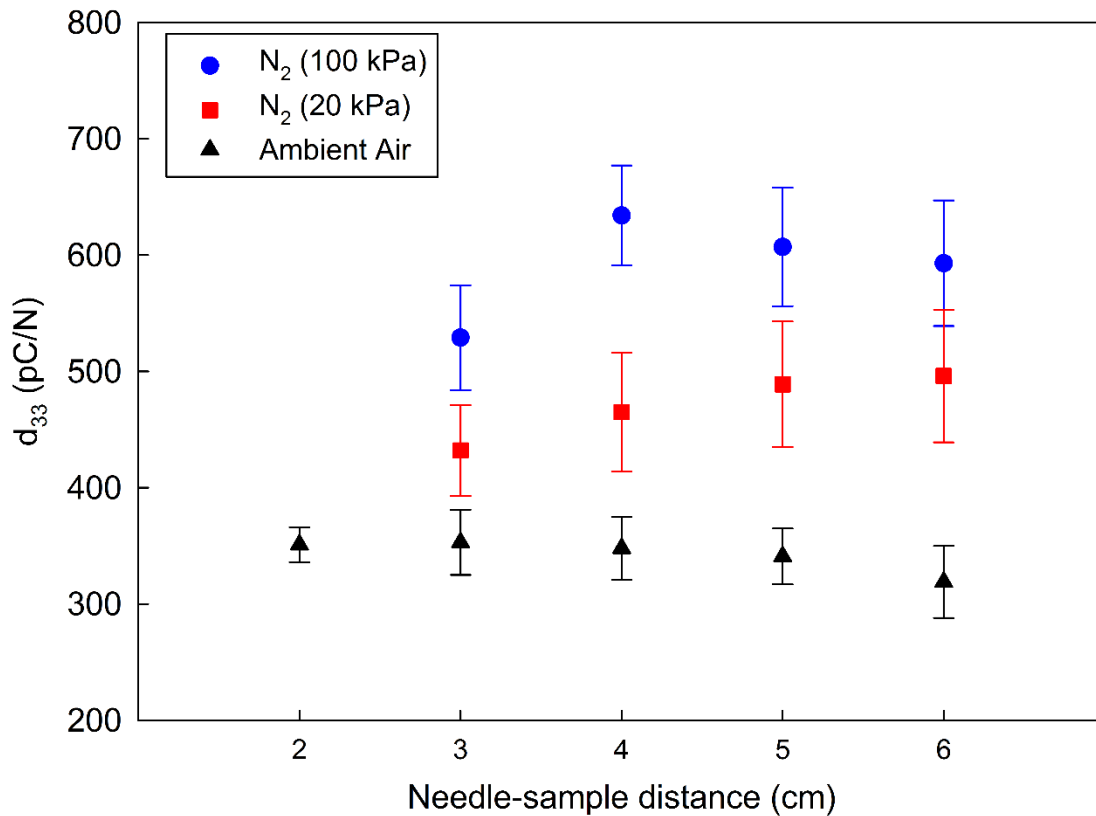


Figure 3.3 Piezoelectric coefficient (d_{33}) as a function of needle-sample distance under air and different N₂ atmospheres.

Under a N₂ atmosphere, the piezoelectric coefficient is influenced by the needle-sample distance. In fact, the charging voltage is more important when a higher N₂ pressure is applied, resulting in higher piezoelectric coefficients. Also, higher N₂ pressure leads to higher gas pressure inside the cells via N₂ diffusion. Therefore, more and more voids exhibit a breakdown field lower than the applied electric field and will get electrically charged, leading to a higher piezoelectric d_{33} coefficient [Paajanen et al. (2001)]. Moreover, the voltage

evolves proportionally to the needle-sample distance. For example, the maximum charging voltage corresponding to a needle-sample distance of 3 cm is -9 kV compared to -15 kV at 4 cm. This is associated to a piezoelectric coefficient increase reaching 634 pC/N at 4 cm (an improvement of about 20%). This charging voltage stabilizes from a certain needle-sample distance (4 cm in our case). However, the piezoelectric coefficient decreases at higher needle-sample distance because nonuniform corona charging occurs over the whole film surface at large distances [Mohebbi *et al.* (2017b)].

This good value (634 pC/N) can mainly be explained by the optimized cellular structure of the S2n-6.4 film. As reported in our previous work, sample S2n-6.4-1.8 has a fine and uniform morphology (relative foam density of 0.62 and high cell density of 5.9×10^6 cells/cm³) with a well-developed eye-like cellular structure (cell AR of around 4 in both longitudinal and transversal directions: AR-L = 4.7 and AR-T = 3.8) which are required for piezoelectric applications. However, the film S2n-3.2-1.8 presents a less-developed eye-like cellular structure (AR-L = 3.0 and AR-T = 2.4) and a lower cell density (3.79×10^6 cells/cm³). This implies less surface area available for charging as well as higher elastic stiffness leading to lower d_{33} (see **Equation 3.1**). It must be noted that d_{33} was measured according to **Equation 3.2** using 2 different pressures (2 and 11 kPa) leading to similar d_{33} values. Therefore, for the next step, only the lowest pressure (2 kPa) was used to determine the piezoelectric coefficient.

3.3.2. Morphology effect on the piezoelectric coefficient and elastic stiffness

Two different TPT were used as postprocessing methods to obtain an optimized eye-like cellular structure with different cell AR as reported in **Figure 3.4**. From these samples, typical SEM micrographs of samples S2n-6.4 and S2n-3.2 before and after the TPT are presented in **Figure 3.4** for both longitudinal (L) and transversal (T) directions. Their corresponding film thickness, cell size (in both L and T directions), AR and cell density, as well as the resulting piezoelectric coefficient are reported in **Table 3.1**. It can be seen in

Figure 3.4 that all the samples had an eye-shaped cell structure due to the biaxial stretching associated to the blown-film extrusion process. The original sample (S2n-6.4), which was the most optimized untreated sample, had an average AR-L of 4.7 and AR-T of 3.8. On the other hand, the treated sample (S2n-6.4-TPT1) presented more elongation in both L and T directions, leading to a 52% increase in AR-L (7.2) and a 21% increase in AR-T (4.7), and showing the effectiveness of TPT1 (stepwise increase of temperature) in further cellular structure stretching. However, TPT2 (rapid increase of temperature) led to a morphological degradation as the cell AR decreased in both directions. In this case, the N₂ molecules did not have enough time to accumulate at cells extremities, leading to a more important expansion in the thickness direction compared to dilatation in the longitudinal and transversal directions. Therefore, less elongated cells with lower AR values were obtained.

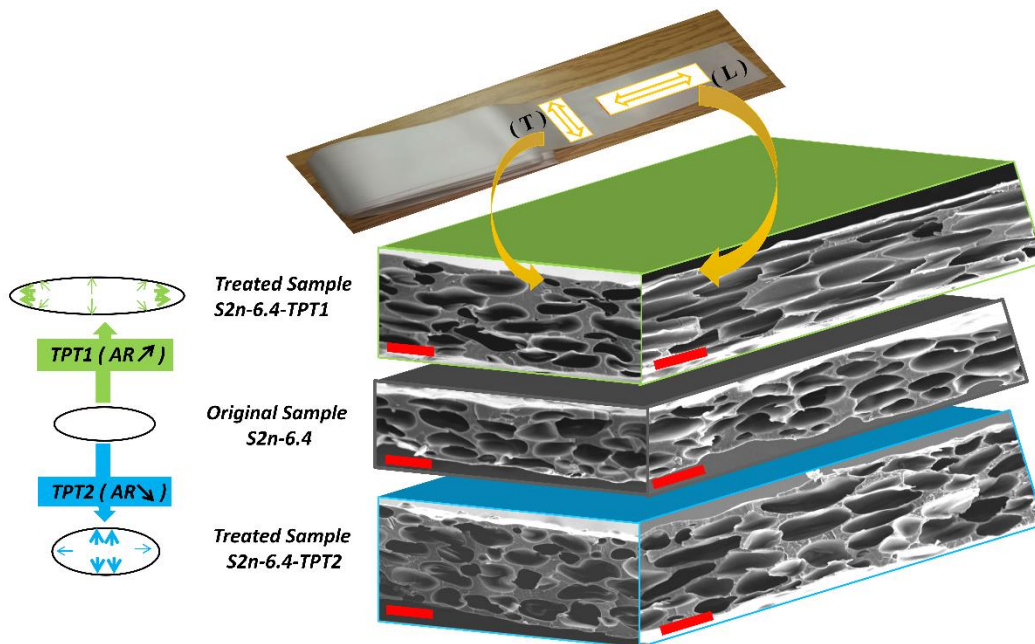


Figure 3.4 Typical structures of the original and TPT samples (S2n-6.4). (Red lines represent a 100- μm scale).

Both TPT were applied on sample S2n-3.2 for comparison, and the same AR trends were observed: a significant cell flattening in both directions (AR-L = 6.6 and AR-T = 4.1) for TPT1 against a cell shape degradation under TPT2 (AR-L = 2.4 and AR-T = 2.4).

As represented in **Table 3.1** and **Figure 3.5**, the values for AR-L and AR-T are linked to the piezoelectric coefficients obtained. A value of 935 pC/N was obtained for S2n-6.4-TPT1. To the best of our knowledge, this piezoelectric coefficient is very high compared to the literature available on polyethylene ferroelectrets (around 400 pC/N) [*Qiu et al. (2008); Tajitsu (2011)*] and better than the best coefficients obtained for PP ferroelectrets (800 pC/N) [*Branaa et al. (2011)*], which are the most developed ferroelectrets. The results are in agreement with the literature stating that the piezoelectric activity is inversely proportional to the cell AR. Several parameters were combined to obtain this value: high cell deformation in both direction (AR-L = 7.2 and AR-T = 4.7), good cell density (48.3×10^5 cell/cm³), and optimized corona charging parameters (charging voltage of -21 kV, needle-sample distance of 4 cm, and charging time of 1 minute under 5 MPa of N₂).

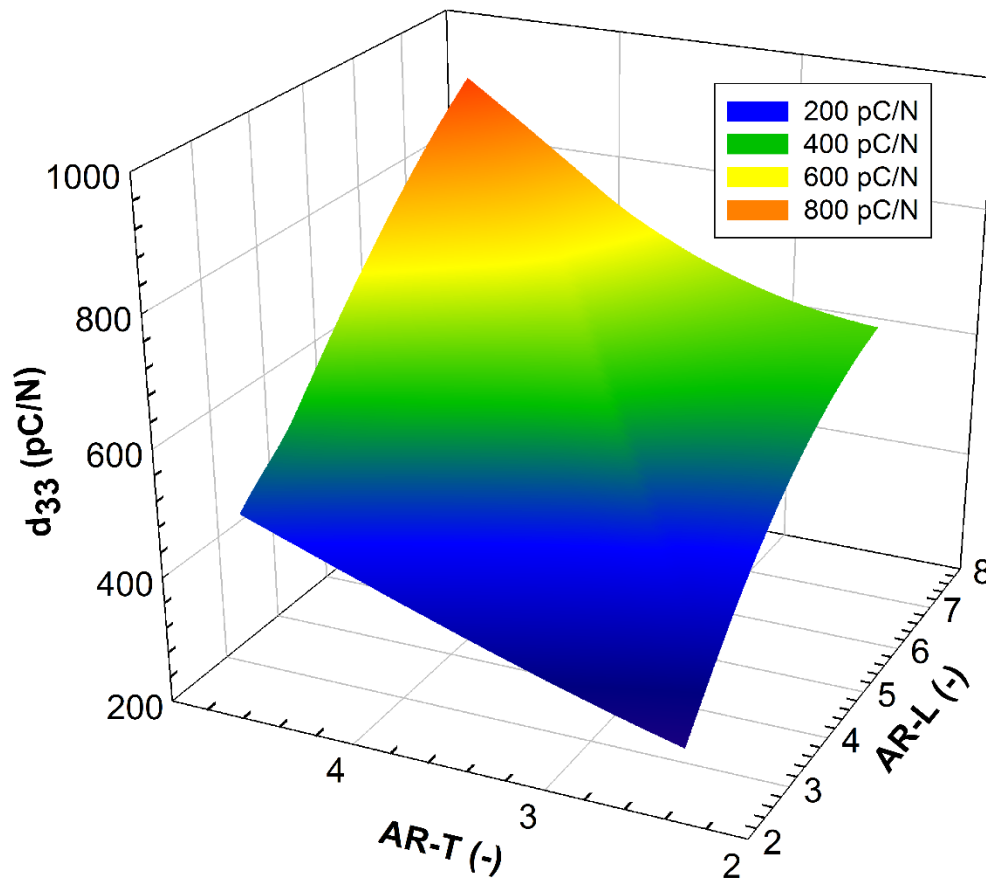


Figure 3.5 Relationships between the piezoelectric coefficient (d_{33}) and the aspect ratio in both longitudinal (AR-L) and transversal (AR-T) directions.

3.3.3 Elastic stiffness and piezoelectric coefficient correlations

The antiresonance frequency was determined by a capacitance analysis (real and imaginary parts) as a function of frequency as presented in **Figure 3.6**. In a typical curve, a resonance peak appears at around 65 kHz for the real (C') and imaginary (C'') components. The same value was obtained for the different samples analyzed, which can be explained by the relatively narrow window of sample densities [Sborikas *et al.* (2013)].

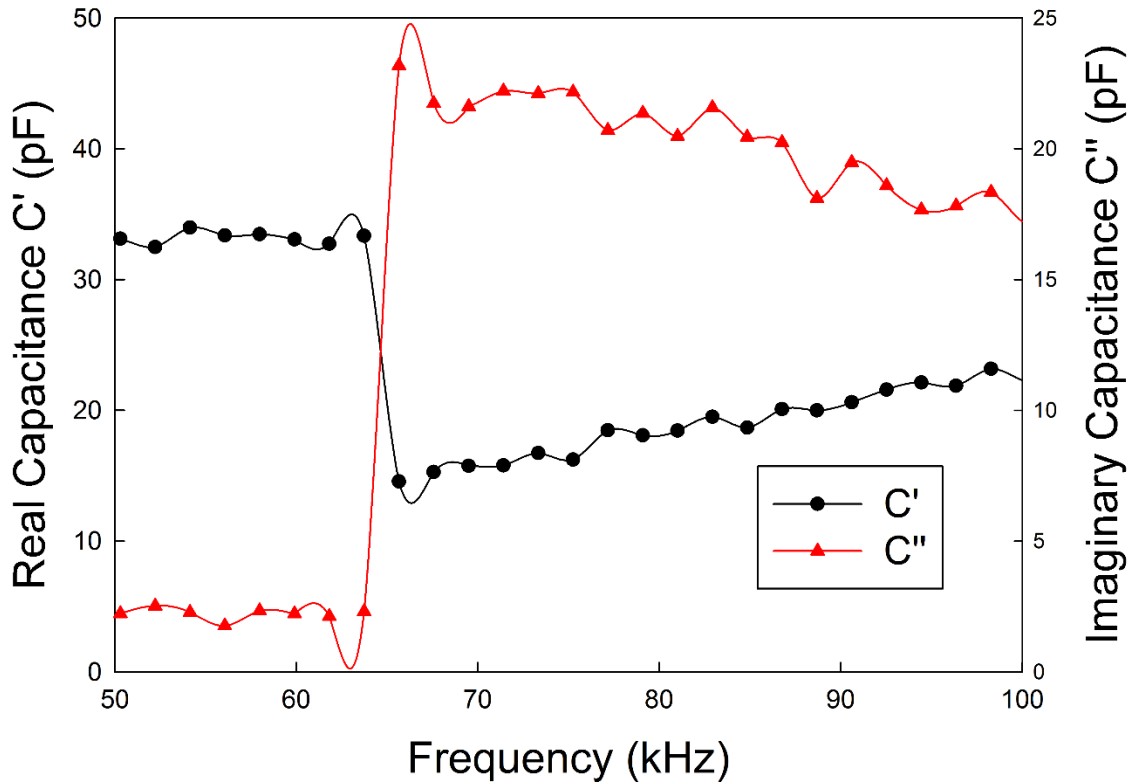


Figure 3.6 Experimental dielectric spectrum of S2n-6.4-TPT1 ferroelectret sample.

Taking into account the film density and thickness, compressive moduli between 0.18 and 1.19 MPa are reported in **Table 3.2**. These values are considered as approximations since **Equation 3.4** strictly holds for homogeneous samples. In any case, the Young moduli of S2n-6.4 and S2n-6.4-TPT1 are much smaller than typical values reported in the literature. This indicates that biaxial stretching was very effective to reduce the elastic stiffness of these films compared to uniaxial stretching. This is in agreement with the literature reporting that Young modulus (c_{33}) is inversely proportional to the cell AR, a/b , where a and b are the cell's length and height, respectively. This means that flatter cells produce lower Young modulus explaining the low values obtained since the cells are stretched in 2 directions [Tuncer (2005)]. To the best of our knowledge, the most optimized c_{33} values reported are 6 MPa for PE ferroelectrets and 0.9 MPa for PP ferroelectrets. [Qiu et al. (2008); Branaa et al. (2011)]. This explains the relatively large d_{33} coefficients obtained in this work for the optimized films.

Table 3.2 Properties of the cellular polyethylene films.

Sample	Antiresonance frequency (f_a) (kHz)	Film density (ρ) (kg/m³)	Film thickness (s) (μm)	Elastic stiffness (c_{33}) (MPa)
S2n-3.2	Around 65	483	266	0.58
S2n-3.2-TPT1		561	174	0.29
S2n-3.2-TPT2		430	401	1.19
S2n-6.4		576	139	0.19
S2n-6.4-TPT1		490	151	0.18
S2n-6.4-TPT2		519	171	0.26

The results obtained confirm that the elastic stiffness (c_{33}) and piezoelectric coefficient (d_{33}) are inversely proportional, and this is in agreement with the literature reporting that “softer” ferroelectret deforms more under pressure, leading to better piezoelectric activity (see **Equation 3.1**). For example, sample S2n-3.2-TPT2 had a relatively high elastic stiffness of 1.16 MPa leading to a d_{33} coefficient of 281 pC/N, while sample S2n-6.4-TPT1 had an optimized elastic stiffness of 0.18 MPa (84% lower) corresponding to a much higher d_{33} coefficient of 935 pC/N (around 3 times higher). Despite its important role, it is clear that the

elastic stiffness is not the only parameter affecting the piezoelectric coefficient (see **Equation 3.1**). Thus, more work would be needed to further understand the effect of film morphology on its piezoelectric activity. For comparison and validation, the d_{33} values from the quasi-static method (**Equation 3.1**) were compared to the resonance method (**Equation 3.4**) using $k_t = 0.073$ as determined via **Equation 3.6** [Neugschwandtner et al. (2000)].

It can be seen in **Table 3.3** that both quasi-static (**Equation 3.2**) and resonance (**Equation 3.5**) methods led to similar d_{33} values (maximum difference of 21%) within experimental uncertainty for these complex structures and measurements. Nevertheless, the resonance method is expected to produce higher uncertainties as several parameters need to be experimentally determined.

Table 3.3 The values of d_{33} determined by two different methods (quasi-static and resonance).

Sample	Quasi-static method (pC/N)	Resonance method (pC/N)	Difference (%)
S2n-3.2	354	428	21
S2n-3.2-TPT1	783	605	-23
S2n-3.2-TPT2	281	299	6
S2n-6.4	634	747	18
S2n-6.4-TPT1	935	768	-18
S2n-6.4-TPT2	568	639	13

3.3.4. Improving the d_{33} piezoelectric coefficient by using reverse charging

To further optimize the samples produced, another optimization step was investigated: multiple charging on a single film. In this technique, the films were charged 2 times by reversing their position (flip-over) under the corona discharge. So a first corona discharge was applied for 60 seconds under the optimized conditions described in **Section 3.3.1**, and the exposed side to the corona discharge was metallized to neutralize surface charges and preserve internal charges [Tajitsu (2011)]. The sample was then placed upside down under the corona charging setup and charged again under the same conditions. Thus, the firstly exposed and metallized side is now the grounded side of the sample. In this case, the internal electric field is reversed in the cells and added to the initial external applied electric field. This results in a modification of the gas breakdown dynamics inside the cells inducing stronger internal discharges and higher surface charge [Tajitsu (2011)]. The newly exposed side is then metallized, and the sample is removed for characterization.

Since the literature also reports that multilayered ferroelectret films give better d_{33} piezoelectric coefficient than a single layer [Qiu et al. (2007b)], three-layer films of the final sample with optimized conditions were superposed by attaching the positive and negative charges to the surface with the same charge. The d_{33} coefficient obtained was around 2550 pC/N, which is the best value obtained of all our samples. Obviously, the output of each single cellular PE film is added in the hybrid system; therefore, the piezoelectric sensitivity of the hybrid multilayer system is the sum of each single cellular PE film. This charging method provides good results, as seen in **Table 3.4**, with a 54% improvement of the piezoelectric d_{33} coefficient for two time charged films. Furthermore, the d_{33} coefficient was multiplied by 3 in the case of multilayered film (3 layered/2 time charged sample) reaching a very high value of 2550 pC/N. For the latter, a relatively higher standard deviation was obtained because the layer assembly is very sensitive and requires special precautions to eliminate interfacial defects. This procedure can also be optimized in future works. Finally, the complete process from film manufacturing to characterization is summarized in **Figure 3.7**.

Table 3.3 Piezoelectric coefficient (d_{33}) of multicharged cellular polyethylene films.

Sample S2n-6.4-TPT1	d_{33} (pC/N)
1 time charged	935 (54)
2 time charged	1440 (180)
3 layered/2 time charged	2550 (420)

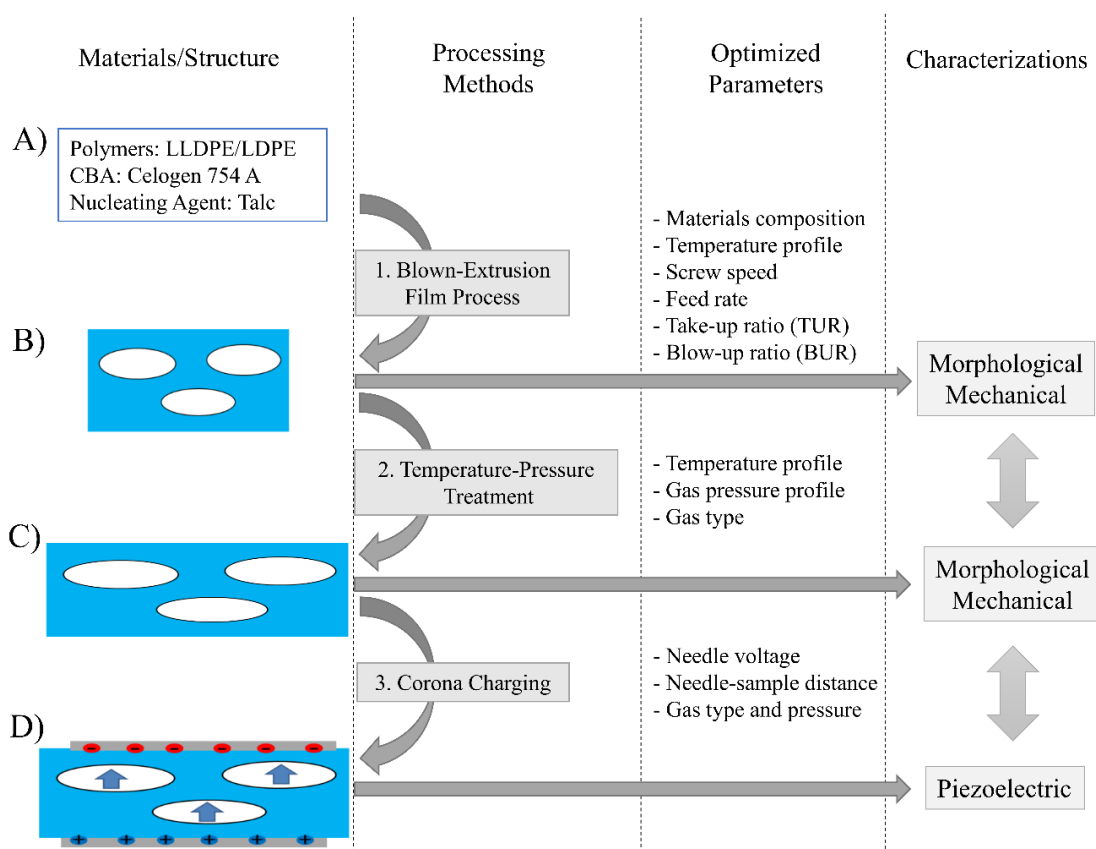


Figure 3.7 Schematic representation of the developed process from manufacturing to characterization: (A) materials used, (B) biaxially stretched cellular PE films manufactured via optimized extrusion-blown film process, (C) cellular PE films with optimized morphology following a postprocessing temperature-pressure treatment (TPT), and (D) charged PE cellular films (ferroelectrets).

3.4. CONCLUSION

In this work, biaxially stretched polymer foams with well-defined cellular structures were prepared from polyethylene (PE) via an optimized blown-film extrusion process. The effect of corona charging parameters and the temperature/pressure as a postprocessing treatment on the piezoelectric response was then investigated. For the optimized samples produced, a substantial improvement of the d_{33} coefficient was obtained by a combined multiple and reverse charging method reaching a maximum of value of 2550 pC/N.

The originality of this work lies in its treatment of all the steps leading to optimized ferroelectret films: the cellular structure manufacturing (biaxially stretched cellular films using optimized extrusion-blown film process), postprocessing treatments (thermal-pressure treatment), and linking the morphological, mechanical, and piezoelectric properties together to obtain the best piezoelectric coefficient. The choice of polyethylene is also innovative since it is very seldom studied as a ferroelectret material. The obtained results are considered as an important development in the production of ferroelectrets based on low-cost materials like polyethylene. Therefore, it can be a very attractive material for the large-scale production of electret-based sensors and transducers.

For future developments, gases with higher electrical strength than N_2 should be tested, as they can better retain high effective charge density. Another recommendation is to develop a mechanism allowing more stretching in both longitudinal and transversal directions to determine the limits of d_{33} optimization. It should also be noted that the piezoelectric coefficient is not the only parameter controlling the ferroelectrets quality, as piezoelectric stability in terms of temperature and time stability is also important. This behavior is currently being optimized, and the results will be reported in a future paper.

ACKNOWLEDGEMENTS

Financial support from the Natural Sciences and Engineering Research Council of Canada (NSERC) and Fonds Québécois de la Recherche sur la Nature et les Technologies (FRQNT) was received for this work. Material samples were kindly supplied by Exxon Mobil (LLDPE), Nova Chemicals (LDPE), and Imerys (talc). The technical support from Mr. Yann Giroux is highly appreciated.

CHAPITRE 4. TIME AND THERMAL STABILITY IMPROVEMENT OF POLYETHYLENE FERROELECTRETS

RÉSUMÉ

Des ferroélectrets avec de bons coefficients piézoélectriques ont été produits à base de polyéthylène cellulaire (PE) en utilisant le procédé d'extrusion-gonflage. La valeur du coefficient piézoélectrique quasi statique (d_{33}) obtenue (935 pC/N) est bien supérieure aux valeurs typiques du polypropylène (PP) qui est le polymère le plus utilisé pour les applications piézoélectriques. On essaie ici d'améliorer la stabilité du coefficient piézoélectrique en fonction de la température et du temps. Pour ce faire, des traitements ont été appliqués sur les films afin d'améliorer leur microstructure. Tout d'abord, la cristallinité des films a été augmentée via un recuit thermique à 80°C pendant 5 minutes, ce qui a entraîné une augmentation de 32% de la valeur initiale du d_{33} et une certaine amélioration de sa stabilité temporelle. Cependant, le traitement thermique n'a pas apporté d'amélioration significative de la stabilité thermique, puisque les films traités ont presque complètement perdu leur activité piézoélectrique (96%) à 80°C. Par conséquent, les films ont été traités avec de l'acide orthophosphorique, ce qui a entraîné des améliorations substantielles de la stabilité de la charge, en particulier à une température plus élevée. Globalement, il a été possible d'augmenter la température de service continu (CST) des ferroélectrets à base de PE de 40 à 80°C, ce qui est similaire au CST typique du PP.

ABSTRACT

Ferroelectrets with good piezoelectric coefficients have been produced based on cellular polyethylene (PE) via extrusion film blowing. The quasi-static piezoelectric coefficient (d_{33}) value obtained (935 pC/N) was well above typical values for polypropylene (PP), considered as the workhorse of piezoelectric polymers. Here, a focus is made at increasing the time and thermal stability of their piezoelectric activity. To do so, treatments were applied on the films to improve their microstructure. Firstly, films crystallinity was increased via thermal annealing at 80°C for 5 minutes, leading to a 32% increase of the initial d_{33} value as well as its time stability. However, thermal treatment did not give a significant thermal stability improvement, since the treated films almost completely lost their piezoelectric activity (96%) at 80°C. Therefore, the films were treated with orthophosphoric acid resulting in substantial charge stability improvements, especially at higher temperature. Overall, it was possible to increase the continuous service temperature (CST) of PE ferroelectrets from 40 to 80°C which is similar to the typical CST of PP.

Keywords: Polyethylene; ferroelectrets; piezoelectric stability; chemical and thermal treatments.

Ouassim Hamdi, Frej Mighri, Denis Rodrigue (2018d) Time and thermal stability improvement of polyethylene ferroelectrets. *Journal of Applied Polymer Science*. Submitted.

4.1. INTRODUCTION

Cellular polymers (or polymer foams) are two-phase expanded polymers containing a gaseous phase in the form of bubbles (or cells) dispersed in a solid continuous phase (polymer matrix). Cellular structures are generally produced by the introduction of a blowing agent (chemical or physical) in a polymer matrix [Notario et al. (2016); Coccorullo et al. (2008); Mohebbi et al. (2015)]. In addition, different types of particles can be added, such as nucleating agents, to improve the processability and final structure. It is known that the cellular morphology is the main parameter controlling foam properties such as light weight, excellent specific stiffness, high fatigue life, thermal stability, acoustic/electrical/thermal insulation and so on [Collias et al. (1995); Colton et al. (1987a)].

The concept of ferroelectrets, which are electrically charged non-polar cellular films exhibiting good piezoelectric activity, has gained increasing attention recently [Graz et al. (2016); Kirjavainen (1987)]. These materials can be used as sensors or actuators by conversion between electrical and mechanical signals. A detailed review on ferroelectrets processing and properties is available in our previous review article [Hamdi et al. (2018a)].

Recently, a high number of foamed polymers (such as polyesters and fluoroethylenepropylene) have been developed and identified as ferroelectrets [Rychkova et al. (2012)]. But polyolefins, such as PE and PP, have several advantages like their lower costs, better processability and they are more environmentally friendly (mostly recyclability) than other polymers such as fluorocarbons [Rychkova et al. (2012)]. While cellular PP is already an established ferroelectret material, the piezoelectric properties of PE have not been intensively investigated [Nakayama et al. (2009); Tajitsu (2011); Altafim et al. (2012)]. The main reason for this is the low thermal and time stability of the stored charges in this polymer. In fact, the literature reports that the piezoelectric coefficient of cellular PE films starts to decay rapidly around 40°C (compared to 60°C for PP), while at 90°C these ferroelectrets lose almost completely their electric charge (decaying to zero at 100°C) [Rychkova et al. (2012); Paajanen et al. (2000); Neugschwandtner et al. (2001)].

The stability of the piezoelectric coefficient of ferroelectrets is a critical factor from an application point of view. This electromechanical property originates from the charges

between electric dipoles and from the cellular structure, which can change the dipole moment in response to an external stress [Qui (2016); Thyssen et al. (2015); Fang (2010); Mellinger et al. (2006); Harris et al. (2014)]. Obviously, the cellular structure stability is limited by temperature when approaching the polymer melting point (T_m).

However, T_m is generally much higher than the temperature of charge de-trapping, which depends on both chemical composition and structure of the polymer matrix. At higher temperatures, the charges have more thermal energy leading to their mobility and eventually to de-trapping; the higher the temperature, the more charges are lost. In fact, the interfaces between amorphous and crystalline regions in the polymer are believed to be obstacles to electric charge drift [Qui (2016); Thyssen et al. (2015); Fang (2010); Mellinger et al. (2006); Harris et al. (2014)]. Therefore, a film with more interfacial area should better retain its charge, producing stronger and more stable piezoelectric effects. Similarly, it was shown that a higher crystallinity degree gives a better charge stability as a function of temperature and time [Qui (2016)].

Different chemical treatments have also been used for surface modification of ferroelectrets. This modification was shown to be efficient at improving the charge trapping stability. In fact, the treatment of PP ferroelectret with fluorine gas or PE ferroelectrets with phosphorus trichloride (PCl_3) or orthophosphoric acid (H_3PO_4) all resulted in significantly enhanced charge stability in terms of temperature and time [Qui (2016); Thyssen et al. (2015); Fang (2010); Mellinger et al. (2006); Harris et al. (2014)]. For instance, the half-value temperature (i.e. the temperature at which the surface potential decays to half of its initial value) for PE films treated with PCl_3 vapors was found to increase by 55°C compared to virgin films. PE modification with H_3PO_4 also led to significant thermal stability enhancement by about 60°C [Qui (2016)].

In our previous work [Hamdi et al. (2018b); Hamdi et al. (2018c)], cellular films based on PE with high piezoelectric properties ($d_{33} = 935$ pC/N) were successfully produced by controlling the cellular morphology in terms of the cells aspect ratios in both the longitudinal and transversal directions, as well as the cell density and the film density. The d_{33} values

obtained were well above typical values for PP (around 800 pC/N [Mohebbi *et al.* (2017c)]) considered as the workhorse of piezoelectric polymers. However, to use PE as a substitute for PP, the optimization of the charge stability, which is the main objective of this work, is of the utmost importance. To do so, thermal and chemical treatments were applied to determine their effect on the time and thermal stability of cellular PE piezoelectric activity.

4.2. EXPERIMENTAL

4.2.1. Materials used and film preparation procedure

The material used in this study was a biaxially stretched foamed PE film with an eye-like cellular morphology. A blend of linear low-density polyethylene (LLDPE 8555 from Exxon Mobil Chemical, Irving, TX, USA) and low density polyethylene (LDPE LF-0219-A from NOVA Chemicals, Calgary, AB, Canada) was used as the matrix polymeric system.

The samples were produced through an optimized continuous chemical foaming process via extrusion film blowing using 2% of Celogen 754A (Lion Copolymer Company, USA) as a chemical blowing agent and talc (Jetfine 3CC, Imerys Talc, USA) as a nucleating agent. A thermal pressure treatment (TPT) was applied to improve the films morphological properties: a stepwise temperature increase at constant pressure (5 MPa). The temperature was increased from 25 to 81°C at a rate of 19°C/10min then maintained at 81°C for 14 min for stabilization. Then, the pressure was kept constant during sample slow cooling until ambient temperature to retain the final cell structure produced. This phase took about 2 h. Finally, a corona charging process was imposed to give the films piezoelectric properties. The samples were charged under nitrogen (N₂) at a pressure of 100 kPa with a needle-sample distance of 4 cm, which was shown to give the best piezoelectric properties. More details on the film production and morphological analysis can be found in our previous work [Hamdi *et al.* (2018c)]. The optimized film had a good piezoelectric coefficient d_{33} reaching 935 pC/N for film S1 (previously coded 2n-6.4-TPT1 in [Hamdi *et al.* (2018c)]). This sample has a density of 490 kg/m³, a longitudinal cell aspect ratio (AR-L) of 7.2, a transversal cell aspect ratio (AR-T) of 4.7 and a cell density of 4.83x10⁶ cell/cm³.

Annealing is a process where a sample is brought to a certain temperature, kept for a period of time and then cooled to room temperature [Ghassemi *et al.* (2017)]. Generally, annealing influences polymer microstructure. This method was used to increase the cellular film crystallinity. An oven was used to increase the cellular PE film temperature (50 and 80°C). The effect of annealing time was also studied by leaving the samples in the oven for different periods (1 to 60 min). The specimens were finally cooled to room temperature and used for characterization. The annealed samples were coded according to the annealing temperature and time. For example, S1-80-5 refers to sample S1 annealed at 80°C for 5 min.

A chemical treatment was also performed to improve the piezoelectric stability. The PE cellular films were treated with orthophosphoric acid PA (H₃PO₄, 85% concentration, Fisher Chemical, China) through complete immersion for 24 h at 60°C [Rychkova *et al.* (2012)]. After removal from the acid, film surfaces were thoroughly rinsed with water. The samples treated with phosphoric acid were coded by adding PA. For example, S1/PA-80-5 refers to sample S1 treated by phosphoric acid and then annealed at 80°C for 5 min, while S1-80-5/PA is the sample thermally and then chemically treated at the mentioned conditions.

4.2.2. Differential Scanning Calorimetry (DSC) characterization

A differential scanning calorimeter DSC7 (Perkin Elmer, USA) was used to study the crystallinity degree of the cellular PE films. Around 5 mg of each specimen was placed in aluminum pans and then heated from 50 to 180°C at 10°C/min. The degree of crystallinity (X_c) was calculated as:

$$X_c = \frac{\Delta H_{exp}}{\Delta H^*} * \frac{1}{w_f} \quad (4.1)$$

where ΔH_{exp} is the experimental heat of crystallization, ΔH^* is the enthalpy of the fully crystalline PE ($\Delta H^* = 293$ J/g [Mark (2004); Rigato *et al.* (2012)]) and w_f is the PE weight fraction in the composite/blend.

4.2.3. Piezoelectric coefficient measurement

The piezoelectric coefficient is defined as the electric charge density generated per unit stress (or pressure) applied across the material at zero or very low frequency (few Hz) as:

$$d_{33} = Q/F = \sigma/p \quad (4.2)$$

where Q (C) is the charge generated on the electrodes, F (N) is the applied force and σ (C/m²) is the charge density generated upon applying a mechanical pressure p (Pa). A quasi-static setup was used to measure the piezoelectric coefficient d_{33} by applying a direct piezoelectric effect. A force of 0.5 N was applied to the sample and the induced charge was detected by a programmable electrometer (Keithley 6514, USA). The procedure was repeated three times for each sample and the average values with their standard deviations are reported.

4.2.4. Fourier-transform infrared (FTIR) spectroscopy characterization

The infrared spectra were recorded with a Nicolet Magna 860 Fourier transform spectrometer (Thermo-Nicolet, USA) to detect any changes in the chemical composition of the chemically treated PE surface [Bernard *et al.* (2007)]. A total of 128 interferograms were acquired, co-added and Fourier -transformed, using a Happ-Genzel apodization function to give a spectral resolution of 4 cm⁻¹ in the spectral range of 3800 to 800 cm⁻¹. The data were processed by the Grams 386 software (Galactic Industries Corporation, USA).

4.2.5. Morphological and density characterizations

A JEOL JSM-840A scanning electron microscope (SEM) was used for the morphological characterization in both longitudinal (L) and transversal (T) directions. First, cryogenic fracture of the film was done in liquid nitrogen. Then, the fractured surface was coated with a thin layer of Au/Pd and images were taken at different magnifications. The cells were approximated as ellipsoids and the major/minor axes were extracted via the Image Pro Plus software. Due to cell deformation, the cell density (N , cells/cm³) was approximated by [Gosselin *et al.* (2005)]:

$$N = N_1 * (N_2)^{\frac{1}{2}} \quad (4.3)$$

where N_1 and N_2 (cells/cm²) are the surface cell densities in the longitudinal and transversal directions, respectively.

A Quantachrome (USA) Ultrapyc 1200e gas (nitrogen) pycnometer was used to measure the foam density. The reported values correspond to the average of a minimum of five measurements.

4.3. RESULTS AND DISCUSSION

4.3.1. Effect of the annealing temperature and time on crystallinity

Thermal annealing at temperatures between the glass transition (T_g) and melt temperature (T_m) is a common strategy to improve the crystallinity of semi-crystalline polymers. The lower the heating temperature, the longer the time needed to achieve maximum crystallinity. However, annealing using temperatures closer to T_m can cause undesirable melting and recrystallization (i.e. loss of existing crystallites) [Viswanath *et al.* (2016)]. A compromise should be made to determine the best temperature/time combination for annealing.

Figure 4.1 shows the degree of crystallinity (%) of the sample S1 as a function of annealing time and temperature. The results show the expected behavior: the crystallinity initially increases until a maximum is reached, followed by a decrease at longer time. This drop is explained by the over-melting effect which destroys the existing crystallites leading to non-ideal recrystallization [Viswanath *et al.* (2016)]. Between these extremes, a maximum value of 41% and 32% was respectively achieved after 5 min of annealing at 80°C and 50°C, compared to the untreated sample which has a crystallinity of 31% (dashed line on **Figure 4.1**).

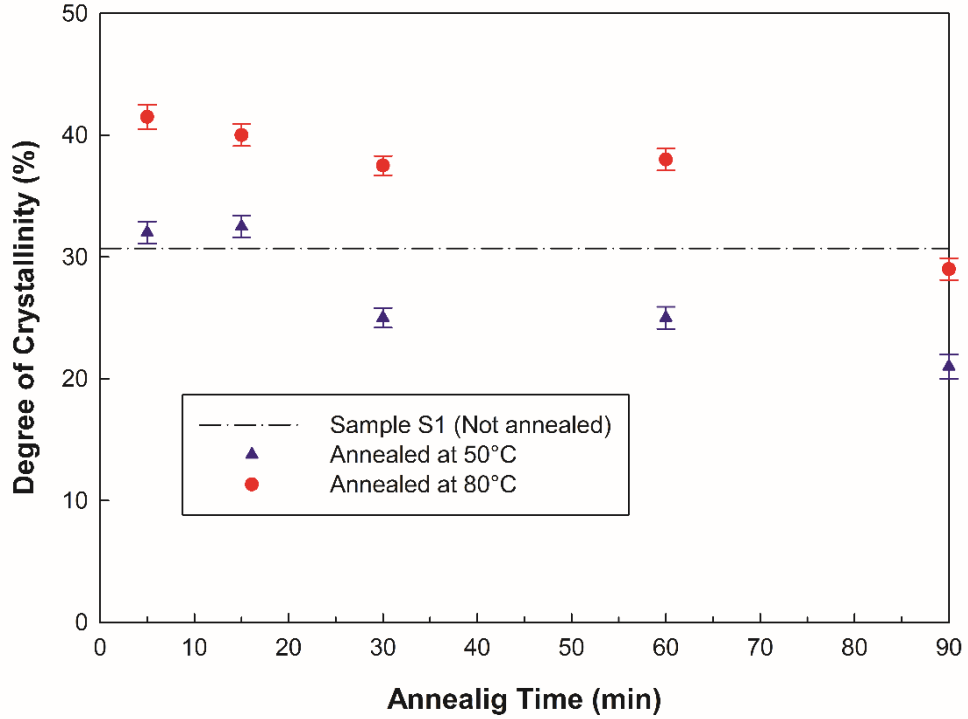


Figure 4.1 Effect of annealing temperature and time on PE cellular films crystallinity.

4.3.2. Effect of polymer crystallinity on the piezoelectric stability of the cellular film

Figure 4.2 shows the long-term decay of the piezoelectric d_{33} coefficient at room temperature for samples S1 (degree of crystallinity = 30.7%) and S1-80-5 (degree of crystallinity = 41.5%). Curve fitting (dashed lines) of the experimental results was performed with SigmaPlot 11.0 using the following exponential equation:

$$d_{33} = y_0 + a * \exp(-bt) \quad (4.4)$$

where t is the characterization time (days) and the corresponding fitting parameters y_0 (pC/N), a (pC/N) and b (day^{-1}) for both characterized samples S1 and S1-80-5 are presented in **Table 4.1**. The coefficient of correlation (R^2) is close to 0.99 in all cases.

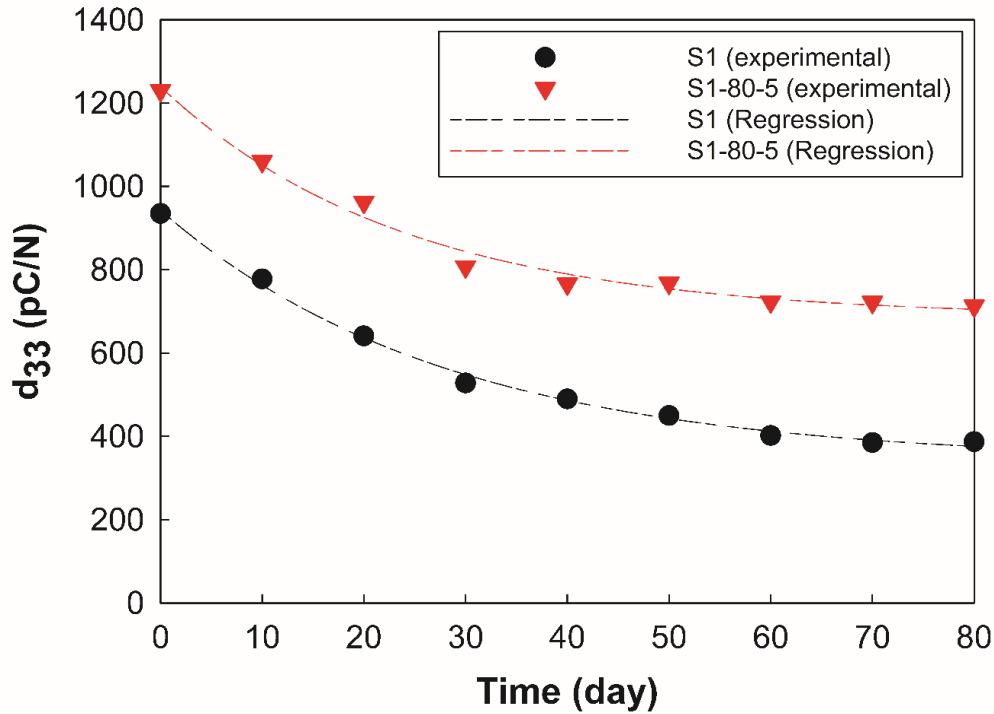


Figure 4.2 Variation of the piezoelectric coefficient with respect to time.

Table 4.1 Fitting parameters for **Equation 4.4** based on the data of **Figure 4.2**.

Sample	y_0 (pC/N)	a (pC/N)	b (day ⁻¹)	R^2
S1	340	602	0.0355	0.996
S1-80-5	685	554	0.0418	0.985

The d_{33} decay rate decreases with time and 48% of the initial value is retained after 50 days for sample S1 compared to 62% for sample S1-80-5. Similarly, the value of y_0 (which can be associated to the stabilized value of d_{33}) for the sample S1-80-5 is higher than that of sample S1, not only in terms of absolute value (685 pC/N compared to 340 pC/N), but also in terms of the retained percentage (55% compared to 37%). Nevertheless, both samples decay at the same rate since their time constants (b) are similar (0.036 vs. 0.042 day⁻¹).

The results of **Figure 4.2** show that increasing the crystallinity significantly improved the time stability of PE ferroelectrets. Moreover, the initial value of the piezoelectric coefficient for S1-80-5 (1230 pC/N) is higher by around 32% than that of the sample S1 (935 pC/N).

However, the annealing treatment did not give enough thermal stability improvement since the treated film almost lost all their piezoelectric activity (around 96%) at 80°C. Therefore, chemical treatment was performed and its effect on the thermal stability of the samples is presented in the following sections.

4.3.3. Effect of the chemical treatment on piezoelectric stability of the cellular films

Chemical treatment with phosphoric acid is believed to improve the piezoelectric properties mainly in terms of thermal stability [Qui (2016)]. As mentioned above in Section II, our samples were treated at 60°C for 24 h and the three following combinations of chemical and thermal treatments have been used:

- (1) Chemical treatment was directly applied to sample S1 (coded S1/PA).
- (2) Annealing was applied to S1 before chemical treatment (sample coded S1-80-5/PA).
- (3) Chemical treatment was applied to S1 before annealing at 80°C for 5 min (coded S1/PA-80-5).

Table 4.2 shows the density, the thickness and the aspect ratio (AR) in both longitudinal (L) and transversal (T) directions of untreated and chemically treated S1 samples. The results show that samples S1/PA, S1-80-5/PA and S1/PA-80-5 presented very similar morphology compared to S1-80-5. These samples were slightly thicker (~ 162 µm) with lower density (~ 450 kg/m³) compared to S1 with a crystallinity of around 37%. Their cell AR slightly decreased in the longitudinal (by around 2%) and transversal (12%) directions. This confirms the assumption that the cells of S1 were inflated during the first few minutes of their exposure to a high temperature (60°C for the chemical treatment or 80°C for the thermal treatment). This is why only the morphology of S1/PA sample was presented and discussed here as representative of the treated sample. Its typical cellular structure and morphological properties are presented in **Figure 4.3** and **Table 4.2**, respectively.

Table 4.2 Morphological parameters of untreated and treated samples S1. (Values in parentheses represent standard deviations).

Sample code	Film density (kg/m ³)	Film thickness (μm)	AR-L (-)	AR-T (-)
S1	490 (14)	151 (4)	7.2 (2.9)	4.7 (1.9)
S1-80-5	443 (11)	158 (9)	6.9 (2.2)	3.9 (1.1)
S1/PA	450 (8)	162 (11)	7.0 (2.2)	4.1 (1.2)
S1/PA-R	437 (9)	166 (3)	7.1 (3.0)	3.7 (1.0)
S1-80-5/PA	440 (6)	165 (10)	6.9 (1.8)	3.9 (0.9)

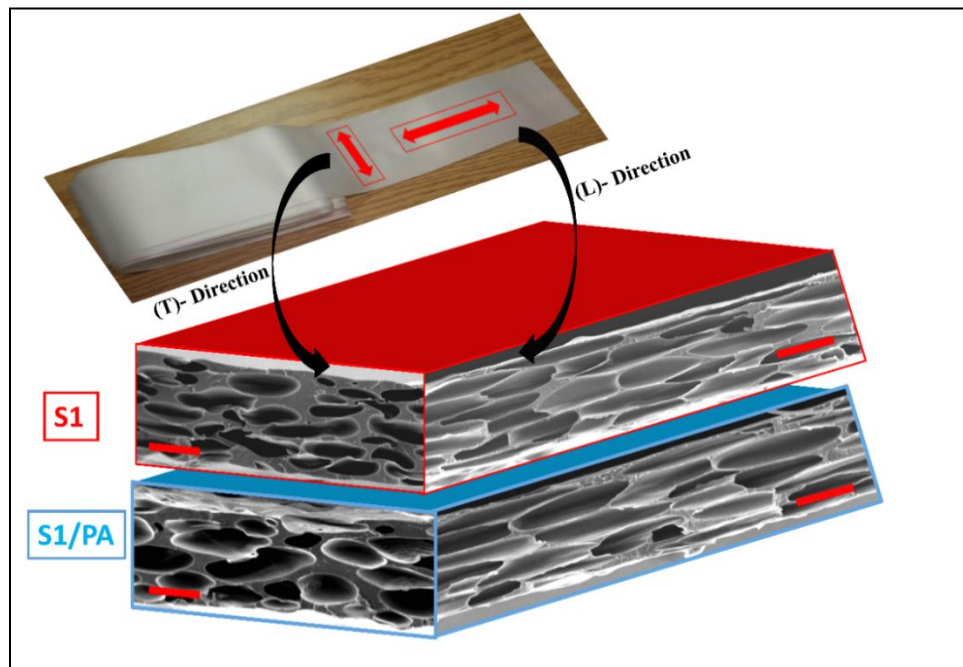


Figure 4.3 Typical cellular structures of the untreated sample (S1) and treated sample (S1/PA). Red lines represent a 100 μm scale.

Table 4.3 and **Figure 4.4** present the positive effect of the chemical treatment on the piezoelectric coefficient thermal stability. In fact, d_{33} substantially decrease by 71%, 87% and 96% when sample S1 is placed for 1 h in an oven at 40, 60 and 80°C, respectively.

However, when the sample is chemically treated, smaller decreases were observed for S1/PA: 11%, 27% and 79%, respectively. Thus, a piezoelectric coefficient of 280 pC/N at 80°C is obtained, which is still a relatively good value despite the decrease recorded. Moreover, S1/PA also presented good results in terms of time stability (similar S1-80-5). In fact, this sample led to a d_{33} stabilization after 50 days at a value of 792 pC/N (i.e. 60% of its initial value compared to 62% for S1-80-5). This confirms that the chemical treatment was more efficient than the thermal one, since it enhanced both time and thermal stability (**Table 4.3**).

Table 4.3 d_{33} (pC/N) of the untreated and treated samples as a function of temperature. (Values in parentheses represent standard deviations).

Conditions	S1	S1-80-5	S1/PA
20°C	935 (54)	1230 (76)	1315 (92)
40°C	270 (62)	307 (51)	1170 (110)
60°C	124 (17)	120 (22)	959 (77)
80°C	44 (17)	46 (19)	280 (55)
After 50 days at 20°C	450 (50)	768 (79)	792 (76)

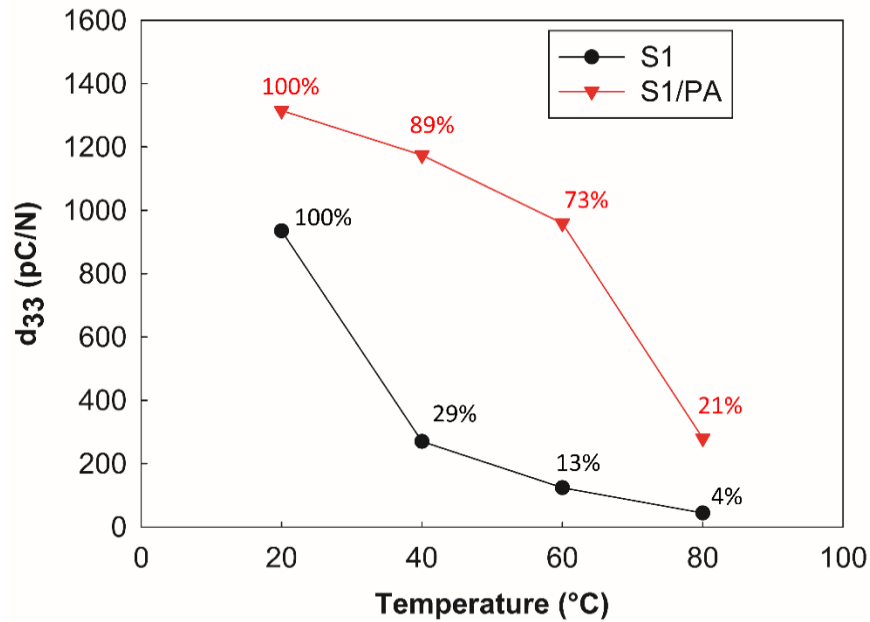


Figure 4.4 Piezoelectric coefficient d_{33} and its corresponding decrease in (%) at different temperatures.

Figure 4.5 presents three SEM pictures of S1/PA sample at various magnifications to identify the effect of the chemical treatment on the microstructure and to understand the origin of the d_{33} improvements. Sample S1 presents some nanometric cavities on the films surface and internal cell walls. This texture change is related to the phosphoric acid attack. In fact, previous work showed that H_3PO_4 treatments shift the surface-charge decay in LDPE to higher temperatures by up to $60^\circ C$ due to the generation of island-like structures containing phosphorus and oxygen, resulting in deeper surface traps [Rychkov *et al.* (2011); Anta *et al.* (2002); Meunier *et al.* (2001)].

This surface chemical composition change of the chemically treated PE surface can also be clearly seen in the FTIR spectra of **Figure 4.6**. In the main figure, the FTIR spectrum of S1/PA was slightly translated downwards with respect to the S1 spectrum in order to differentiate the curves since they are practically identical from 1400 to 3800 cm^{-1} . In the inset, spectra between 800 to 1400 cm^{-1} are shown with their corresponding transmittances. Sample S1/PA treated with orthophosphoric acid exhibits an absorption band between 1020 and 1260 cm^{-1} , a broad band attributed to the stretching vibrations of phosphorus-containing structures ($P=O$ and $P-O-CH_3$) [Rychkova *et al.* (2012)]. Such changes on the surface of a polymer film can create potential barriers in the band structure of polymer electrets and better charges capture. In fact, these structures (phosphorus-containing groups) act as energetically deep traps leading to improved electret stability. These traps are deeper than those present in the non-treated samples. The formation of these new traps is attributed to changes in the chemical composition of the polymer surface because of the treatment. Indeed, molecular-modelling calculations reported that traps related to chemical defects and impurities are deeper than the so-called physical traps (in our case developed via chemical blowing agent) [Rychkov *et al.* (2011); Anta *et al.* (2002); Meunier *et al.* (2001)].

Therefore, when the charges escape shallow traps, they move across a short distance laterally or transversally to be trapped in the nearest new deep trap, which explains the difference between the untreated and treated samples. Another possible reason for the better electret charge stability of the phosphoric acid treated sample is a decrease in PE molecular mobility.

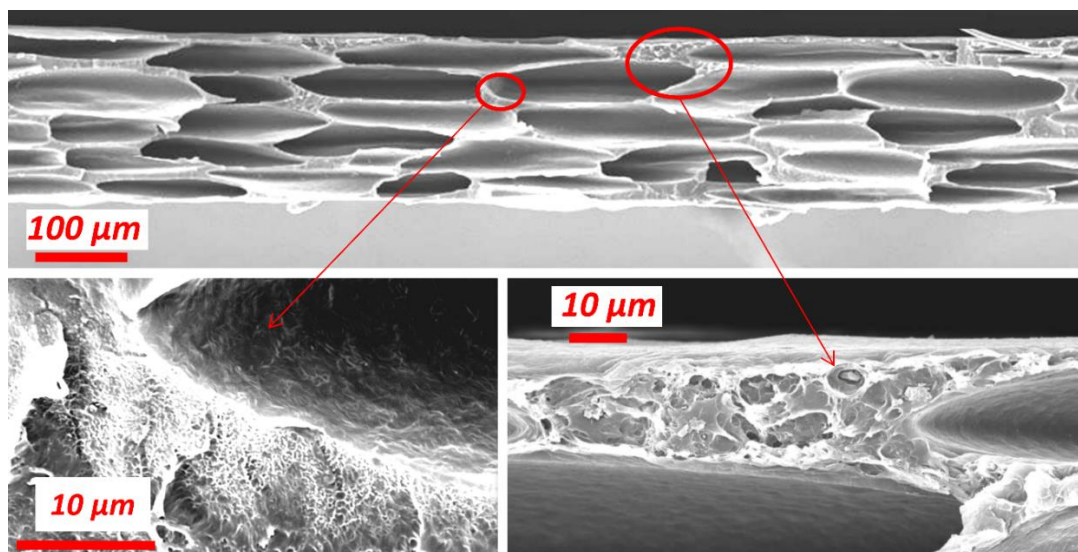


Figure 4.5 Typical SEM pictures of sample S1/PA at different magnifications.

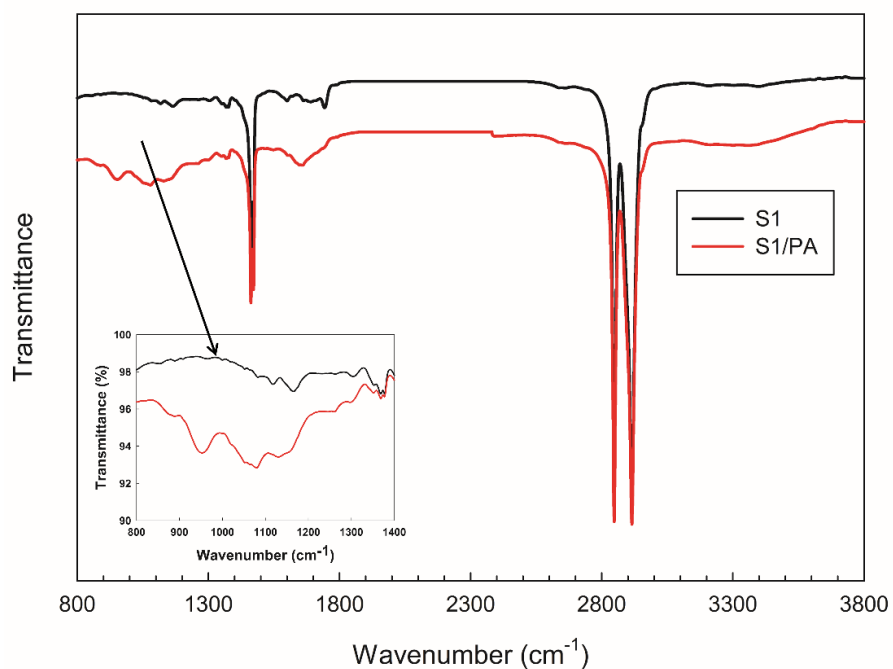


Figure 4.6 FTIR spectra of samples S1 and S1/PA.

It has been reported that phosphorus-containing structures have a dipole moment facilitating intermolecular interactions [Anta *et al.* (2002); Meunier *et al.* (2001)]. This might be the structural origin for the deeper traps formed during the modification. The attachment of new chemical structures to the surface molecules also decreases the molecular mobility, another

possible reason for the overall enhancement of the charge stability [Qiu *et al.* (2008)]. All these factors decrease the probability of thermal activation of charges from the surface traps, allowing an important fraction of these charges to stay on the modified surface, even up to 80°C, despite being close to the PE melting temperature.

4.3.4. Improvement of d_{33} piezoelectric coefficient using reverse charging and multi-layered films

As described in our previous work [Hamdi *et al.* (2018b); Hamdi *et al.* (2018c)], two charging techniques can be combined to improve the piezoelectric coefficient. Firstly, the films were charged two times by reversing their position (flip-over) under the corona discharge (reverse charging method) [Branaa *et al.* (2011)], and then three-layer films of the reversely charged sample were superposed by attaching the positive and negative charges to the surface with the same charge [Qui *et al.* (2007b)]. This allowed a multiplication of the d_{33} value. A schematic view of a multi-layer ferroelectret PE system is presented in **Figure 4.7**. The combined method has also been applied to S1/PA and the results are summarized in **Table 4.4**.

As expected, the combined method gave the best piezoelectric properties with a d_{33} of 3270 pC/N, which represents a 148% increase compared to single charged films. The piezoelectric coefficient obtained at 80°C (670 pC/N) and after stabilization (1580 pC/N) are also very high despite their decrease. To the best of the authors' knowledge, these results are higher than any polyolefin ferroelectrets based cellular films, including PP [Tajitsu (2011); Mohebbi *et al.* (2017c)].

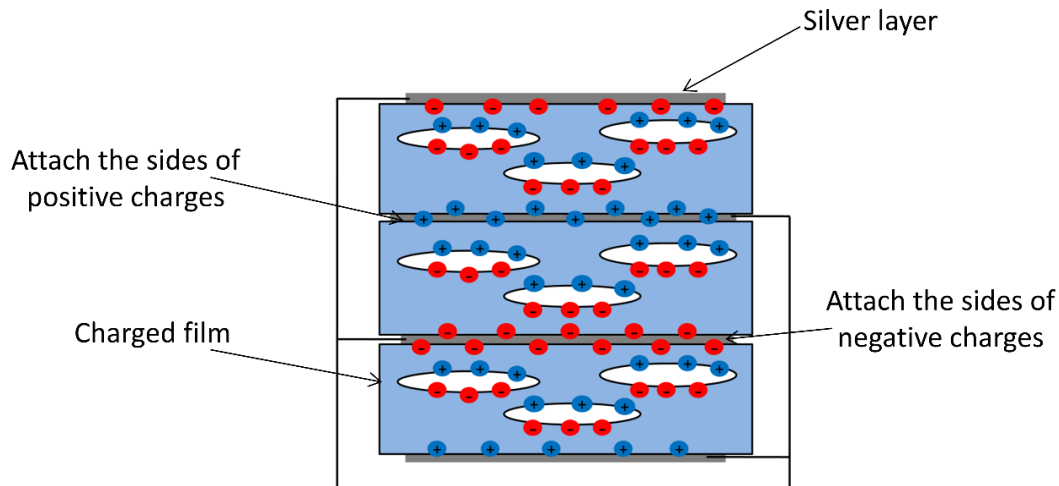


Figure 4.7 Schematic view of a multi-layer ferroelectret PE system.

Table 4.4 Initial d_{33} values (pC/N), as well as their time and thermal stability for three-layered reversely charged cellular polyethylene films. (Values in parentheses represent standard deviations).

S1/PA	d_{33} directly after charging	d_{33} at 80°C	d_{33} after 50 days (stabilization)
1 time charged	1315 (92)	280 (55)	792 (76)
Reversed charging	1850 (120)	411 (32)	980 (100)
3 layered/reversed charging (combined)	3270 (560)	670 (120)	1580 (160)

We believe that these results have a considerable practical value for electret devices since surface modification will allow the use of these devices at temperatures above room temperature, opening the door to more applications. Practically, the electrets made from modified PE films can compete with PP based electrets having typical values around 800 pC/N [Mohebbi et al. (2017c)]. Our PE optimized films are better in terms of initial piezoelectric coefficient (3220 pC/N), time stability (1580 pC/N after 50 days) and

continuous service temperature (80°C). The processing steps and parameters leading to S1/PA are summarized in **Figure 4.8**.

Processing steps	Parameters
1 Blown extrusion film process	-Materials composition: LLDPE, LDPE, Celogen, Talc -Temperature profile: 162–165–172–172–170–166–147°C -Screw speed: 120 rpm -Feed rate: 22 g/min -Take-up ratio (TUR)=6.4 -Blow-up ratio (BUR)=1.8 } Biaxial stretching
2 Thermal Pressure Treatment	-Temperature profile: Stepwise temperature increase to 81 °C -Gas pressure: 5MPa -Gas type and pressure: Nitrogen (5 MPa)
3 Chemical treatment	-Chemical agent: Phosphoric acid -Temperature: 60°C -Period: 24 h
4 Corona charging	-Needle voltage: -21KV (for 60 s) -Needle-sample distance: 4 cm -Gas type and pressure: Nitrogen (100 kPa)
5 3-layered reverse charging	-Reverse charging -Three superposed films

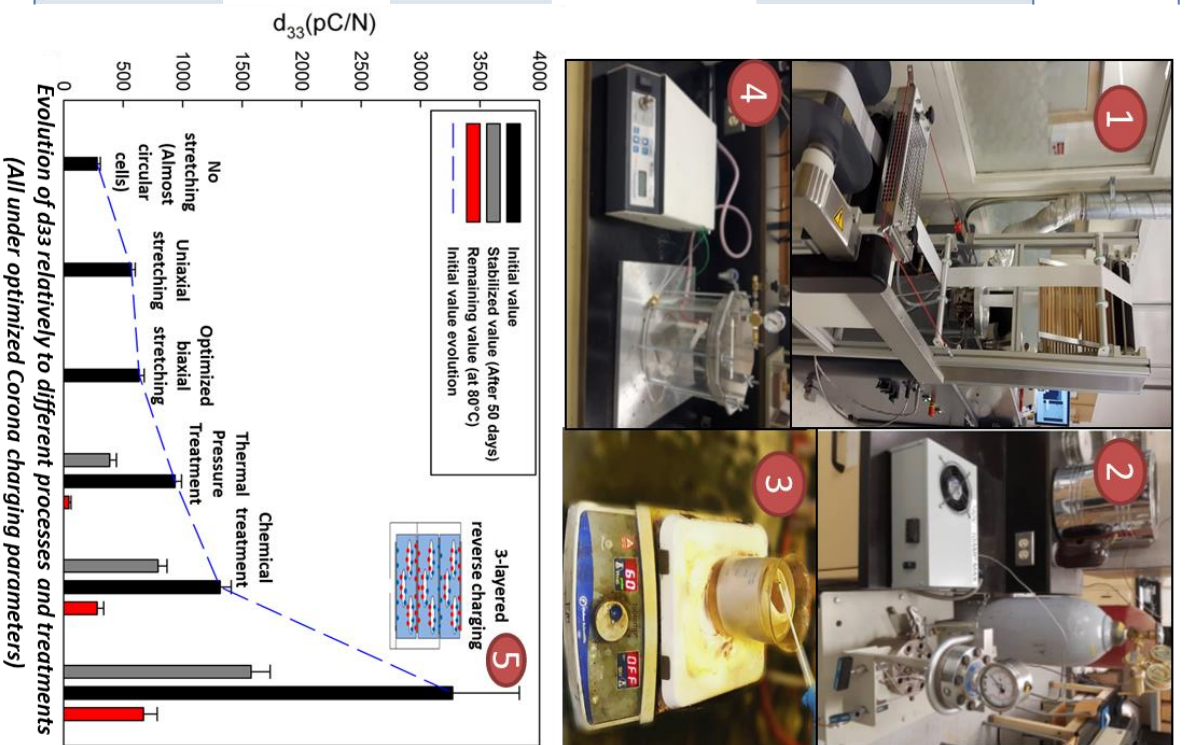


Figure 4.8 Processing steps and parameters leading to the optimized sample S1/PA.

4.4. CONCLUSIONS

This work represents a new step in our objective towards better piezoelectric properties of cellular polyethylene (PE) films. These films were manufactured by a continuous extrusion film-blowing process to provide substantial biaxial stretching, which is important to decrease the elastic stiffness in the thickness direction, and to provide more surface for charge capturing via cell deformation.

Pressure/temperature treatments were applied to further control the cellular morphology of the films. The next step was electric charging by corona discharge producing cellular films with piezoelectric activity. Further improvement was obtained by optimizing the gas used (nitrogen) and its pressure (15 psi) combined with processing conditions such as the charging voltage and the needle/sample distance.

Finally, thermal (annealing) and chemical (phosphoric acid) treatments have been proposed to further control the microstructure of these films and to provide good time and thermal stability. Each step allowed improving these ferroelectret PE films with important piezoelectric properties that can be exploited for large-scale production of electret-based sensors and transducers.

Overall, the chemical treatment was found to be the most efficient, and the best sample was S1/PA which was optimized via chemical treatment with phosphoric acid at 60°C for 24 h. This sample had a density of 450 kg/m³, a thickness of 162 μm, a longitudinal cell aspect ratio (AR-L) of 7, a transversal cell aspect ratio (AR-T) of 4.1, but also presented changes on the polymer surface (phosphorus-containing groups) acting as energetically deep traps able to provide better electret stability. The piezoelectric properties reported are very high (even compared to PP which is the most used polyolefin in this field) with an initial d_{33} of 1315 pC/N stabilizing after 50 days at 792 pC/N, and a good thermal stability since the films remains charged with good piezoelectric coefficients (280 pC/N) at 80°C. The values were further improved when a three-layered reverse charging method was applied, giving an initial d_{33} of 3270 pC/N, a stabilized d_{33} of 1580 pC/N after 50 days and a coefficient of 641 pC/N at 80°C.

ACKNOWLEDGEMENTS

Financial support from the Natural Sciences and Engineering Research Council of Canada (NSERC) and Fonds Québécois de la Recherche sur la Nature et les Technologies (FRQNT) was received for this work. Materials samples were kindly supplied by Exxon Mobil (LLDPE), Nova Chemicals (LDPE) and Imerys (talc). The technical support from Mr. Yann Giroux was highly appreciated.

CONCLUSION ET RECOMMANDATIONS

CONCLUSIONS GÉNÉRALES

Ce travail constitue une contribution dans le domaine de la mise en œuvre de films polymères cellulaires utilisant le procédé d'extrusion-gonflage. Ce procédé a été choisi pour imposer un étirement biaxial à la structure cellulaire pendant sa formation. Les matériaux sélectionnés sont le polyéthylène linéaire de basse densité (LLDPE) et le polyéthylène de basse densité (LDPE) comme matrice, l'azodicarbonamide comme agent gonflant chimique et le talc comme agent de nucléation. Les paramètres de mise en œuvre, à savoir le profil de température, la vitesse de rotation des vis, le débit d'alimentation, le taux d'étirement (TUR), le taux de gonflement (BUR), ainsi que la composition de la matrice ont tous été optimisés pour produire une structure cellulaire homogène ayant des morphologies bien définies. La présence de 1 % de talc (agent de nucléation) a permis d'obtenir une structure plus riche et plus homogène, tandis que l'ajout de 20% de LDPE a permis d'avoir une bonne résistance élongationnelle à l'état fondu (*melt strength*).

Ensuite, un chargement corona a été appliqué pour produire un matériau piézoélectrique. Les paramètres de chargement ont d'abord été optimisés en termes de tension de charge, de distance entre l'aiguille et l'échantillon, ainsi que du type et la pression du gaz utilisé. Leur effet sur le coefficient piézoélectrique quasi-statique (d_{33}) a été étudié en détails. Les résultats ont montré que les échantillons chargés sous azote (N_2) à 100 kPa avaient un meilleur coefficient d_{33} que ceux chargés sous air ambiant ou sous N_2 à 20 kPa, puisque la tension corona augmente avec l'augmentation de la pression du gaz, ce qui permet une meilleure séparation des charges à l'intérieur de l'échantillon. De plus, deux différents traitements de pression et température ont été imposés pour obtenir une structure cellulaire de forme ellipsoïdale allongée avec différents ratios de forme (AR) pour chaque direction (longitudinale et transversale). Les résultats ont montré que plus les cellules étaient étirées (AR plus élevés), plus les coefficients d_{33} étaient élevés parce que les structures cellulaires étirées sont plus flexibles et provoquent une déformation plus importante lors de l'application d'une contrainte mécanique.

Enfin, un traitement chimique (acide phosphorique) a été appliqué et a permis des améliorations de l'activité piézoélectrique surtout au niveau de la stabilité thermique. À la suite de ces étapes, un échantillon optimisé (S1/PA) avec une densité de 450 kg/m³, une épaisseur de 162 µm, un facteur de forme longitudinale (AR-L) de 7.0 et un facteur de forme transversale (AR-T) de 4.1 a été fabriqué. Les propriétés piézoélectriques rapportées étaient très élevées, même comparées au polypropylène (PP) qui est la polyoléfine la plus utilisée dans ce domaine. Dans ce cas, un d_{33} initial de 1315 pC/N se stabilisant après 50 jours à 792 pC/N et une bonne stabilité thermique ont été observés car les films restent chargés avec de bons coefficients piézoélectriques (280 pC/N) jusqu'à des températures de 80°C. Ces valeurs ont été encore améliorées par l'application d'un procédé combiné d'inversement de charge et d'empilement de trois couches, donnant un d_{33} initial de 3270 pC/N, un d_{33} stabilisé de 1580 pC/N après 50 jours et une valeur de 641 pC/N à 80°C. Ces films de polyéthylène cellulaires aux propriétés piézoélectriques importantes peuvent maintenant être exploités pour la production à grande échelle de capteurs et de transducteurs à base d'électrets.

Pour résumer, on peut dire que ce travail a traité toutes les étapes conduisant à l'optimisation des ferroélectrets en utilisant le polymère le plus disponible (polyéthylène) et un procédé très utilisé au niveau industriel (extrusion-gonflage). Ces choix, innovants pour une telle application (piézoélectrique), ont posé plusieurs défis à savoir la faible résistance à l'état fondu et la faible stabilité piézoélectrique du LLDPE. Plusieurs optimisations aux niveaux de la mise en œuvre, des traitements Pression-Température, du chargement électrique et du traitement chimique ont été effectuées afin d'améliorer les différentes propriétés morphologiques, mécaniques, structurales et piézoélectriques des films cellulaires fabriqués. Ceci a permis l'obtention de films aux propriétés piézoélectriques importantes pouvant maintenant être exploités pour la production à grande échelle, ce qui constitue un avancement important au niveau du développement des matériaux piézoélectriques à faible coût pouvant être utilisés dans différents domaines tels que la médecine, la sécurité, l'environnement, le sport et les transports.

RECOMMANDATIONS

Ce travail de recherche est articulé autour de l'optimisation des propriétés piézoélectriques des films cellulaires à base de polyéthylène (et leur mélange). Les propriétés morphologiques, mécaniques, microstructurales et piézoélectriques ont été investiguées et contrôlées.

Cependant, certains aspects n'ont pas été étudiés dans ce projet par choix ou à cause de limitation de temps ou de matériel. Ces aspects présentent tout de même un intérêt scientifique pour des travaux futurs. Ainsi, des travaux supplémentaires pourraient être menés pour combler ce manque de connaissances. Les aspects suivants doivent être pris en compte lors de ces travaux ultérieurs:

- Développer un mécanisme permettant d'étirer davantage les films cellulaires dans les directions longitudinale et transversale afin de déterminer les limites de l'optimisation du coefficient d_{33} . Ceci pourrait être possible par exemple en concevant un entrefer de la filière avec une épaisseur supérieure à celle utilisée dans ce projet (0.8 mm). Ceci permettrait un étirage biaxial plus important, ce qui peut encore améliorer le coefficient piézoélectrique. On pourrait aussi utiliser une matrice principalement en LDPE, ce qui permettrait un meilleur étirement. Néanmoins, il faudrait toutefois conserver une certaine consistance du film cellulaire (résistance mécanique).
- Fabriquer des films moussés par voie physique en utilisant le N_2 ou le CO_2 comme agent moussant, permettrait de produire une nouvelle gamme de morphologies cellulaires (densité, forme et taille des cellules). Ainsi, une comparaison avec les résultats déjà obtenus dans ce projet (par voie chimique) serait utile afin de mieux comprendre l'effet de la structure sur les différentes propriétés physiques des films moussés.
- L'utilisation des techniques de caractérisations piézoélectriques basées sur d'autres méthodes, telles que la résonance et les méthodes dynamiques, serait intéressante pour comparer avec les résultats quasi-statiques de ce travail.

- L'air et l'azote ont été utilisés à l'intérieur des cellules durant le processus de chargement électrique par le procédé corona. Il serait intéressant d'étudier d'autres gaz ayant une plus haute résistance électrique pour optimiser davantage les paramètres de chargement électrique. On peut penser par exemple à l'hexafluorure de soufre SF₆ dont le champ disruptif est environ trois fois supérieur à celui de l'air [*Paajanen et al., 2001*].
- Le traitement chimique avec l'acide phosphorique a fait ses preuves au niveau de l'amélioration de la stabilité du coefficient piézoélectrique. Plus de travail pourrait être fait pour optimiser les conditions de traitement (concentration, température et temps), ainsi que le type d'acide. On peut penser par exemple au traitement des films de polyéthylène moussés avec le trichlorure de phosphore (PCl₃) ou avec de la vapeur de tétrachlorure de titane (TiCl₄) qui ont démontré aussi leur efficacité en termes de stabilités piézoélectriques (thermique et temporelle) [*Qui (2016); Thyssen et al. (2015); Fang (2010); Mellinger et al. (2006)*]. Une comparaison pourrait ainsi être faite avec les résultats obtenus dans ce projet concernant le traitement par acide orthophosphorique et un choix du traitement optimal pourrait être déduit.
- On pense que les propriétés morphologiques, mécaniques et piézoélectriques présentent des corrélations élevées. Dans ce contexte, le développement d'un modèle reliant ces différentes propriétés pourrait être très intéressant puisqu'il permettrait une optimisation des différentes étapes intervenant dans la fabrication des films cellulaires et pourrait conduire à une amélioration de l'activité piézoélectrique.

Références

- Abraham CS (2011) A review of ferroelectric materials and their applications. *Ferroelectrics* 138: 307-309.
- Altafim RAP, Qiu X, Wirges W, Gerhard R, Altafim R.A.C, Basso H.C, Jenninger W, Wagner J (2009) Template-based fluoroethylenepropylene piezoelectrets with tubular channels for transducer applications. *Journal of Applied Physics* 106: 014106.
- Altafim RAP, Rychkov D, Wirges W, Gerhard R, Basso HC, Altafim RAC, Melzer M (2012) Laminated tubular-channel ferroelectret systems from low-density polyethylene (LDPE) films and from fluoro-ethylene-propylene (FEP) copolymer films – A comparison. *IEEE Transactions on Dielectrics and Electrical Insulation* 19: 1116-1123.
- An Z, Zhao M, Yao J, Zhang Y, Xia Z (2009) Improved piezoelectric properties of cellular polypropylene ferroelectrets by chemical modification. *Applied Physics A - Materials* 95: 801-806.
- Anta JA, Marcelli G, Meunier M, Quirkec N (2002) Models of electron trapping and transport in polyethylene: Current–voltage characteristics. *Journal of Applied Physics* 92: 1002-1008.
- Audet E (2015) Films cellulaires en polypropylène chargé de talc et de carbonate de calcium utilisés comme matériaux piézoélectriques: optimisation de la structure cellulaire par étirage bi-axial et par gonflement sous atmosphère d'azote. *Laval University: Master Thesis*.
- Bae SS (2005) Preparation of polypropylene foams with micro/nanocellular morphology using a Sorbitol-based nucleating agent. *University of Toronto: Master Thesis*.
- Baldwin DF, Suh NP, Park CB, Cha SW (1994) Super-Microcellular Foamed Materials. *U.S. Patent* 5334356.
- Bauer S (2006) Piezo-, pyro- and ferroelectrets: soft transducer materials for electromechanical energy conversion. *IEEE Transactions on Dielectrics and Electrical Insulation* 13: 953-962.
- Bauer S, Gerhard-Mulhaupt R, Sessler GM (2004) Ferroelectrets: Soft electroactive foams for transducers. *Physics Today* 57: 37-43.
- Behravesh AH, Park CB, Cheung LK, Venter RD (1996) Extrusion of polypropylene foams with hydrocerol and isopentane. *Journal of Vinyl and Additive Technology* 2: 349-357.
- Belhora F, Hajjaji A, Le M-Q, Mazroui M, Guyomar D, Boughaleb Y, Touhtouh S, Lebrun L (2014) Combination of electrostrictive polymers composites and electrets for energy harvesting capability. *Polymers for Advanced Technologies* 25: 969-974.
- Bernard G, Auger M, Soucy J, Pouliot R (2007) Physical characterization of the stratum corneum of an in vitro psoriatic skin model by ATR-FTIR and Raman spectroscopies, *Biochimica et Biophysica Acta* 1770: 1317-1323.
- Branaa GO, Segoviab PL, Magranera F, Quijano A (2011) Influence of corona charging in cellular polyethylene film. *Journal of Physics: 13th International Conference on Electrostatics* 301: 012054.

Butler TI (2005) *Film Extrusion Manual: process, materials, properties. Tappi Press (Second edition): Atlanta.*

Cantor K (2006) *Blown Film Extrusion Munich: Carl Hanser Verlag ISBN 3-446-22741-5.*

Chen L, Rende D, Schadler LS, Ozisik R (2013) Polymer nanocomposite foams. *Journal of Materials Chemistry A 1: 3837-3850.*

Coccorullo I, Maio L.D, Montesano S, Incarnato L (2008) Theoretical and experimental study of foaming process with chain extended recycled PET. *Express Polymer Letters 3 :84-96.*

Collais DI, Baird DG (1995) Tensile toughness of microcellular foams of polystyrene, styrene-acrylonitrile copolymer, and polycarbonate, and the effect of dissolved gas on the tensile toughness of the same polymer matrices and microcellular foams. *Polymer Engineering & Science 35: 1167-1177.*

Colton JS (1988) Making Microcellular Foams from Crystalline Polymers. *Plastics Engineering 44: 53-55.*

Colton JS, Suh NP (1986) The nucleation of microcellular thermoplastic foam: process model and experimental results. *Advanced Manufacturing Processes 1: 341-364.*

Colton JS, Suh NP (1987a) The nucleation of microcellular thermoplastic foam with additives: Part I: Theoretical considerations. *Polymer Engineering and Science 27: 485-492.*

Colton JS, Suh NP (1987b) The nucleation of microcellular thermoplastic foam with additives: Part II: Experimental results and discussions. *Polymer Engineering and Science 27: 493-499.*

Curie J, Curie P (1880) Development by pressure of polar electricity in hemihedral crystals with inclined faces. *Bulletin De La Société Chimique De France 3: 90-93.*

Dagdeviren C, Joe P, Tuzman OL, Park K, Lee KJ, Shi Y, Huang Y, Rojers J.A (2016) Recent progress in flexible and stretchable piezoelectric devices for mechanical energy harvesting, sensing and actuation. *Extreme Mechanics Letters 9: 269-281.*

Defay E (2013) Dielectricity, Piezoelectricity, Pyroelectricity and Ferroelectricity, In: Defay E, *Integration of Ferroelectric and Piezoelectric Thin Films: Concepts and Applications for Microsystems, London: ISTE Ltd and John Wiley & Sons, Inc., 1-24.*

Ding J, Shangguan J, Ma W, Zhong Q (2013) Foaming behavior of microcellular foam polypropylene/modified nano calcium carbonate composites. *Journal of Applied Polymer Science 128: 3639-3651.*

Dobkin BH, Dorsch A (2011) The promise of mHealth: Daily activity monitoring and outcome assessments by wearable sensors. *Neurorehabil Neural Repair 25: 788-798.*

Dorigato A, Amato M, Pegoretti A (2012) Thermo-mechanical properties of high-density polyethylene – fumed silica nanocomposites: effect of filler surface area and treatment. *Journal of Polymer Research 19: 9889.*

Doring J, Bovtun V, Bartusch J, Erhard A, Kreutzbruck M, Yakymenko Y (2010) Nonlinear

electromechanical response of the ferroelectret ultrasonic transducers. *Applied Physics A-Mater* 100: 479-485.

Ende DAV, Kempen SEV, Wu X, Groen WA, Randall CA (2012) Dielectrophoretically structured piezoelectric composites with high aspect ratio piezoelectric particles inclusions. *Journal of Applied Physics* 111: 124107.

Fang P (2010) Preparation and Investigation of Polymer-Foam Films and Polymer-Layer Systems for Ferroelectrets. *University of Potsdam: Doctoral Thesis*.

Fang P, Hollander L, Wirges W, Gerhard R (2012) Piezoelectric d_{33} coefficients in foamed and layered polymer piezoelectrets from dynamic mechano-electrical experiments, electro-mechanical resonance spectroscopy and acoustic-transducer measurements. *Measurement Science and Technology* 23:1-9.

Fang P, Ma X, Li X, Qiu X, Gerhard R, Zhang X, Li G (2008) Fabrication, Structure characterization, and performance testing of piezoelectret-Film sensors for recording body motion. *IEEE Sensors Journal* 18: 401-412.

Fang P, Qiu X, Wirges W, Gerhard R, Zirkel L (2010) Polyethylene-naphthalate (PEN) ferroelectrets: cellular structure, piezoelectricity and thermal stability. *IEEE Transactions on Dielectrics and Electrical Insulation* 17: 1079-1087.

Fang P, Wegener M, Wirges W, Gerhard R (2007) Cellular polyethylene-naphthalate ferroelectrets: foaming in supercritical carbon dioxide, structural and electrical preparation, and resulting piezoelectricity. *Applied Physics Letters* 90: 192908.

Fang P, Wirges W, Wegener M, Zirkel L, Gerhard R (2008) Cellular polyethylene-naphthalate films for ferroelectret applications: foaming, inflation and stretching, assessment of electromechanically relevant structural features. *E-Polymers* 8: 487-495.

Gamache E (2010) Soufflage de gaine - Description du procédé. *Techniques de l'ingénieur Reference AM3702*.

Gerhard-Mulhaupt R (2002) Less can be more. Holes in polymers lead to a new paradigm of piezoelectric materials for electret transducers. *IEEE Transactions on Dielectrics and Electrical Insulation* 9: 850-859.

Ghassemi A, Moghaddamzadeh S, Duchesne C, Rodrigue D (2017) Effect of annealing on gas permeability and mechanical properties of polylactic acid/talc composite films. *Journal of Plastic Film & Sheeting*, 33: 361-383.

Gibson LJ, Ashby M (1997) Cellular Solids: structure and properties, In: *Solid state science*, Cambridge University Press.

Gosselin R, Rodrigue D (2005) Cell morphology analysis of high density polymer foams. *Polymer Testing* 24: 1027-1035.

Graz I, Mellinger A (2016) Polymer Electrets and Ferroelectrets as EAPs: Fundamentals, In: Carpi F, *Electromechanically Active Polymers. Polymers and Polymeric Composites: A Reference Series*, Springer, London.

Hamdi O, Mighri F, Rodrigue D (2018a) Piezoelectric cellular polymer films: Fabrication, properties and applications. *AIMS Materials and Science* 5: 845-869.

Hamdi O, Mighri F, Rodrigue D (2018b) Optimization of the cellular morphology of biaxially stretched thin polyethylene foams produced by extrusion film blowing. *Cellular Polymers* 37: 153-168.

Hamdi O, Mighri F, Rodrigue D (2018c) Piezoelectric properties improvement of polyethylene ferroelectrets using post-processing treatments. *Polymers for Advanced Technologies* 1-9.

Hamdi O, Mighri F, Rodrigue D (2018d) Time and thermal stability improvement of polyethylene ferroelectrets. *Journal of Applied Polymer Science*. Submitted.

Han X, Zeng C, Lee LJ, Koelling KW, Tomasko DL (2003) Extrusion of polystyrene nanocomposite foams with supercritical CO₂. *Polymer Engineering and Science*, 43:1261-1275.

Harris S, Mellinger A (2014) Towards a better understanding of dielectric barrier discharges in ferroelectrets: Paschen breakdown fields in micrometer sized voids. *Journal of Applied Physics* 115: 163302.

Harrison JS, Ounaies Z (2002) Piezoelectric polymers, In: *Encyclopedia of Polymer Science and Technology* 474–498.

Hillenbrand J, Haberzettl S, Motz T, Sessler G (2011) Electret accelerometers: physics and dynamic characterization. *Journal of the Acoustical Society of America* 129: 3682-3687.

Hillenbrand J, Kodejska M, Garcin Y, Seggern HV and Sessler GM (2010) High sensitivity piezoelectret film accelerometers. *IEEE Transactions on Dielectrics and Electrical Insulation* 17: 1021-1027.

Hillenbrand J, Kodejska M, Garcin Y, Seggern HV, Sessler GM (2010) High sensitivity piezoelectret film accelerometers. *IEEE Transactions on Dielectrics and Electrical Insulation* 17: 1021-1027.

Hillenbrand J, Sessler G, Zhang X (1999) Verification of a model for the piezoelectric d₃₃ coefficient of cellular electret films. *Journal of Applied Physics* 98: 0641051.

Hossieny N (2010) Morphology and properties of polymer/carbon nanotube nanocomposite foams prepared by super critical carbon dioxide. *The Florida State University: Doctoral Thesis*.

Huang HX (2005) HDPE/PA-6 blends: Influence of screw shear intensity and HDPE melt viscosity on phase morphology development. *Journal of Materials Science* 40: 1777-1779.

Huang HX, Jiang G, Mao SQ (2005) Effect of flow fields on morphology of PP/Nano/CaCO₃ composite and its rheological behavior. *ASME International Mechanical Engineering Congress and Exposition* 80830: 567-574.

Huang HX, Wang JK, Sun XH (2008) Improving of cell structure of microcellular foams based on polypropylene/high-density polyethylene blends. *Journal of Materials Science* 44: 69-85.

Information of 2020 armor products (USA). Available from: <http://www.2020armor.com/>. (Last visit:

May 2019).

Information of the company B-Band (Finland). Available from: <http://www.b-band.com/>. (Last visit: May 2019).

Information of the company Emfit (Finland). Available from: <https://www.emfit.com/>. (Last visit: Mai 2019).

Information of the company Xonano smart foam (USA). Available from: <http://www.xonano.com/>. (Last visit: May 2019).

Jarrasse N, Nicol C, Touillet A, Richer F, Martinet N, Paysant J, De Graaf JB (2017) Classification of phantom finger, hand, wrist, and elbow voluntary gestures in transhumeral amputees with sEMG. *IEEE Transactions on Neural Systems and Rehabilitation Engineering* 25: 71-80.

Kim H, Kobayashi S, Abdur Rahim MA, Zhang MJ, Khusainova A, Hillmyer MA, Abdala AA (2011) Graphene/polyethylene nanocomposites: Effect of polyethylene functionalization and blending methods. *Polymer* 52: 1837-1846.

Kim JY (2013) Parylene C as a new piezoelectric material. *California Institute of Technology: Doctoral Thesis*.

Kirjavainen K (1987) Electromechanical film and procedure for manufacturing same. *U.S. Patent, No: 4654546*.

Klempner D, Frisch KC (1991) Handbook of Polymeric Foams and Foam Technology. *Hanser Publishers: Munich*.

Kogler A, Buchberger G, Schwodiauer R, Bauer S (2011) Ferroelectret based Flexible Keyboards and Tactile Sensors. *14th International Symposium on Electrets* 201-202.

Kolarik R (2012) Modeling of film blowing process for non-Newtonian fluids by using variational principles. *Tomas Bata University: Doctoral thesis*.

Kolarik R, Zatloukal M (2011) Modeling of Nonisothermal Film Blowing. *Journal of Applied Polymer Science* 122: 2807-2820.

Koliatene F (2009) Contribution à l'étude de l'existence des décharges dans les systèmes de l'avionique 'Contribution to the study of the existence of discharges in avionics systems'. *Université de Toulouse: Doctoral Thesis*.

Kumar V (1993) Microcellular polymers: Novel materials for the 21st century. *Cellular Polymers* 12: 207-223.

Kumar V, Suh NP (1990) A Process for Making Microcellular Thermoplastic Parts. *Polymer Engineering and Science* 30: 1323-1329.

Kumar V, Weller JE, Montecillo R (1992) Microcellular PVC. *Journal of Vinyl Technology* 14: 191-197.

- Laffargue J (2003) Étude et modélisation des instabilités du procédé de soufflage de gaine. *École Nationale Supérieure des Mines de Paris: Doctoral thesis.*
- Lambert CH (1991) Applications and opportunities for cellular polymers in automobiles. *RAPRA Technology, Conference Proceedings: London.*
- Lang S, Muensit S (2006) Review of some lesser-known applications of piezoelectric and pyroelectric polymers. *Applied Physics A 85:125-134.*
- Lechner MD (2005) Springer Handbook of Condensed Matter and Materials Data. Werner M, Hans W. *Springer Berlin Heidelberg Publisher 477-522.*
- Lee CH, Lee KJ, Jeong HG, Kim SW (2000) Growth of gas bubbles in the foam extrusion process, *Advances in Polymer Technology 19: 97-112.*
- Lee EK (2010) Novel Manufacturing Processes for Polymer Bead Foams. *University of Toronto: Doctoral Thesis.*
- Lee ST (2000) Foam Extrusion Principles and Practice. *Technomic Publishing Company: CRC Press 4: 81-124.*
- Lei W (2017) Ferroelectret nanogenerator (FENG) for mechanical energy harvesting and self-powered flexible electronics. *Michigan State University: Doctoral Thesis.*
- Leung S (2009) Mechanisms of cell nucleation, growth, and coarsening in plastic foaming: theory, simulation, and experiment. *University of Toronto: Doctoral thesis.*
- Li W, Torres D, Diaz R, Diaz R, Wang Z, Wu C, Wang C, Wang ZL, Sepulveda N (2017) Nanogenerator-based dual-functional and self-powered thin patch loudspeaker or microphone for flexible electronics. *Nature Communications 8: 15310.*
- Li X, Fisher M, Rymer WZ, Zhou P (2015) Application of the F-response for estimating motor unit number and amplitude distribution in hand muscles of stroke survivors. *IEEE Transactions on Neural Systems and Rehabilitation Engineering 24: 674-681.*
- Li Y, Zeng C (2013) Low-temperature CO₂-assisted assembly of cyclic olefin copolymer ferroelectrets of high piezoelectricity and thermal stability. *Macromolecular Chemistry and Physics 214: 2733-2738.*
- Lindner M, Hoislbauer H, Schwodiaue, R, Bauer-Gogonea S, Bauer S (2004) Charged cellular polymers with ferroelectric behavior. *IEEE Transactions on Dielectrics and Electrical Insulation 11: 255-263.*
- Liu F (1998) Processing of polyethylene and polypropylene foams in rotational molding. *University of Toronto: Master Thesis.*
- Mark HF (2004) Encyclopedia of polymer science and technology, *Wiley, 3rd edition, New York.*
- Mellinger A (2003) Dielectric resonance spectroscopy: a versatile tool in the quest for better piezoelectric polymers. *IEEE Dielectrics and Electrical Insulation Society 10: 842-861.*

- Mellinger A, Wegener M, Wirges W, Gerhard-Multhaupt R (2011) Thermally stable dynamic piezoelectricity in sandwich films of porous and nonporous amorphous fluoropolymer. *Applied Physics Letters* 79: 1851-1854.
- Mellinger A, Wegener W, Wirges W, Gerhard-Multhaupt R (2006) Thermal and temporal stability of ferroelectret films made from cellular polypropylene/air Composites. *Ferroelectrics* 331: 189-199.
- Meunier M, Quirke N, Aslanides A (2001) Molecular modeling of electron traps in polymer insulators: Chemical defects and impurities. *Journal of Chemical Physics* 115: 2876-2881.
- Mohebbi A, Mighri F, Ajjji A, Rodrigue D (2015) Current issues and challenges in polypropylene foaming: A review. *Cellular Polymers* 34: 299-337.
- Mohebbi A, Mighri F, Ajjji A, Rodrigue D (2017a) Effect of processing conditions on the cellular morphology of polypropylene foamed films for piezoelectric applications. *Cellular Polymers* 36: 13-34.
- Mohebbi A, Mighri F, Ajjji A, Rodrigue D (2017b) Polymer ferroelectret based on polypropylene foam: piezoelectric properties prediction using dynamic mechanical analysis. *Polymers for Advanced Technology* 28: 476-483.
- Mohebbi A, Mighri F, Ajjji A, Rodrigue D (2018) Cellular polymer ferroelectret: A review on their development and their piezoelectric properties. *Advances in Polymer Technology* 37: 468-483.
- Montanari GC, Mazzanti G, Ciani F, Paaajanen F (2004) Effect of gas expansion on charging behavior of quasi-piezoelectric cellular PP. *The 17th Annual Meeting of the IEEE Lasers and Electro-Optics Society* 153-157.
- Nakayama M, Uenaka Y, Kataoka S, Oda Y, Yamamoto K, Tajitsu Y (2009) Piezoelectricity of ferroelectret porous polyethylene thin film. *Journal of Applied Physics* 48: 09KE05.
- Nawaby AV, Zhang ZY (2004) Solubility and Diffusivity, In: Gendron R, *Thermoplastic Foam Processing: Principles and Development*. Boca Raton, FL: CRC Press 1-42.
- Neuschwandtner GS, Schwödianer R, Gogonea SB, Bauer S (2001) Piezo- and pyroelectricity of a polymer-foam space-charge electrets. *Journal of Applied Physics* 89: 4503-4511.
- Neuschwandtner GS, Schwödianer R, Vieytes M, Bauer-Gogonea S, Bauer S, Hillenbrand J, Kressmann R, Sessler GM, Paaajanen M, Lekkala J (2000) Large and broadband piezoelectricity in smart polymer-foam space-charge electrets. *Applied Physics Letters* 77: 3827-3829.
- Ni SS, Li T, Ma J (2009) Polymeric piezoelectric cantilever and tubular actuators. *Polymers for Advanced Technologies* 21: 591-597.
- Ning C, Zhou Z, Tan G, Zhu Y, Mao C (2018) Electroactive polymers for tissue regeneration: Developments and perspectives. *Progress in Polymer Science* 81: 144-162.
- Nofar M, Majithiya K, Kuboki T, Park CB (2012) The foamability of low-melt-strength linear polypropylene with nanoclay and coupling agent. *Journal of Cellular Plastics* 48: 271-287.

Notario B, Pinto J, Rodriguez-Perez MA (2016) Nanoporous polymeric materials: A new class of materials with enhanced properties. *Progress in Materials Science* 78: 93-139.

Okolieocha C, Koppl T, Kerling S, Tolle FJ, Fathi A, Mülhaupt R, Altstadt V (2015) Influence of graphene on the cell morphology and mechanical properties of extruded polystyrene foam. *Journal of Cellular Plastics* 51: 413-426.

Paaanen M, Lekkala J, Kirjavainen K (2000) ElectroMechanical Film (EMFi) - a new multipurpose electret material *Sensors and Actuators A: Physical*, 84: 95-102.

Paaanen M, Wegener M, Gerhard-Mulhaupt R (2001) Understanding the role of the gas in the voids during corona charging of cellular electret films-a way to enhance their piezoelectricity. *Journal of Physics D: Applied Physics* 34: 2482-2488.

Padasalkar GG, Shaikh JM, Syed YD, Tamboli SH, Phutane PS (2015) A Review on Piezoelectricity. *International Journal of Advanced Research in Electrical, Electronics and Instrumentation Engineering* 4: 8231-8235.

Pandey A, Shukla S, Shukla V (2015) Innovation and application of piezoelectric materials: a theoretical approach. *International Journal of Advanced Technology in Engineering and Science* 3: 1413-1417.

Park CB, Baldwin DF, Suh NP (2004) Effect of the pressure drop rate on cell nucleation in continuous processing of microcellular polymers. *Polymer Engineering and Science* 35: 432-440.

Park CB, Cheung LK (1997) A study of cell nucleation in the extrusion of polypropylene foams. *Polymer Engineering and Science* 37: 1-10.

Park CB, Suh NP (1996) Filamentary extrusion of microcellular polymers using a rapid decompressive element. *Polymer Engineering and Science* 36: 34-48.

Patel S, Park H, Bonato P, Chan L, Rodgers M (2012) A review of wearable sensors and systems with application in rehabilitation. *Journal of Neuroengineering and Rehabilitation* 9: 1-17.

Qaiss A, Saidi H, Fassi-Fehri O, Bousmina M (2012) Cellular polypropylene-based piezoelectric films. *Polymer Engineering and Science* 52: 2637-2644.

Qiu X, Gerhard R, Mellinger A (2011) Turning polymer foams or polymer-film systems into ferroelectrets: dielectric barrier discharges in voids. *IEEE Transactions on Dielectrics and Electrical Insulation* 18: 34-42.

Qiu X, Mellinger A, Gerhard R (2008) Influence of gas pressure in the voids during charging on the piezoelectricity of ferroelectrets. *Journal of Applied Physics* 92: 052901.

Qiu X, Mellinger A, Wegener M, Wirges W, Gerhard R (2007a) Barrier discharges in cellular polypropylene ferroelectrets: How do they influence the electromechanical properties. *Journal of Applied Physics* 101: 104112.

Qiu X, Rychkov D, Wirges W (2015) Properties and applications of ferroelectrets. *The Nano-Micro Interface: Bridging the Micro and Nano Worlds, Wiley, Second Edition* 14: 271-288.

Qiu X, Xia Z, Wang F (2007b) Piezoelectricity of single and multi-layer cellular polypropylene film electrets. *Frontiers of Materials Science in China* 1: 72-75.

Qui X (2016) Polymer Electrets and Ferroelectrets as EAPs: Materials, electromechanically Active Polymers. *Polymers and Polymer Composites* 25: 561-589.

Qui X, Xia Z, Wang F (2007) Piezoelectricity of single and multi-layer cellular polypropylene film electrets. *Frontiers of Materials Science in China*, 1: 72-75.

Rachtanapun P, Selke SEM, Matuana LM (2004a) Effect of the high-density polyethylene melt index on the microcellular foaming of high-density polyethylene/polypropylene blends. *Journal of Applied Polymer Science* 93: 364–371.

Rachtanapun P, Selke SEM, Matuana, LM (2004b) Relationship between cell morphology and impact strength of microcellular foamed high-density polyethylene/polypropylene blends. *Polymer Engineering and Science* 44: 1551-1560.

Ramadan KS, Sameoto D, Evoy S (2014) A review of piezoelectric polymers as functional materials for electromechanical transducers. *Smart Materials Structures* 23: 1-26.

Reimund GM (2002) Less can be more. Holes in polymers lead to a new paradigm of piezoelectric materials for electret transducers. *IEEE Transactions on Dielectrics and Electrical Insulation* 9: 850-859.

Rodrigue D, Gosselin R (2002) The effect of calcium carbonate particle size on LDPE foam morphology. *Blowing Agents and Foaming Processes Conference* 16: 157-166.

Rychkov D, Altafim RAP (2016) Polymer Electrets and Ferroelectrets as EAPs: Models, Electromechanically Active Polymers. *Polymers and Polymeric Composites: A Reference*, 28: 646-657.

Rychkov D, Kuznetsov A, Rychkov A (2011) Electret properties of polyethylene and polytetrafluoroethylene films with chemically modified surface, *IEEE Transactions on Dielectrics and Electrical Insulation* 18: 8-14.

Rychkova D, Altafim RAP, Qiu X, Gerhard R (2012) Treatment with orthophosphoric acid enhances the thermal stability of the piezoelectricity in low-density polyethylene ferroelectrets. *Journal of Applied Physics* 111: 124105.

Saarimaki E, Paaajanen M, Savijarvi A, Minkkinen H, Wegener M, Voronina O, Schulze R, Wirges W, Gerhard MR (2006) Novel heat durable electromechanical film: processing for electromechanical and electret applications. *IEEE Transactions on Dielectrics and Electrical Insulation* 13: 963-972.

Savolainen A, Kirjavainen K (1989) Electrothermomechanical film. Part I. Design and characteristics. *Journal of Macromolecular Science, Chemistry* A26: 583-591

Sborikas M, Wegener M (2013) Cellular-foam polypropylene ferroelectrets with increased film thickness and reduced resonance frequency. *Applied Physics Letters* 103: 252901.

Schirmer HG, Kumar V (2003) Novel reduced-density materials by solid-state extrusion: Proof-of-concept experiments. *Cellular Polymers* 23: 369-385.

- Sessler GM, Hillenbrand J (1999) Electromechanical response of cellular electrets films. *Applied Physics Letters* 75: 3405-3407.
- Setter N, Damjanovic D, Eng L, Fox G, Gevorgian S, Hong S, Kingon A, Kohlstedt H, Park NY, Stephenson GB, Stolitchnov I, Taganstev AK, Taylor DV, Yamada T, Streiffer S (2006) Ferroelectric thin films: Review of materials, properties, and applications. *Journal of Applied Physics* 100: 051606.
- Shi J (2017) Ferro-electrets material in human body energy harvesting. *University of Southampton: Doctoral Thesis*.
- Suh KW, Park CP, Maurer M, Tusim MH, Genova RD, Broos R, Sophiea DP (2000) Lightweight Cellular Plastics. *Advanced Materials* 12: 1779-1789.
- Tajitsu Y (2011) Piezoelectric Properties of ferroelectret. *Ferroelectrics* 415: 57-66.
- Thyssen A, Almdal K, Thomsen EV (2015) Electret Stability Related to the Crystallinity in Polypropylene. *IEEE Sensors* 1-4.
- Torquato S (2001) *Random Heterogeneous Materials: Microstructure and macroscopic properties*, New York: Springer Science & Business Media.
- Tuncer E (2005) Numerical calculations of effective elastic properties of two cellular structures. *Journal of Physics D: Applied Physics* 38: 497-503.
- Tuncer E, Wegener M (2006) Soft polymeric composites for electro-mechanical applications: predicting and designing their properties by numerical simulations, In: *Dillon KI, Soft Condensed Matter: New Research*, Nova Science publishers, Hauppauge, 217-275.
- Viswanath V, Maity S, R.B. Jason, I.C. Laura, E.G. Russell E (2016) Enhanced crystallinity of polymer nanofibers without loss of nanofibrous morphology via heterogeneous photothermal annealing. *Macromolecules* 49: 9484-9492
- Wagner MH, Kheirandish S, Stange J, Münstedt H (2006) Modeling Elongational Viscosity of Blends of Linear and Long-Chain Branched Polypropylenes. *Rheology Acta* 46: 211-221.
- Wagner MH, Kheirandish S, Yamaguchi M (2004) Quantitative analysis of melt elongational behavior of LLDPE/LDPE blends. *Rheologica Acta* 44: 198-218.
- Wan YP, Zhong Z (2012) Effective electromechanical properties of cellular piezoelectret: A review. *Acta Mechanica Sinica* 28: 951-959.
- Wang C, Ying S, Xiao Z (2013) Preparation of short carbon fiber/polypropylene fine-celled foams in supercritical CO₂. *Journal of Cellular Plastics* 49: 65-82.
- Wegener M (2010) Piezoelectric polymer foams: Transducer mechanism and preparation as well as touch-sensor and ultrasonic-transducer properties. *Behavior and Mechanics of Multifunctional Materials and Composites* 7644: 76441A.
- Wegener M, Bergweiler S, Wirges W, Pucher A, Tuncer E, Mulhaupt RG (2005) Piezoelectric two-layer stacks of cellular polypropylene ferroelectrets: transducer response at audio and ultrasound

frequencies. *IEEE Transactions on Ultrasonics, Ferroelectrics, and Frequency Control* 52: 1601-1607.

Wegener M, Tuncer E, Gerhard-Multhaupt R, Bauer S (2006) Elastic properties and electromechanical coupling factor of inflated polypropylene ferroelectrets. *IEEE Conference on Electrical Insulation and Dielectric Phenomena* 752-755.

Wegener M, Wirges W (2004a) Optimized electromechanical properties and applications of cellular Polypropylene—a new voided space-charge electret material, In: Fecht HJ, Werner M, *The nano-micro interface: Bridging the micro and nano worlds*, Wiley-VCH Verlag, Weinheim 303-317.

Wegener M, Wirges W, Dietrich JP, Gerhard-Multhaupt R (2005) Polyethylene terephthalate (PETP) foams as ferroelectrets. *12th International Symposium on Electrets* 28-30.

Wegener M, Wirges W, Fohlmeister J, Tiersch B, Gerhard-Multhaupt R (2004b) Two-step inflation of cellular polypropylene films: void-thickness increase and enhanced electromechanical properties. *Journal of Physics D: Applied Physics* 37: 623-627.

Wirges W, Wegener M, Voronina O, Zirkel L, Gerhard-Multhaupt R (2007) Optimized preparation of elastically soft, highly piezoelectric cellular ferroelectrets from nonvoided poly(ethylene terephthalate) films. *Advanced Functional Materials* 17: 324-329.

Xu B.X, Von SH, Zhukov S, Gross, D (2013) Continuum modeling of charging process and piezoelectricity of ferroelectrets. *Journal of Applied Physics* 114: 094103.

Xu X, Park CB, Xu D, Pop-Iliev R (2003) Effects of die geometry on cell nucleation of PS foams blown with CO₂. *Polymer Engineering and Science* 43: 1378-1390.

Zakaria Z, Ariff ZM, Sipaut CS (2009) Effects of parameter changes on the structure and properties of low-density polyethylene foam. *Journal of Vinyl and Additive Technology* 15: 120-128.

Zhai W, Wang H, Yu J, Dong J, He J (2008) Cell coalescence suppressed by crosslinking structure in polypropylene microcellular foaming. *Polymer Engineering and Science* 48: 1312-1321.

Zhang P, Xia Z, Qiu X, Wang F, Wu X (2005) Influence of charging parameters on piezoelectricity for cellular polypropylene film electrets. *12th International Symposium on Electrets* 39-42.

Zhang X, Hillenbrand J, Sessler GM, Habertzettl S, Lou K (2012) Fluoroethylenepropylene ferroelectrets with patterned microstructure and high, thermally stable piezoelectricity. *Applied Physics A* 107: 621-629.

Zhang H (2010) Scale-up of extrusion foaming process for manufacture of polystyrene foams using carbon dioxide. *University of Toronto: Doctoral Thesis*.

Zheng WG, Lee YH, Park CB (2010) Use of nanoparticles for improving the foaming behaviors of linear PP. *Journal of Applied Polymer Science* 117: 2972-2979.

Zhuo Q, Tian L, Fang P, Li G, Zhang X (2015) A piezoelectret-based approach for touching and slipping detection in robotic hands. *IEEE International Conference on Cyber Technology in Automation, Control, and Intelligent Systems (CYBER)* 918-921.